NASA TECHNICAL NOTE

NASA TN D-5332

c. 1

NASA TN D-5332

MAGNETOSPHERIC DUCT PROPAGATION RESEARCH USING ALOUETTE-2 TOPSIDE-SOUNDER OBSERVATIONS

by Jayaram Ramasastry and Edward J. Walsh

Electronics Research Center
Cambridge, Mass.

NATIONAL AERONAUTICS AND SPACE ADMINISTRATION • WASHINGTON, D. C. • AUGUST 1969

1. Report No. NASA TN D-5332	2. Government Accession No.	3. Recipient's Catalog No.
4. Title and Subtitle: Magnetospheric Duct Propagation Research Using Alouette-2 Topside-Sounder Observations		5. Report Date: August 1969
		6. Performing Organization Code
7. Author(s): Jayaram Ramasastry and Edward J. Walsh		8. Performing Organization Report No. C-71
9. Performing Organization Name and Address: Electronics Research Center Cambridge, Mass. 02139		10. Work Unit No. 188-39-01-01-25
		11. Contract or Grant No.
		13. Type of Report and Period Covered: Technical Note
12. Sponsoring Agency Name and Address: National Aeronautics and Space Administration Washington D.C. 20546		14. Sponsoring Agency Code

15. Supplementary Notes

16. Abstract

Part I of this report presents a discussion of the intense field-aligned propagation activity in the longitudes of Singapore observed by the Alouette-2 topside sounder. The frequency occurence of sequences of ionograms containing conjugate echo traces is discussed in detail and attributed to the presence of field-aligned irregularities over a wide L-value range in the magnetosphere. The Singapore observations are correlated with magnetic activity and conclusions have been drawn about the sources and mechanisms responsible for the formation and maintenance of magnetospheric duct irregularities.

Part II of the report is devoted to the development of a unified model of field-aligned ducts in the magnetosphere from the analysis of the fine structure and diffuseness of the conjugate echo traces observed by the Alouette-2 sounder. The proposed model for the magnetospheric ducts is a large-scale, field-aligned, gaussian enhancement of electron density with a superimposed fine structure of small-scale gaussian ripples so that the large-scale variation has a ribbed rather than a smooth structure. Mathematical and digital ray-tracing analyses of the new model, along with illustrative ionograms which were used in postulating the model, are presented.

17. Key Words Suggested by Author(s)	18. Distribution Statement: Unclassified – Unlimited		
19. Security Classif. (of this report): Unclassified	20. Security Classif. (of this page): Unclassified	21. No. of Pages: 00	22. Price*: $3.00

*For sale by the Clearinghouse for Federal Scientific and Technical Information Springfield, Virginia 22151

MAGNETOSPHERIC DUCT PROPAGATION RESEARCH USING ALOUETTE-2 TOPSIDE-SOUNDER OBSERVATIONS

By Jayaram Ramasastry and Edward J. Walsh
Electronics Research Center

SUMMARY

Part I of this report presents a discussion of the intense field aligned propagation activity in the longitudes of Singapore observed by the Alouette-2 topside sounder. The frequency occurrence of sequences of ionograms containing conjugate echo traces is discussed in detail and attributed to the presence of field-aligned irregularities over a wide L-value range in the magnetosphere. The Singapore observations are correlated with magnetic activity and conclusions have been drawn about the sources and mechanisms responsible for the formation and maintenance of magnetospheric duct irregularities.

Part II of the report is devoted to the development of a unified model of field-aligned ducts in the magnetosphere from the analysis of the fine structure and diffuseness of the conjugate echo traces observed by the Alouette-2 sounder. The proposed model for the magnetospheric ducts is a large-scale, field-aligned, gaussian enhancement of electron density with a superimposed fine structure of small-scale gaussian ripples so that the large-scale variation has a ribbed rather than a smooth structure. Mathematical and digital ray-tracing analyses of the new model, along with illustrative ionograms which were used in postulating the model, are presented.

PART I

FIELD-ALIGNED PROPAGATION ACTIVITY IN THE LONGITUDES OF SINGAPORE

INTRODUCTION

High-frequency (HF) conjugate echoes were first observed by the Alouette-1 sweep-frequency topside sounder (ref. 1) and the Explorer-20 fixed-frequency topside sounder (ref. 2). Muldrew (ref. 3) and Ramasastry, Walsh and Herman (ref. 4) have published occurrence statistics of HF conjugate echoes observed by the Alouette-2 topside sounder. Ramasastry, Walsh and Herman (ref.5) have revealed three types of Alouette-2 ionograms containing symmetric conjugate echo traces and explained them in terms of multiple reflections between the conjugate points of a field line passing through the satellite.

The purpose of this report is to discuss the unusually high percentage of occurrence of HF conjugate echo events as observed by the Alouette-2 topside sounder in the longitudes of Singapore and correlate the ducting phenomenon with magnetic activity. An attempt is made to interpret the duct occurrence statistics in terms of the changing parameters of the satellite orbit and also the non-uniform sounding time.

ALOUETTE-2 TOPSIDE-SOUNDER DATA FROM SINGAPORE

More than 150,000 ionograms from 10 equatorial and mid-latitude stations (Quito, Fort Myers, Santiago, Johannesburg, Kano, Singapore, Winkfield, Orroral Valley, Kuai, and Kashima) and an equal amount of data from high-latitude stations (Ottawa College, Resolute Bay, South Atlantic and Tromsö) have been analyzed to identify those exhibiting conjugate echo traces. In previous work (refs. 4,5), the authors discussed three basic patterns (double-hook, triple-hook, and equatorial) of conjugate echo traces observable in the Alouette-2 topside sounder ionograms. However, the relative percentages of ducting activity observed at various stations have not been reported in the literature hitherto. Loftus, VanZandt and Calvert (ref.2) concluded that conjugate ducting is more frequent in the longitudes of the Americas. Their conclusion was based on Explorer-20 observation of conjugate ducting at the longitudes of the Americas, Hawaii, Australia, Singapore, and South Africa. Observations made by the authors with the Alouette-2 topside sounder contradict previous topside-sounder observations and predictions. From data taken from 10 equatorial and mid-latitude stations analyzed by the authors, the Singapore data especially show some unusual features. For the period November 1965 to November 1966, more than 50 percent of all the ionograms

exhibiting conjugate echoes were recorded at Singapore. For the time period considered, the total sounding time at Singapore is comparable to the total sounding time at each of the other stations. During 1966 the individual soundings at Singapore amounted to 7250 minutes during which period 1467 conjugate echo ionograms were recorded. Any doubt that enhanced total sounding time might have contributed to the increased ducting activity at Singapore is therefore eliminated. In the authors' evaluation of the intensity of ducting activity, they have excluded ionograms exhibiting only combination mode echoes, near-end ducted echoes, and topside spread-F traces. Inclusion of these ionograms by considering them as representing field-aligned propagation phenomena would have greatly enhanced the value of the number of conjugate ducting events observed per minute of sounding time.

Since the same magnetospheric ducts are responsible for guiding the whistler modes also, the whistler occurrence characteristics should agree with the occurrence characteristics of HF-guided modes unless there are other ionospheric phenomena which drastically inhibit their propagation. From VLF whistler data, Helliwell (refs. 6,7) observed that southern hemisphere stations lying along the magnetic meridian which passes through the eastern coast of the U.S.A. have the highest whistler rates of any stations of the world. Helliwell explains this fact as being due to whistlers generated by the high thunderstorm activity along the eastern coast of the U.S.A. Because the thunderstorm activity is just as high in some other areas, such as Central Africa, an alternative explanation has been given by many that the high rate of whistler activity is caused by a great occurrence of whistler-supporting magnetospheric irregularities over South America. Such a hypothesis does not agree with what was observed by the Alouette-2 topside sounder in the longitudes of Singapore.

Figures 1 and 2 show the longitudinal and latitudinal (both geographic and geomagnetic) distribution of the conjugate ducting events monitored at Singapore during 1966.

SEQUENCES IN THE SINGAPORE DATA

The prevailing opinion about magnetospheric ducting is that it occurs according to the altitude, L-value, and local time statistics published by Loftus, VanZandt and Calvert (ref. 2), Muldrew (refs. 1,3) and Ramasastry, Walsh, and Herman (refs. 4,5). No study has hitherto been reported concerning whether or not magnetospheric ducting is observed over a wide range of L-values simultaneously. Sequences of ionograms exhibiting conjugate echo traces provide a partial answer to that question. If sequences do exist frequently, they will dispel the idea that magnetospheric ducts exist only in localized L-shells. On the other hand, the se-

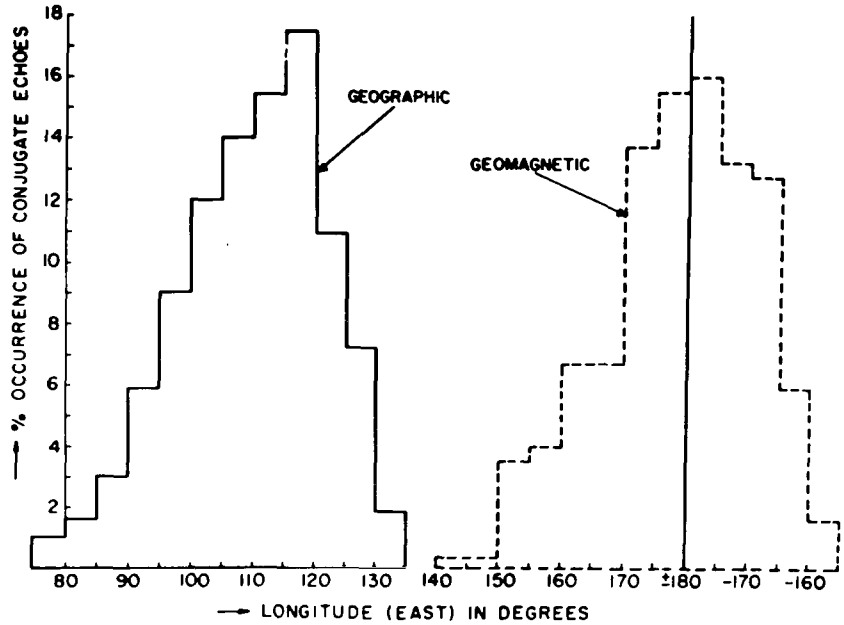

Figure 1 - Longitude distribution of percentage occurrence of conjugate echoes at Singapore during 1966

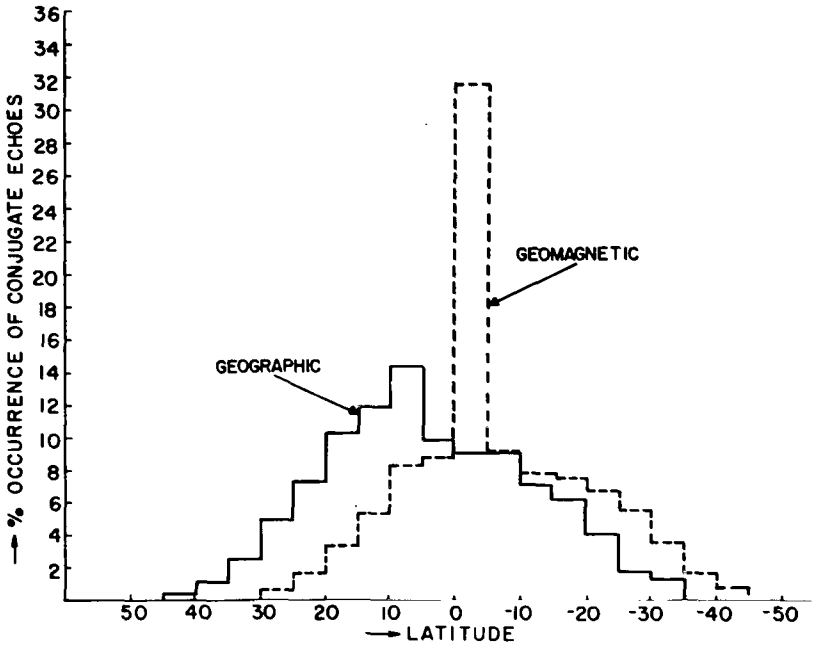

Figure 2 - Latitude distribution of percentage occurrence of conjugate echoes at Singapore during 1966

quences establish the fact that, whenever they are observed, a large portion of the magnetosphere (as described by the L-value range of the sequence) is involved in field-aligned propagation activity. Such information will be very useful not only in understanding the physical mechanisms responsible for the formation of field-aligned ducts in the magnetosphere, but also for planning a satellite experiment to study the field-aligned ducting phenomenon.

Singapore is unique in this respect. More than 75 percent of all the conjugate echo ionograms recorded at Singapore are in the form of sequences. In the remaining 25 percent of the ionograms, the sequences were disrupted by either small sounding times or unusual noise conditions. In all some 73 sequences were observed at Singapore during the year 1966 with an average of 18 ionograms per sequence.

The L-value range corresponding to any one sequence should not be taken to mean that ducting activity was restricted to those corresponding field lines only. In fact, sounding time plays a strong role in determining the length of the sequences and hence the L-value range. The beginning of sounding is not to be mistaken for the onset of a physical mechanism responsible for guiding the HF waves. In many instances, conjugate echo traces were present in the first ionogram recorded after the sounding was started when the satellite was in the vicinity of Singapore. This only means that the initial L-value of the field line passing through the satellite when the sounder was started does not represent the appropriate L-value when the sequence actually began. It may be safely assumed that the onset of the physical mechanism responsible for conjugate ducting had taken place much earlier than when the satellite sounder detected it. This ambiguity cannot be resolved as long as data are not available from the remaining portion of the orbit.

In many other cases, the sequences were abruptly terminated when the sounder was turned off. This gives rise to artificial termination of a physical phenomenon. Hence, the length of the sequence, in many instances, is dependent on the length of the sounding time.

Figure 3a is a sequence of 29 ionograms recorded at Singapore on February 8, 1966, from 16 h., 31 m., 53 s. UT to 16 h., 52 m., 30 s. UT in a South to North pass of the satellite. As in the case of most of the other sequences, the sequence starts when the satellite is in the southern (or northern) hemisphere and continues as the satellite crosses the equator and enters the other hemisphere. Figure 3b shows the satellite positions during the time when the sequence was recorded. Also shown in the figure are the field lines of maximum and minimum L-values corresponding to the sequence. The region between the two field lines indicates

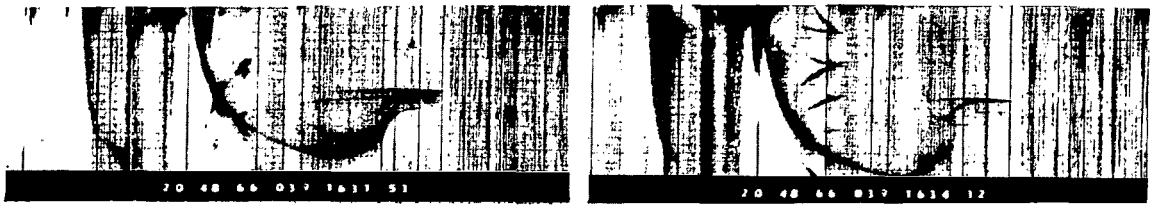

1 6

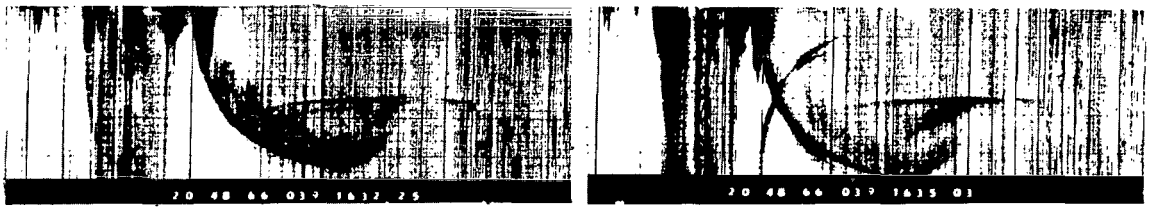

2 7

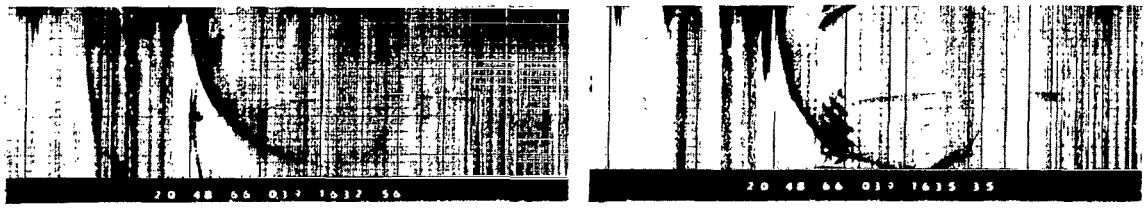

3 8

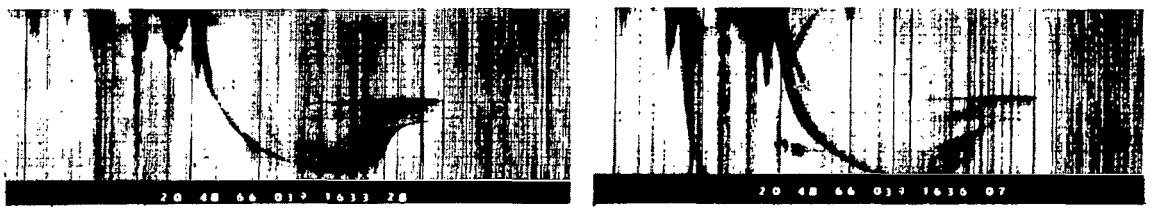

4 9

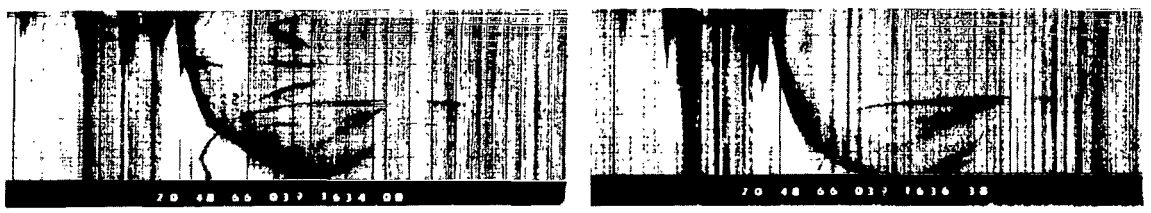

5 10

Figure 3a.-Sequence recorded at Singapore on February 8, 1966, from 16:31:53 UT to 16:52:30 UT in a South to North pass

11

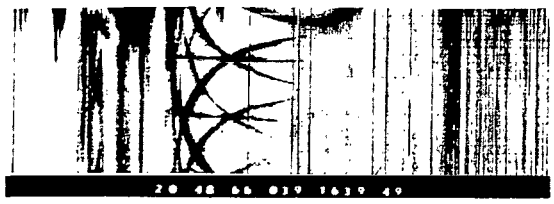

16

12

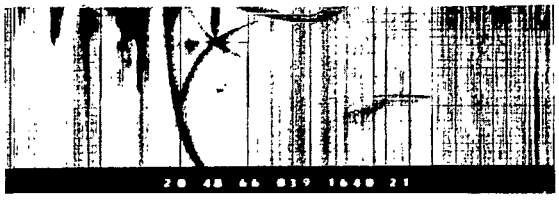

17

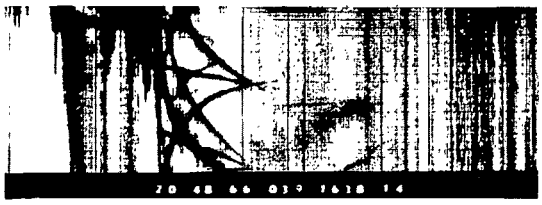

13

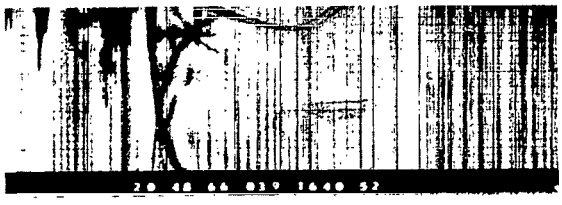

18

14

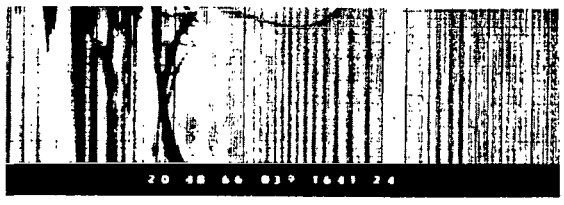

19

15

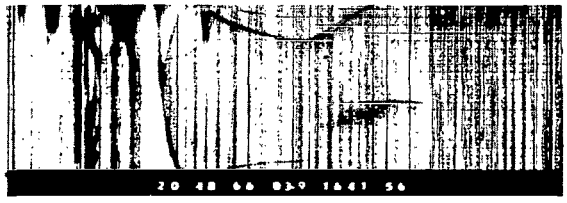

20

Figure 3a.-Sequence recorded at Singapore on February 8, 1966, from 16:31:53 UT to 16:52:30 UT in a South to North pass (cont'd)

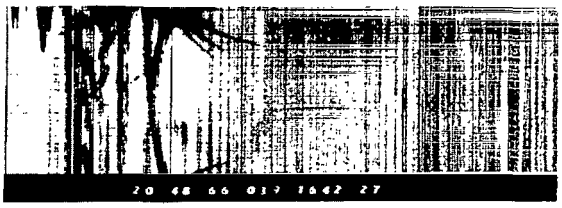

21

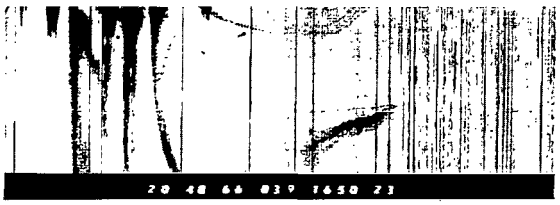

26

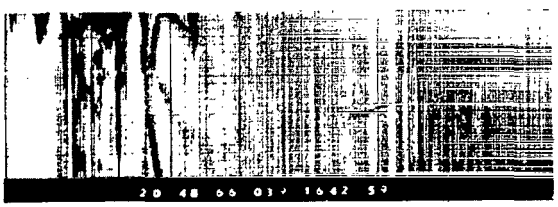

22

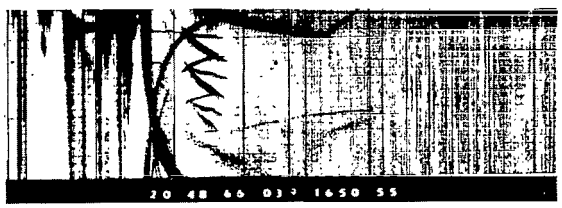

27

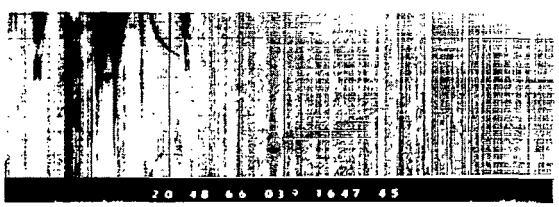

23

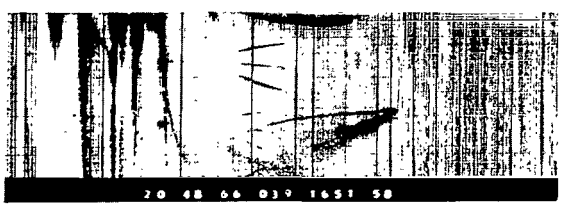

28

24

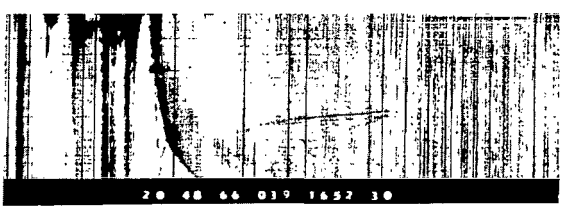

29

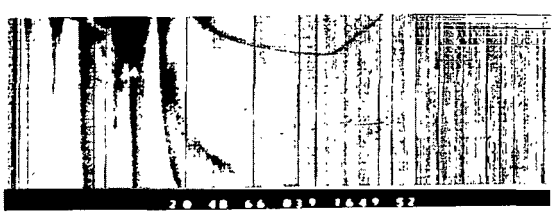

25

Figure 3a.-Sequence recorded at Singapore on February 8, 1966, from 16:31:53 UT to 16:52:30 UT in a South to North pass (concl'd)

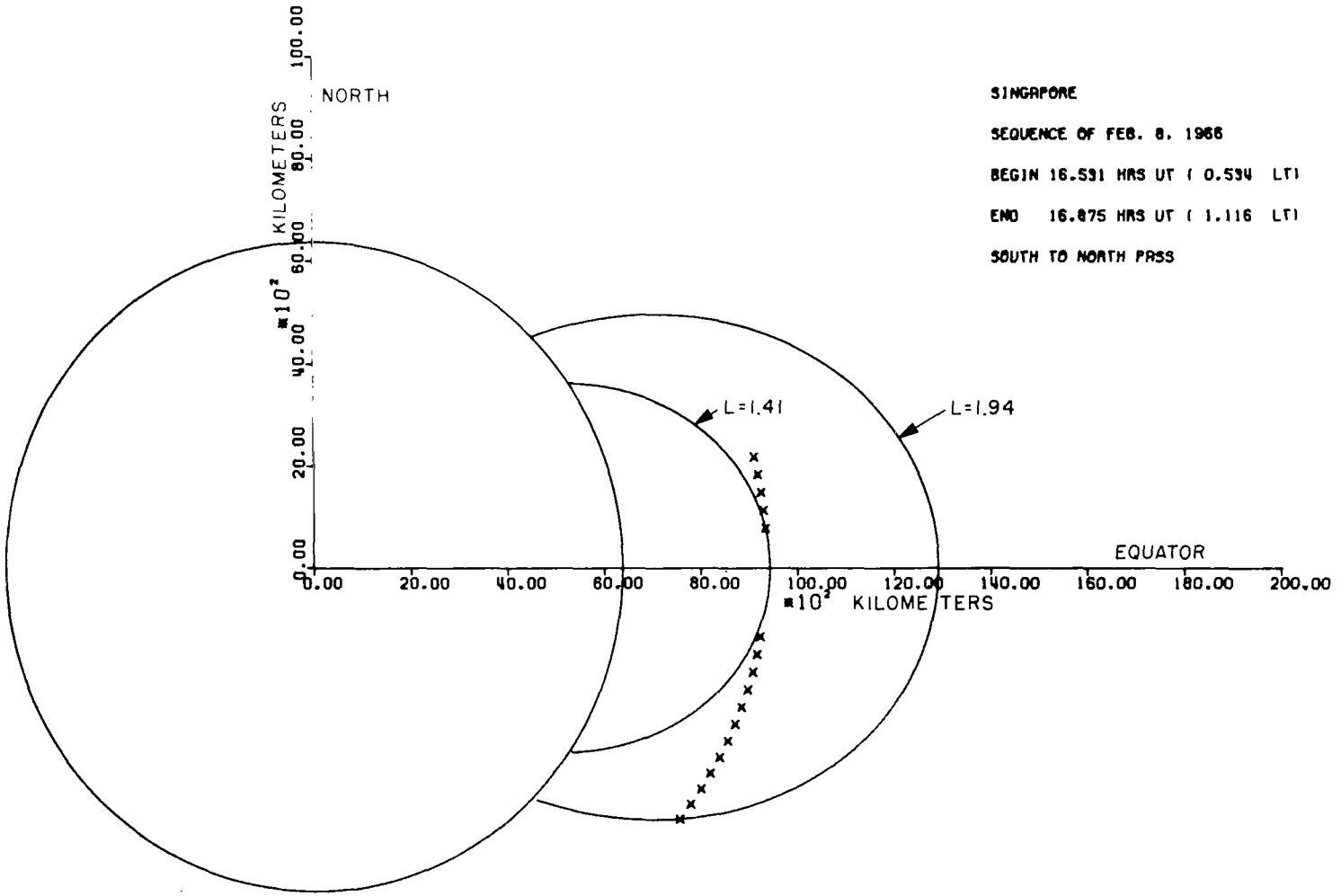

Figure 3b.-Diagram showing the satellite positions corresponding to the ionograms of the sequence observed on February 8, 1966

the portion of the magnetosphere participating in the observed field-aligned propagation activity at the time the sequence was recorded. The termination of a sequence is caused by various factors like abrupt termination of the sounding experiment, presence of conditions unfavorable to monitor conjugate echoes, disappearance of magnetospheric ducts, and so forth. This particular sequence was observed for about 90 percent of the corresponding sounding time. However, during the remaining 10 percent of the sounding time, spread-F activity was very intense on the records. The first ionogram recorded in this sounding period was the beginning of the sequence also. The L-value range of the sequence is 1.94-1.41-1.51. The middle number indicates the L-value of the satellite position when it crossed the equator. During the length of the sequence, the geomagnetic longitude of the satellite changed only by 1.5 degrees, while the geomagnetic latitude changed from 33.26°S to 13.52°N. The satellite was near apogee and the Local Time was 00 h., 32 m., 02 s., when the sequence was recorded.

Another interesting feature of the sequence is the change in the patterns of the echo traces as the satellite moves in from higher latitudes towards the equator and then moves away towards higher latitudes after equatorial crossing. Ramasastry, Walsh, and Herman (refs. 4,5) reported three distinct types of conjugate echo patterns: triple hook, double-hook, and equatorial types. Triple-hook and double-hook patterns are characteristic of wave guidance at relatively high satellite latitudes where the difference in the group delays between the near-end and far-end traces is equal to or greater than 32 msec. This is a necessary condition for the formation of these two types of conjugate echo patterns. In the sequence ionograms 1 through 19 either exhibit or have the potential to exhibit triple-hook and/or double-hook types of traces. Ionograms 20 through 25 reveal the equatorial type of traces. The satellite was close to the equator when these ionograms were recorded, and hence the difference in the group delays between the near-end and far-end traces is smaller than 32 msec, a condition necessary for the formation of equatorial pattern. Ionograms 25 through 29 exhibit, once again, the double-hook and triple-hook patterns as the satellite moves away from the equator.

Figure 4a is a sequence of 36 ionograms recorded on June 7, 1966, from 14 h., 08 m., 24 s., UT to 14 h., 32 m., 08 s., UT in a North to South pass of the satellite. The sequence of ionograms was observed for about 80 percent of the corresponding sounding time. The L-value range is 1.65-1.38-1.83. The change in the satellite longitude (geomagnetic) is 7.15° as the satellite latitude changes from 19.72°N to 32.11°S. The satellite was near apogee and the local time was 22 h., 19 m., 34 s., when the sequence was recorded. Figure 4b shows the satellite trajectory

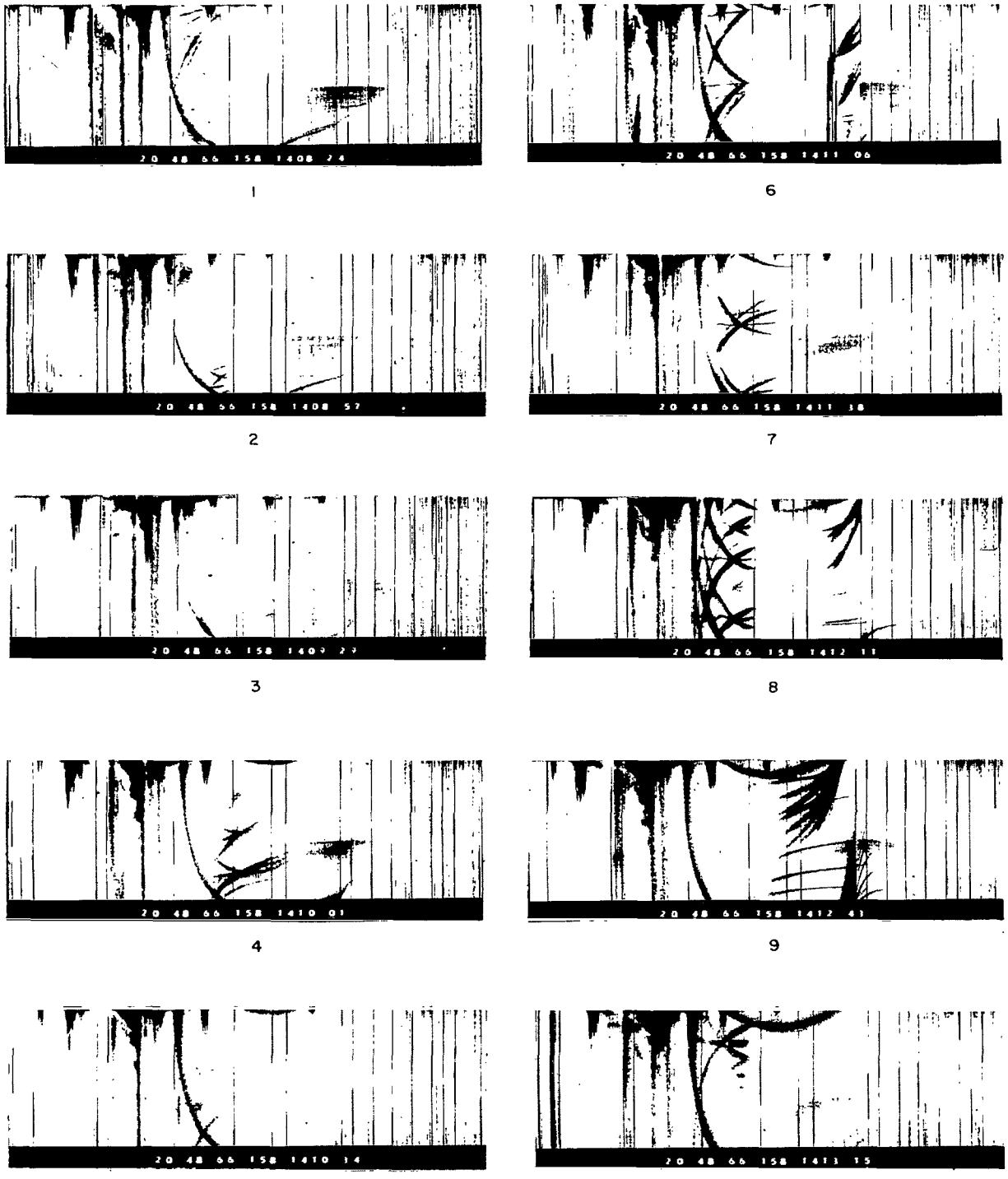

Figure 4a.-Sequence recorded at Singapore on June 7, 1966, from 14:08:24 UT to 14:32:08 UT in a North to South pass

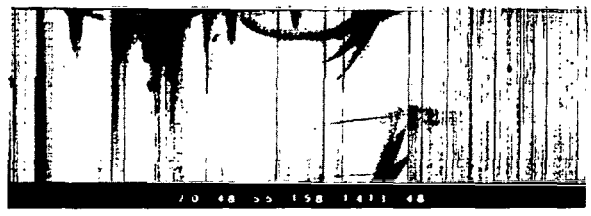

11

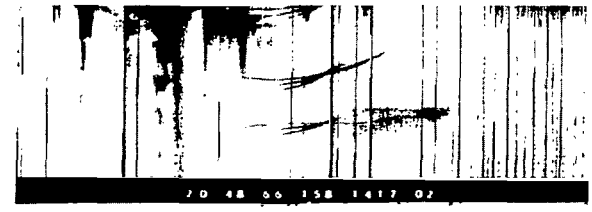

16

12

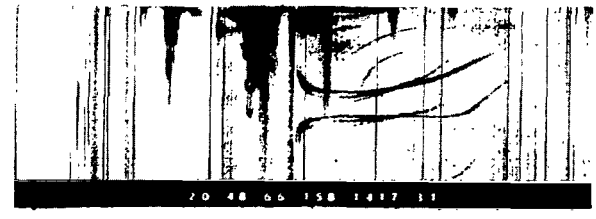

17

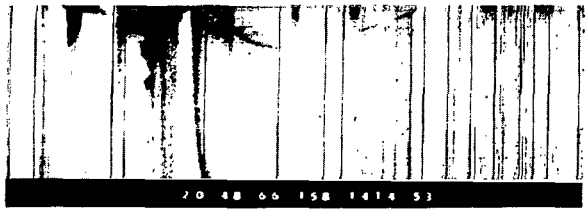

13

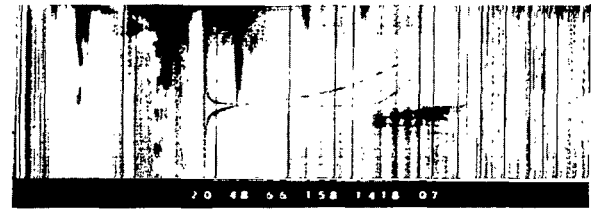

18

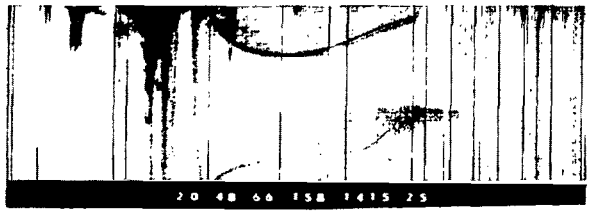

14

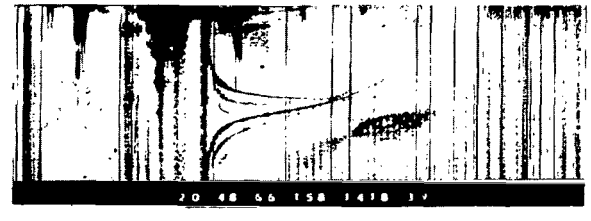

19

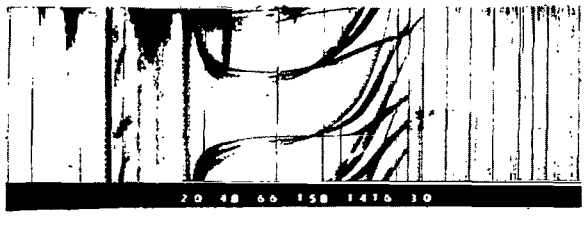

15

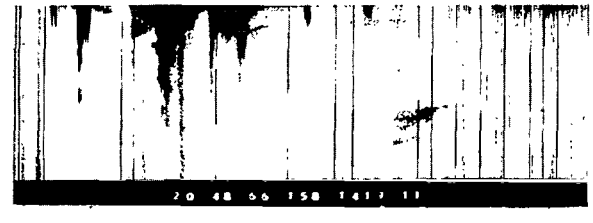

20

Figure 4a.-Sequence recorded at Singapore on June 7, 1966, from 14:08:24 UT to 14:32:08 UT in a North to South pass (cont'd)

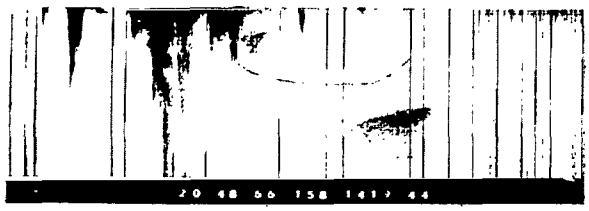

21

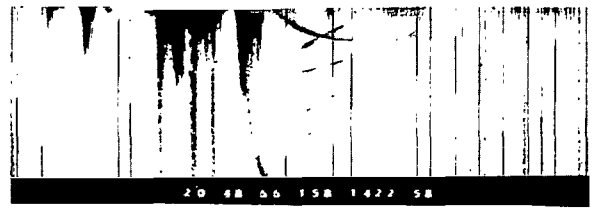

26

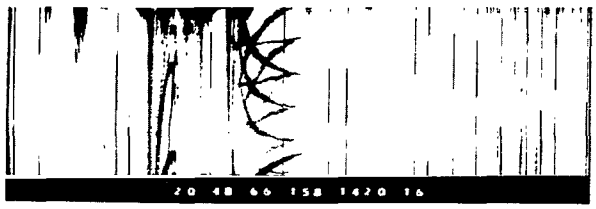

22

27

23

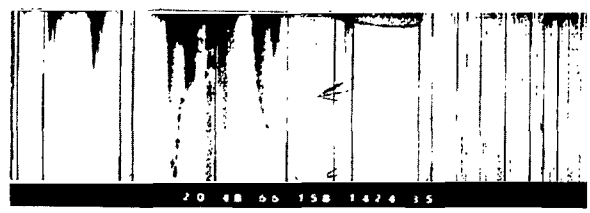

28

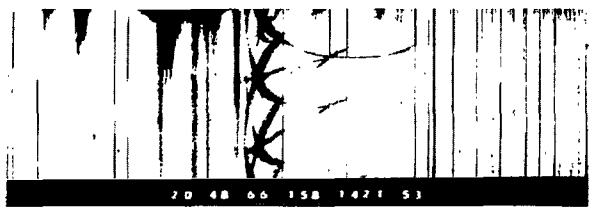

24

29

25

30

Figure 4a.-Sequence recorded at Singapore on June 7, 1966, from 14:08:24 UT to 14:32:08 UT in a North to South pass (cont'd)

31

36

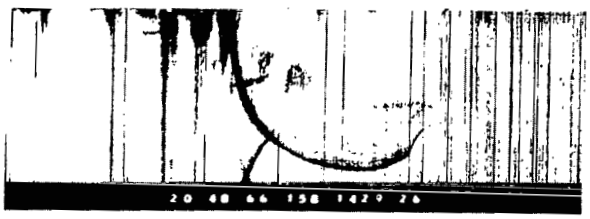

32

33

34

35

Figure 4a.-Sequence recorded at Singapore on June 7, 1966, from 14:08:24 UT to 14:32:08 UT in a North to South pass (concl'd)

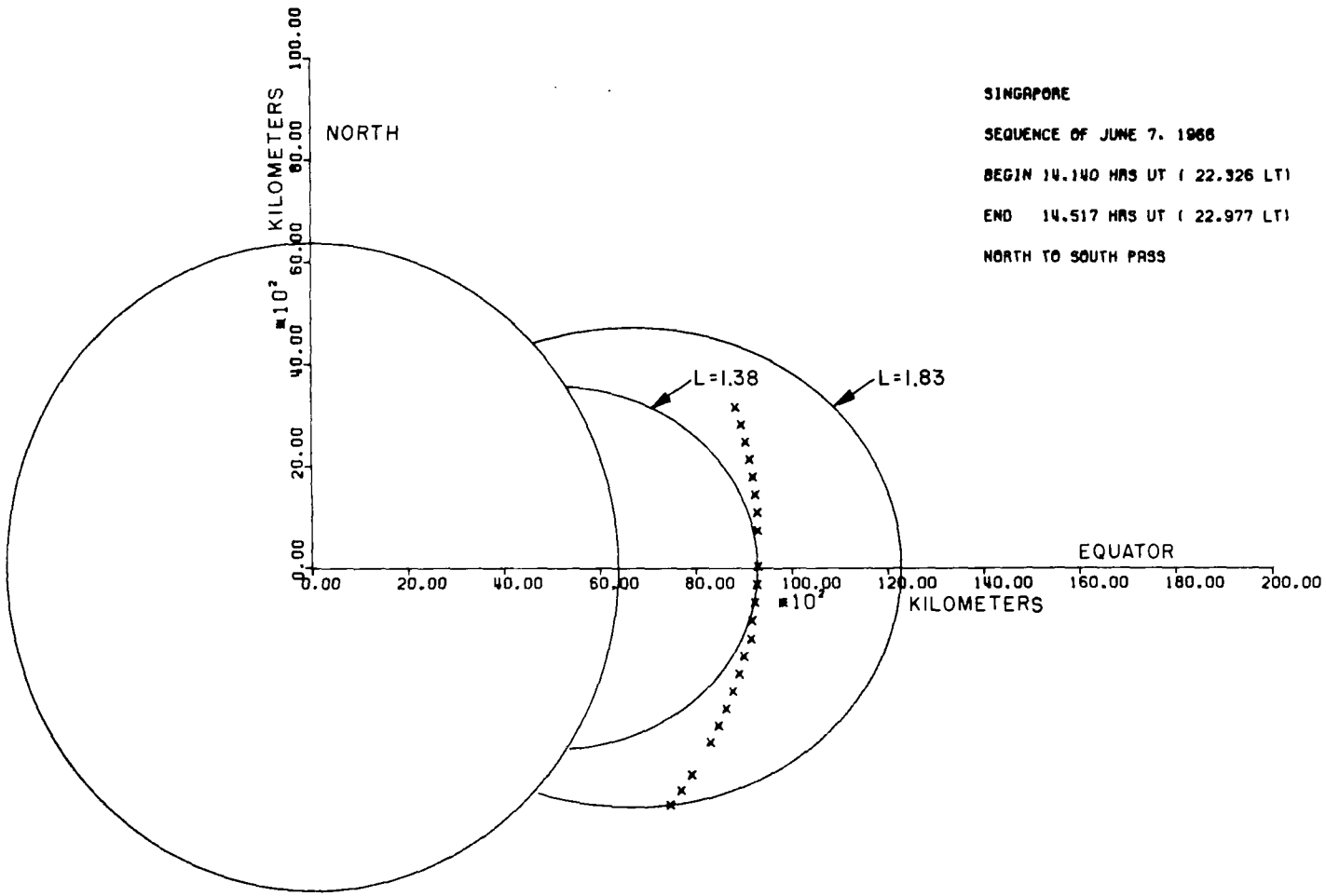

Figure 4b.-Diagram showing the satellite positions corresponding to the ionograms of the sequence observed on June 8, 1966

during the period when the sequence was recorded. Also shown in the figure are the field lines of maximum and minimum L-values corresponding to the sequence. The same remarks made about the patterns of conjugate echo traces observed in the ionograms of the February 8, 1966, sequence hold for this sequence also. However, this sequence is a typical example of beautiful patterns of conjugate echo traces that are observable.

Figure 5a is a sequence of 27 ionograms recorded at Singapore on June 8, 1966, from 14 h., 28 m., 05 s. UT to 14 h., 46 m., 26 s. UT in a North to South pass of the satellite. The sequence was observed for about 65 percent of the corresponding sounding time. Spread-F activity was very high during the remaining part. The L-value range of the sequence is 1.44-1.38-1.55. The change in the satellite longitude (geomagnetic) is 4.35° as the satellite latitude changes from 14.78°N to 25.86°S. Figure 5b shows the satellite trajectory during the period when the sequence was recorded. Also shown in the figure are the field lines of maximum and minimum L-values corresponding to the sequence.

Figure 6a is a sequence of 31 ionograms recorded on August 9, 1966, from 19 h., 28 m., 09 s. UT to 19 h., 45 m., 20 s. UT in a South to North pass of the satellite. The sequence was observed for about 90 percent of the sounding time and the L-value range is 1.63-1.37-1.58. The change in satellite longitude was 2.25° as against the change in latitude from 21.97°S to 16.33°N. An additional feature of this sequence is the wavy nature of the conjugate echo traces. The basic triple-hook, double-hook and equatorial patterns wind and fold into complicated shapes. Figure 6b shows the satellite trajectory during the period when the sequence of August 9, 1966, was recorded.

Table I provides all the pertinent information about the sequences. In some cases, the sequence had already begun when the sounding started while, in some other cases, the sounding is abruptly terminated while the sequence is still continuing. This sequence is considered as a typical example of anomalous ducting activity.

Figure 7 is a scatter plot of altitude versus L-value of every member of all the sequences observed during the year 1966. The high density of data points in the vicinity of L = 1.4 is due not only to the location of the tracking station (Singapore), but also to the way in which the sounder is operated. It has already been pointed out that a majority of the conjugate echo events at Singapore were recorded in the form of sequences. The tracking station is situated close to the equator and the latitude range covered by the satellite is limited. In many cases, even when the sequences began at fairly high L values (higher latitudes), they were abruptly terminated when the satellite was

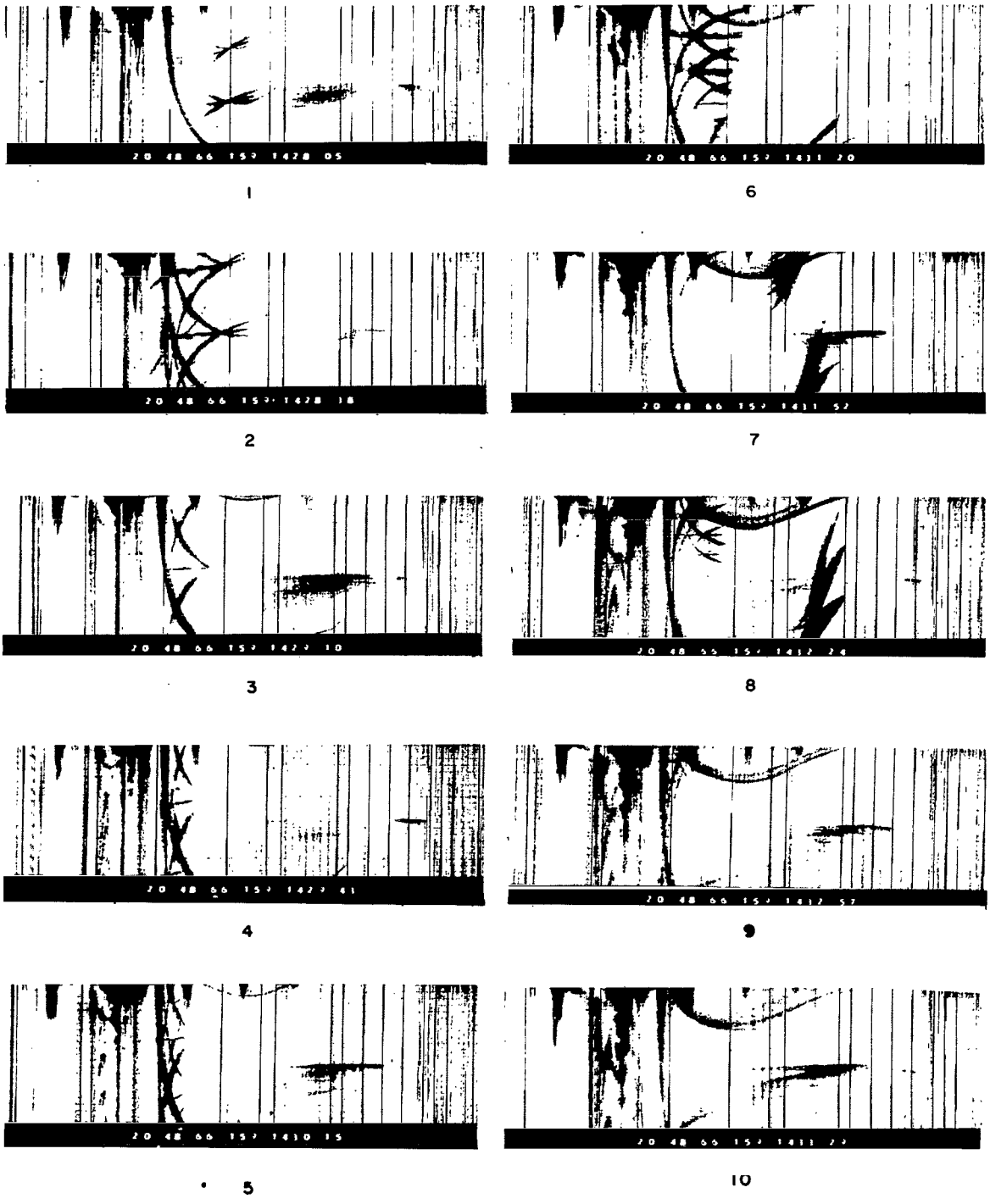

Figure 5a.-Sequence recorded at Singapore on June 8, 1966, from 14:28:05 UT to 14:46:26 UT in a North to South pass

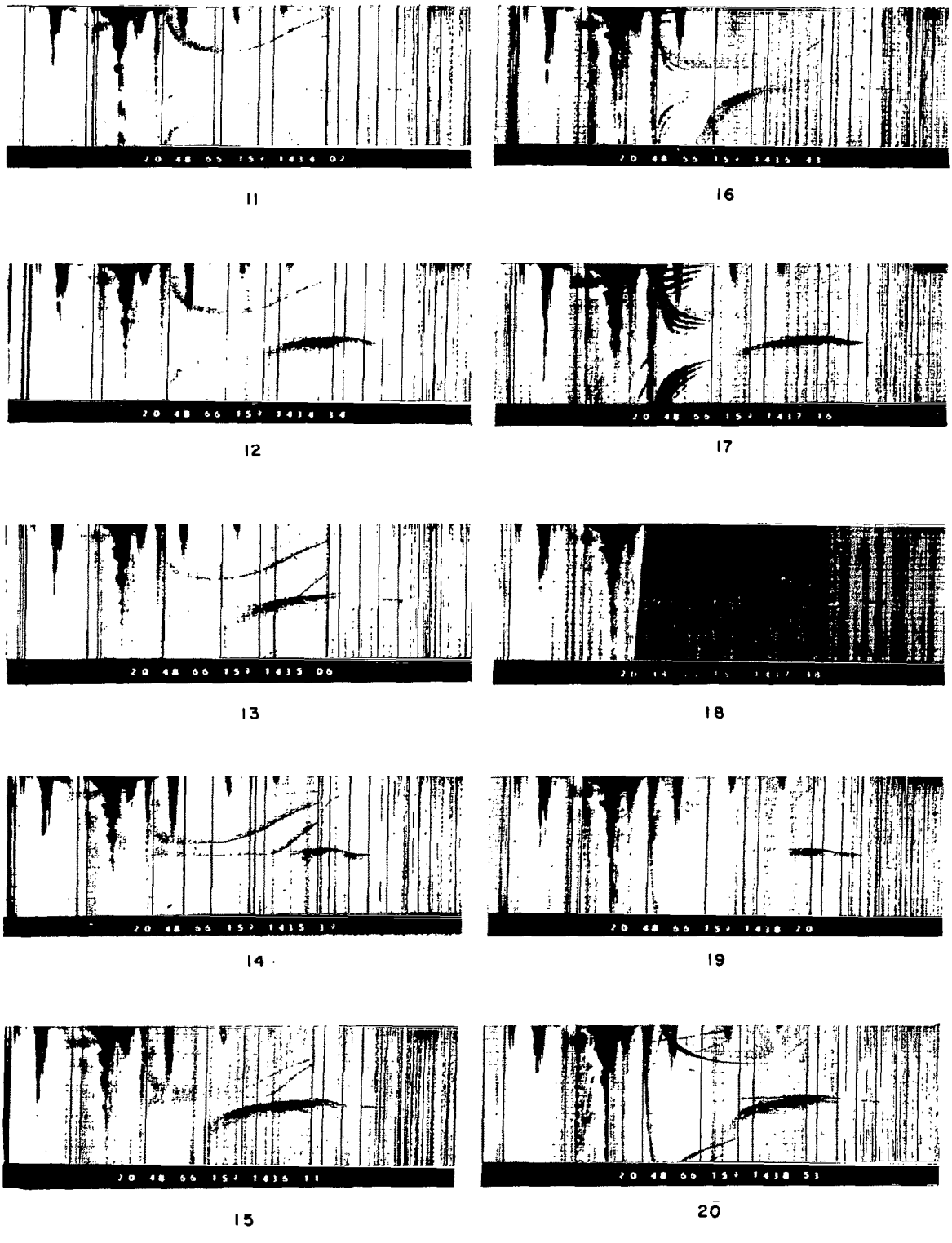

Figure 5a.-Sequence recorded at Singapore on June 8, 1966, from 14:28:05 UT to 14:46:26 UT in a North to South pass (cont'd)

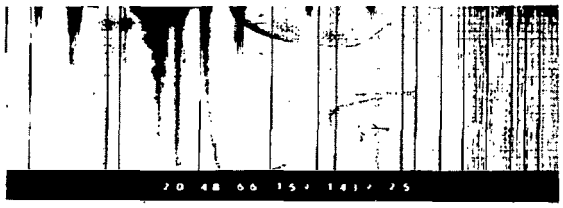

21

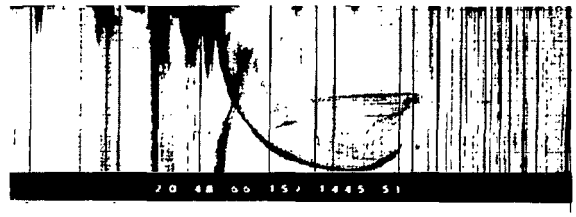

26

22

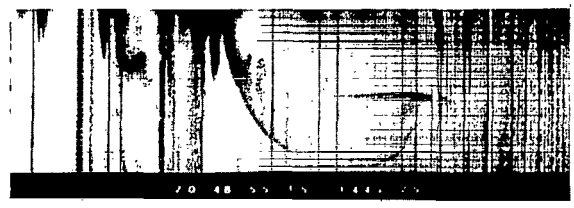

27

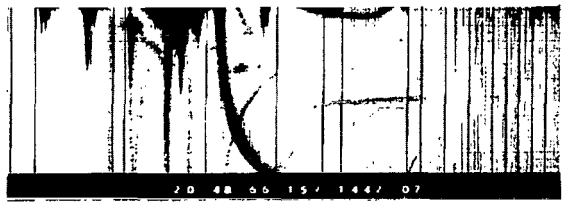

23

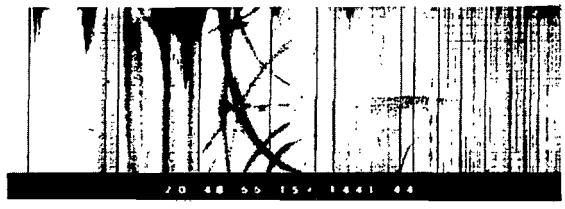

24

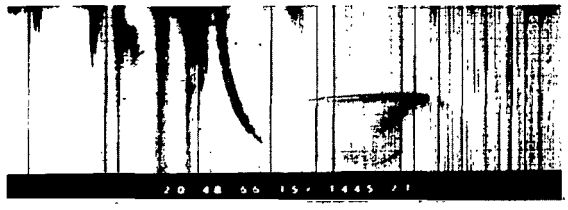

25

Figure 5a.-Sequence recorded at Singapore on June 8, 1966, from 14:28:05 UT to 14:46:26 UT in a North to South pass (concl'd)

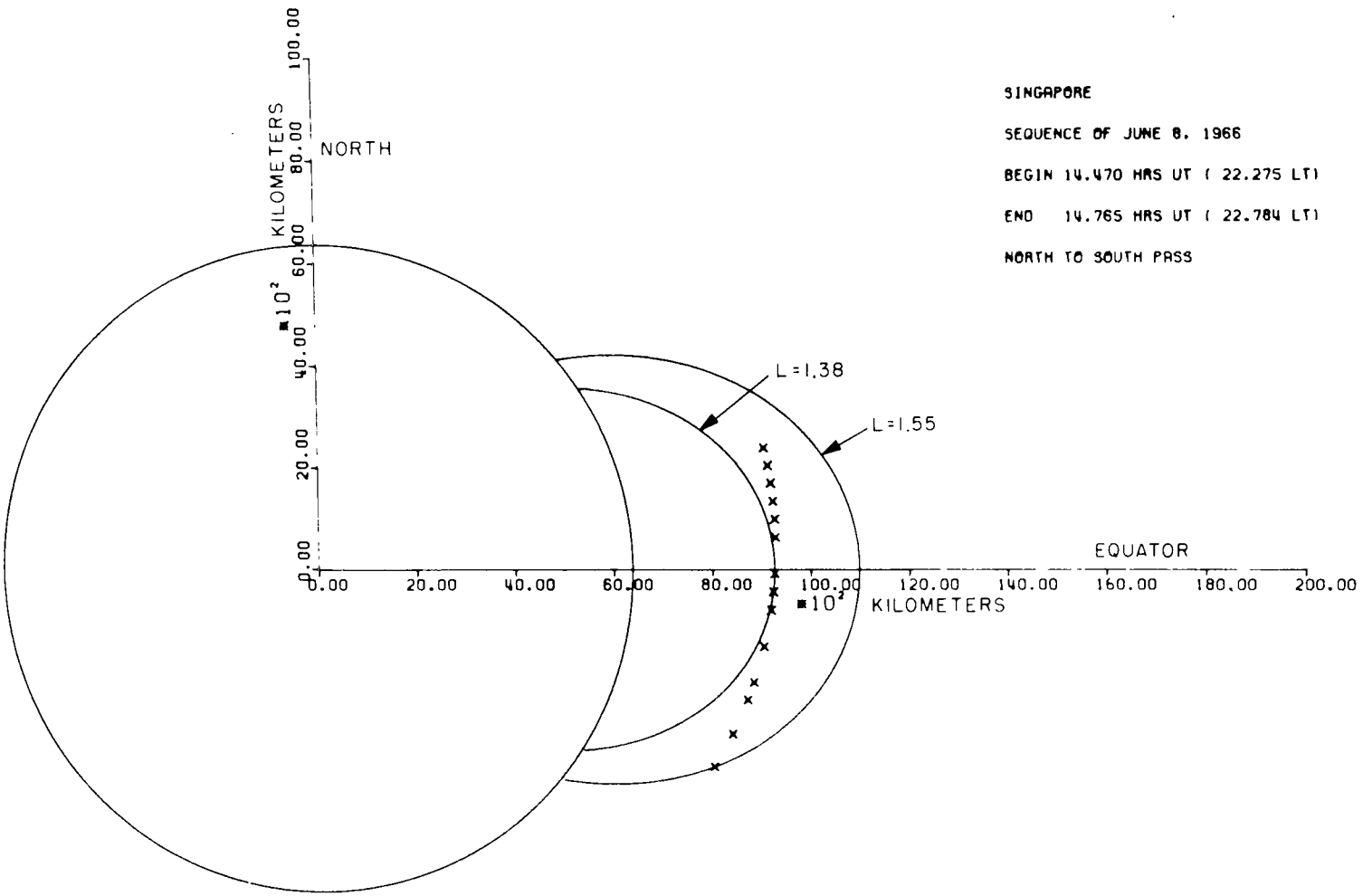

Figure 5b.-Diagram showing the satellite positions corresponding to the ionograms of the sequence observed on June 8, 1966

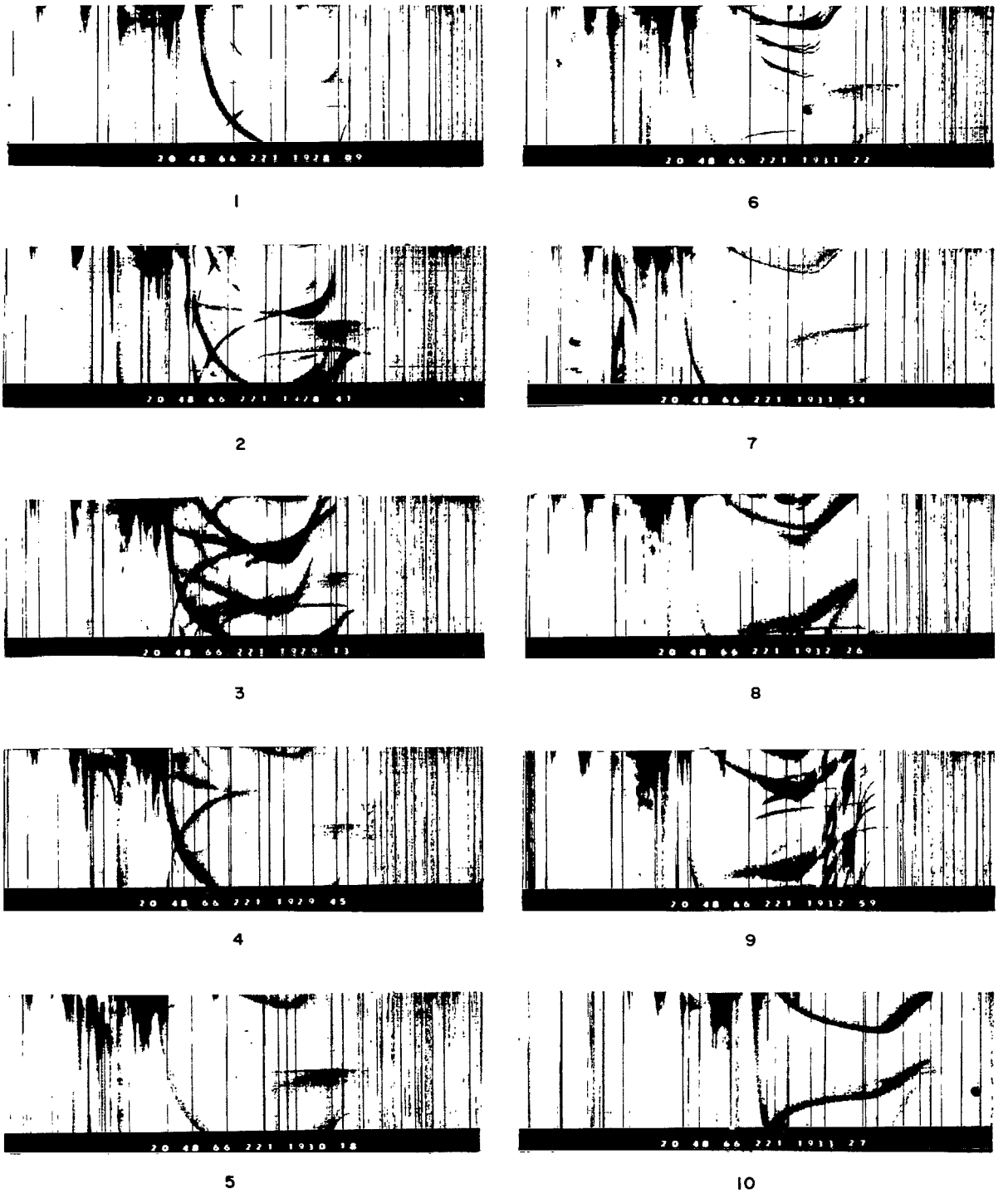

Figure 6a.-Sequence recorded at Singapore on August 9, 1966, from 19:28:09 UT to 19:45:20 UT in a South to North pass

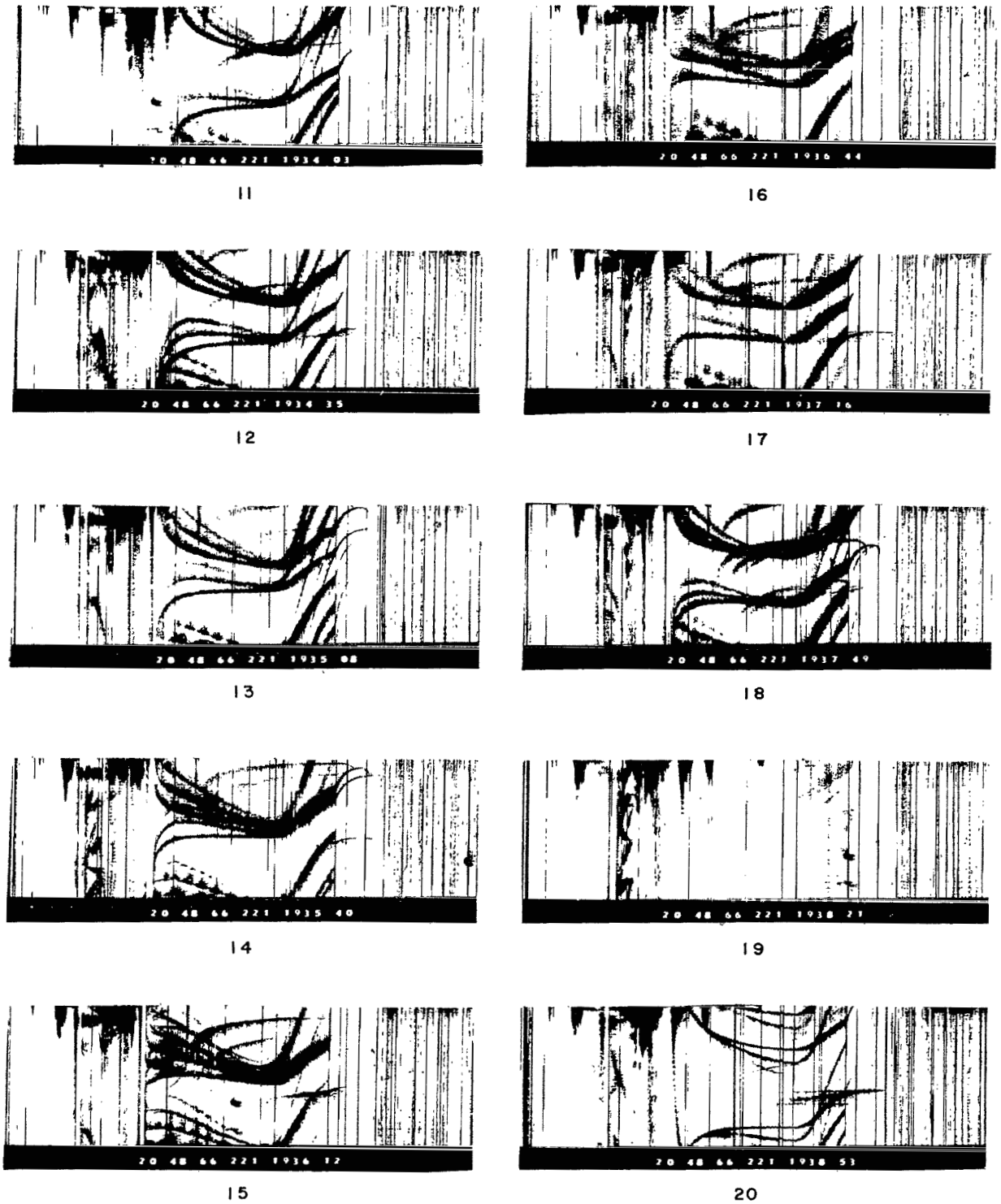

Figure 6a.-Sequence recorded at Singapore on August 9, 1966, from 19:28:08 UT to 19:45:2- UT in a South to North pass (cont'd)

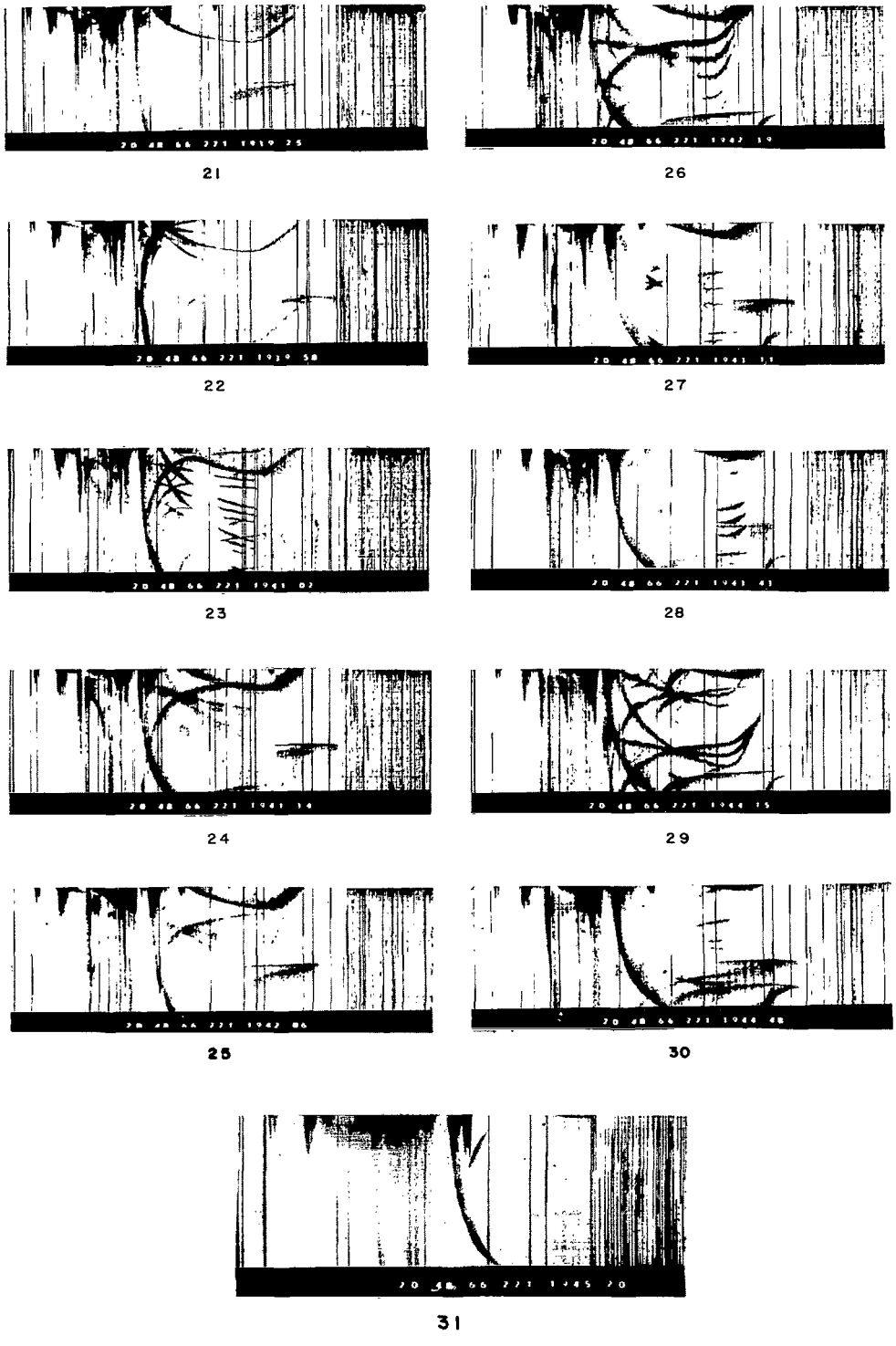

Figure 6a.-Sequence recorded at Singapore on August 9, 1966, from 19:28:09 UT to 19:45:20 UT in a South to North pass (concl'd)

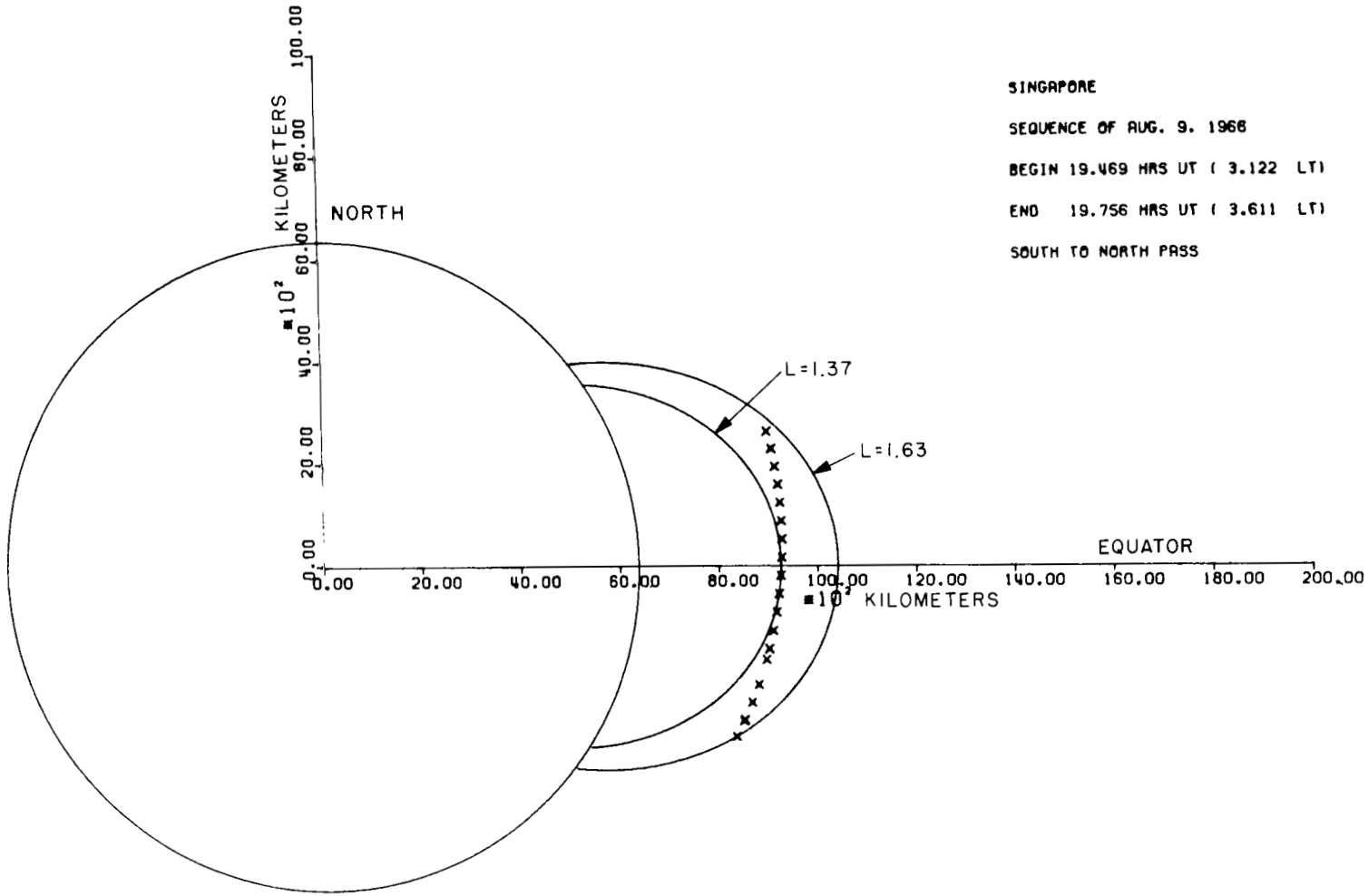

Figure 6b.-Diagram showing the satellite positions corresponding to the ionograms of the sequence observed on August 9, 1966

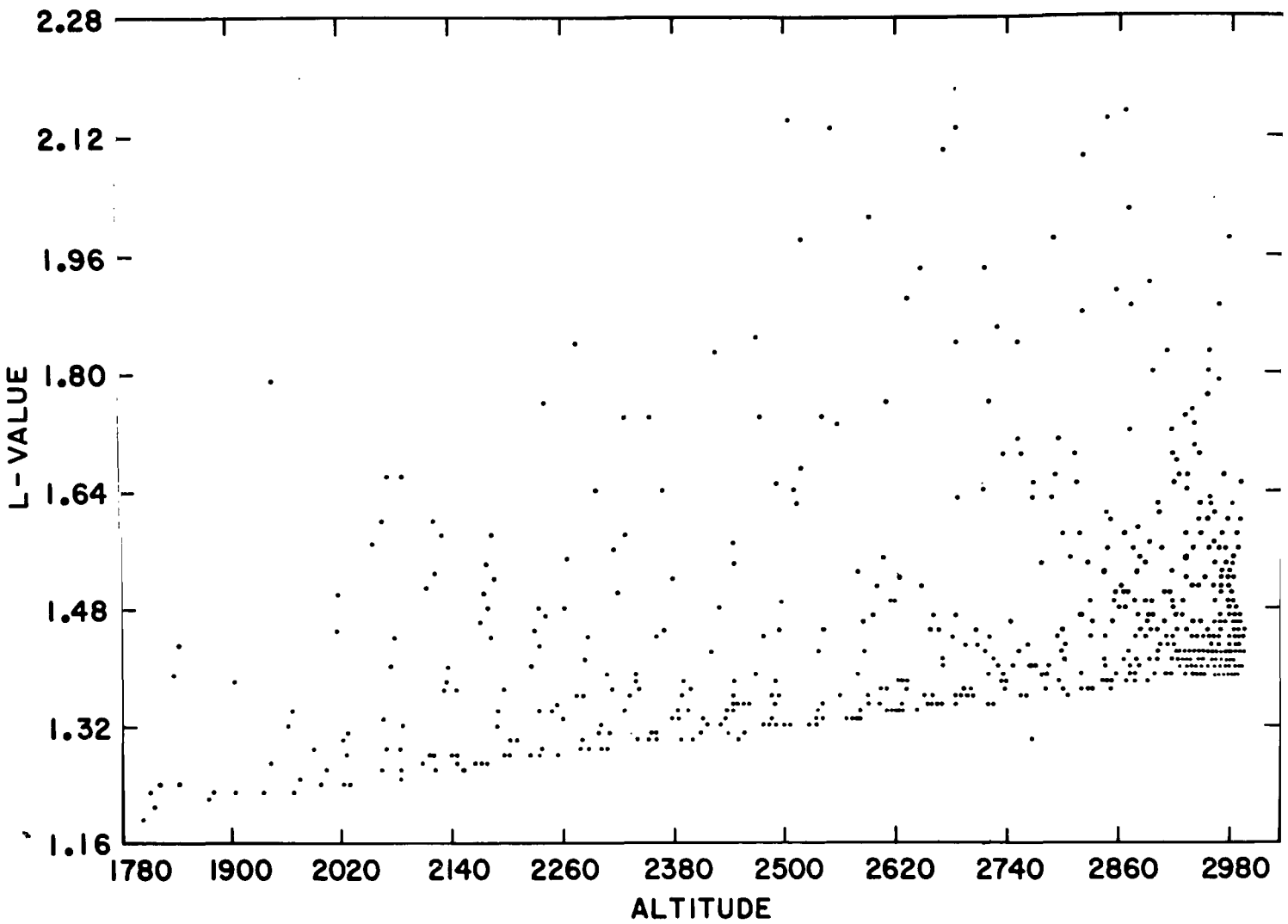

Figure 7.-Scatter plot of altitude versus L-value of every ionogram of all the sequences

TABLE I

ORBITAL INFORMATION OF SEQUENCES OBSERVED AT SINGAPORE DURING 1966

Year	Day	Time Begin (UT)	Duration*	% Fraction of Total Sounding Time	L-value Range	Geomagnetic Latitude Range (deg)	Altitude Range (km)	South to North (S/N) North to South (N/S)	Local Time Range
1966	1	21:40:48	5'35"	27	1.33-1.30-1.53		2206-2296	S/N	5:30:07-5:42:00
	6	21:00:14	9'08"	76	1.39-1.32-1.37		1681-2229	S/N	4:37:37-4:55:55
	22	21:57:18	4'34"	22	1.61-1.98	18.82°N-29.50°N	2901-2976	S/N	3:10:44-3:21:50
	38	18:14:20	31'09"	100	2.13-1.39-2.09	36.84°S-31.87°N	2548-2974-2820	S/N	0:35:53-1:34:19
	39	16:31:52	20'38"	90	1.94-1.41-1.51	33.26°S-13.52°N	2646-2945-2967	S/N	0:32:02-1:06:58
	41	17:08:24	20'10"	95	1.94-1.39-1.51	32.97°S-13.44°N	2715-2982-2944	S/N	0:18:36-0:52:48
	44	16:00:25	19'37"	85	1.98-1.40-1.47	33.34°S-10.77°N	2789-2981-2924	S/N	23:57:00-0:29:53
	45	16:28:52	7'26"	62	1.42-1.39-1.42	9.0°S-6.31°N	2986-2976-2942	S/N	0:07:44-0:19:30
	46	16:39:07	15'54"	66	1.72-1.39-1.44	26.44°S-8.59°N	2911-2967-2909	S/N	23:48:11-0:13:55
	64	13:47:20	29'03"	100	3.02-1.54	45.73°S-21.56°N	2995-2115	S/N	21:24:22-22:18:54
	65	14:20:24	5'49"	30	1.49-1.39	11.50°S-1.70°N	2720-2488	S/N	21:44:42-21:54:32
	73	14:38:16	20'13"	85	2.65-1.27-1.28	42.25°S-4.88°N	2931-2233-2119	S/N	20:44:20-20:59:49
	104	22:44:38	7'20"	35	1.64-2.76	27.66°S-44.72°S	2298-2638	N/S	5:16:44-5:31:59
	105	22:53:20	6'47"	35	1.20-1.44	0.85°S-20.13°S	1752-2183	N/S	4:51:04-5:04:41
	106	21:13:01	12'29"	55	1.28-2.74	12.16°S-44.42°S	2027-2691	N/S	4:51:43-5:17:17
	114	19:24:43	20'53:	90	1.27-1.26-2.79	6.69°N-44.1°S	1943-2064-2892	N/S	3:41:24-4:21:14
	123	20:10:37	10'23"	35	1.49-2.18	12.37°S-34.93°S	2679-2950	N/S	2:03:22-2:30:43
	125	20:36:43	17'54"	85	1.42-1.88	11.61°N-28.21°S	2309-2932	N/S	0:24:50-2:11:17
	126	18:53:53	19'01"	80	1.41-2.18	8.73°N-34.88°S	2384-2978	N/S	2:14:42-2:47:31
	128	19:29:56	12'11"	45	1.42-1.65	7.84°N-19.95°S	2483-2900	N/S	2:01:19-2:21:54
	129	17:47:46	9'03"	100	1.41-1.58	3.67°N-16.88°S	2592-2887	N/S	1:57:47-2:12:47
	130	18:00:14	18'40"	65	1.50-1.82	17.48°N-26.23°S	2356-2970	N/S	1:40:48-2:12:25
	142	15:31:52	10'12"	85	1.46-1.40-1.45	10.66°N-11.15°S	2852-2949-2987	N/S	0:20:53-0:37:37
	143	17:52:05	13'59"	60	1.44-1.40-1.61	8.72°N-22.01°S	2889-2943-2954	N/S	0:14:35-0:37:08
	144	16:02:46	21'32"	75	1.69-1.39-1.69	22.60°N-25.77°S	2735-2971-2916	N/S	23:55:44-0:33:32

TABLE I - Continued

ORBITAL INFORMATION OF SEQUENCES OBSERVED AT SINGAPORE DURING 1966

Year	Day	Time Begin (UT)	Duration*	% Fraction of Total Sounding Time	L-value Range	Geomagnetic Latitude Range (deg)	Altitude Range (km)	South to North(S/N) North to South(N/S)	Local Time Range
1966	146	16:43:52	9'07"	40	1.44-1.39-1.43	8.21°N-11.46°S	2937-2979-2977	N/S	23:53:28-0:08:17
	147	15:00:32	7'34"	65	1.44-1.40-1.42	7.44°N-7.72°S	2957-2985-2980	N/S	23:47:46-23:59:42
	148	17:28:44	4'20"	35	1.44-1.57	11.31°S-20.76°S	2960-2891	N/S	23:54:04-0:00:54
	158	14:08:24	22'37"	80	1.65-1.38-1.83	19.72°N-32.11°S	2985-2911-2425	N/S	22:19:34-03:42:25
	159	14:28:05	17'49"	65	1.55-1.38-1.44	14.78°N-16.41°S	2982-2889-2515	N/S	22:16:30-22:47:02
	161	15:01:52	10'15"	85	1.63-1.45	18.44°N-3.66°S	2982-2809	N/S	21:58:44-22:16:52
	162	13:17:20	20'28"	75	1.70-1.70	21.65°N-25.94°S	2985-2388	N/S	21:49:48-23:46:41
	164	13:53:28	19'51"	85	1.66-1.36-1.58	20.16°N-25.90°S	2970-2789-2327	N/S	21:36:25-22:12:07
	165	14:13:59	8'05"	70	1.50-1.35	13.09°N-4.99°S	2912-2755-2685	N/S	21:35:17-21:49:26
	166	14:39:31	18'18"	75	1.58-1.34-1.55	17.10°N-25.16°S	2930-2719-2266	N/S	21:24:07-21:56:35
	167	12:46:23	18'18"	75	1.79-1.35-1.58	24.61°N-26.48°S	2965-2701-2183	N/S	21:14:06-21:51:25
	168	13:01:19	22'01"	100	1.77-1.34-1.60	23.90°N 27.82°S	2952-2661-2121	N/S	21:04:23-21:45:40
	169	13:17:49	21'29"	90	1.83-1.33-1.50	25.47°N-23.78°S	2952-2658-2174	N/S	20:54:47-21:35:10
	170	13:43:16	15'32"	65	1.43-1.32-1.57	9.40°N-27.51°S	2763-2615-2053	N/S	21:03:02-21:31:12
	171	14:00:14	10'45"	90	1.41-1.32-1.36	8.91°N-15.30°S	2726-2568-2274	N/S	20:54:36-21:14:10
	172	12:14:24	16'37"	80	1.55-1.35-1.50	16.71°N-24.67°S	2808-2590-2018	N/S	20:43:41-21:15:00
	176	13:20:13	11'49"	100	1.91-1.30	27.20°N-0.41°S	2856-2329	N/S	13:20:13-13:32:03
	178	11:56:17	18'14"	90	1.71-1.28-1.45	23.25°N-24.73°S	2750-2307-1775	N/S	19:54:14-20:31:41
	184	11:46:23	9'07"	75	1.37-1.23-1.25	10.67°N-13.51°S	2313-2087-1779	N/S	21:23:28-19:41:42
	185	11:58:19	19'45"	95	1.73-1.24-1.52	24.59°N-30.03°S	2556-2022-1390	N/S	19:02:57-19:46:16
	196	22:13:12	11'49"	100	1.57-1.31-1.36	27.89°S-6.28°N	1455-2083-2199	S/N	5:59:42-6:24:29
	198	22:49:19	10'37"	90	1.43-1.24-1.30	25.19°S-5.22°N	1596-2152-2265	S/N	5:47:31-6:09:25
	201	23:45:29	7'30"	60	1.29-1.27-1.33	11.97°S-6.07°N	1990-2279-2384	S/N	5:34:05-5:47:53
	203	22:15:47	10'41"	90	1.43-1.28-1.32	23.23°S-3.11°N	1842-2363-2414	S/N	5:13:05-5:32:56
	207	21:24:29	16'05"	70	1.45-1.30-1.54	23.04°S-16.41°N	2015-2500-2776	S/N	4:44:49-5:14:53

TABLE I - Concluded

ORBITAL INFORMATION OF SEQUENCES OBSERVED AT SINGAPORE DURING 1966

Year	Day	Time Begin (UT)	Duration*	% Fraction of Total Sounding Time	L-value Range	Geomagnetic Latitude Range (deg)	Altitude Range (km)	South to North(S/N) North to South(N/S)	Local Time Range
1966	208	21:42:58	7'58"	65	1.44-1.31-1.32	21.89°S-1.61°S	2080-2504	S/N	4:38:53-4:53:31
	211	20:29:46	20'49"	90	1.79-1.34-1.59	33.71°S-17.64°N	1944-2622-2879	S/N	4:08:35-4:47:49
	212	20:49:23	20'17"	85	1.66-1.33-1.66	29.91°S-20.29°N	2070-2665-2922	S/N	4:05:06-4:43:23
	217	20:15:22	18'14"	75	1.76-1.36-1.51	31.52°S-13.07°N	2239-2800-2937	S/N	3:28:26-4:01:12
	218	20:35:35	14'27"	70	1.54-1.36-1.45	23.41°S-9.27°N	2443-2831-2921	S/N	3:26:49-3:51:14
	219	18:47:56	22'02"	85	1.84-1.37-1.60	33.09°S-17.98°N	2274-2845-2977	S/N	3:12:36-3:51:43
	221	19:28:09	17'41"	90	1.53-1.37-1.58	21.97°S-16.33°N	2578-2898-2983	S/N	3:07:19-3:36:40
	225	18:43:23	8'38"	75	1.40-1.39-1.48	8.79°S-11.02°N	2873-2947-2985	S/N	2:48:47-3:03:22
	227	19:18:47	14'02"	80	1.41-1.39-1.74	9.98°S-22.79°N	2900-2971-2930	S/N	2:34:05-3:00:00
	228	19:35:46	5'56"	50	1.41-1.39-1.41	9.27°S-3.85°N	2922-2972-2983	S/N	2:26:17-2:35:53
	231	18:25:19	13'16"	100	1.41-1.39-1.55	8.74°S-15.30°N	2961-2984-2930	S/N	2:03:18-2:24:18
	233	18:49:12	20'38"	85	2.42-1.39-1.42	40.94°S-5.59°N	2639-2983-2965	S/N	1:26:35-2:01:55
	234	17:20:13	15'43"	100	1.62-1.40-1.86	7.74°S-27.74°N	2982-2977-2730	S/N	1:45:40-2:15:50
	235	17:32:28	18'25"	70	1.56-1.40-1.66	20.56°S-21.32°N	2936-2976-2790	S/N	1:39:38-2:01:55
	236	17:53:28	12'29"	50	1.44-1.39-1.50	11.69°S-13.18°N	2983-2975-2863	S/N	1:28:08-1:48:11
	236	19:55:16	11'20"	95	1.45-1.41-1.51	10.33°S-14.38°N	2983-2970-2860	S/N	1:27:50-1:46:52
	238	18:18:29	13'01"	55	2.14-1.40	36.20°S-5.57°N	2844-2973	S/N	0:55:44-1:17:53
	239	16:42:14	19'34"	95	1.54-1.39-1.76	18.98°S-25.75°N	2980-2930-2609	S/N	1:02:17-1:38:06
	261	14:58:01	17'49"	85	2.14-1.36	34.47°S-8.71°N	2884-2116	S/N	22:14:24-22:46:37
	267	14:43:41	16'08"	80	1.91-1.33	30.37°S-10.33°N	2678-1830	S/N	21:34:48-22:05:20
	268	14:59:28	7'30"	30	1.86-1.51	28.93°S-17.15°N	2708-2397	S/N	21:23:20-21:37:41
	269	13:17:02	17'10"	70	1.97-1.33	32.01°S-12.25°N	2645-1713	S/N	21:20:02-21:53:17
	300	23:08:17	18'14"	90	1.24-1.22-2.44	7.66°N-40.9°S	1747-1936-2743	N/S	5:38:20-6:14:46

* ' Represents minutes
" Represents seconds

in the other hemisphere near the L-value range of 1.4 (smaller latitudes). This situation was mostly caused by limited sounding time. Out of 461 separate soundings taken during 1966, 217 soundings were taken for 12 minutes each time and 122 were taken for about 21 minutes each time. Therefore, it is not considered that the published statistics of percentage occurrence of conjugate echo events as a function of L-value are either conclusive or truly indicative of the physical extent of the phenomenon.

DEPENDENCE OF TOPSIDE-SOUNDER OBSERVATION OF CONJUGATE DUCTING ON SOUNDING TIME

In any statistical interpretation of the occurrence characteristics of a HF conjugate ducting phenomenon as observed by the topside sounder, one must consider the total amount of time the sounder is operated (i.e., the sounding time) at each sounding. This is particularly important in correlating HF conjugate ducting with magnetic activity.

Figure 8 shows the number of times the sounding was taken as a function of sounding time. The data are for the year 1966 at Singapore. Also shown in the figure are the number of conjugate echo frames observed as a function of sounding. Most of the sounding was performed in ranges of 9 to 12 and 18 to 24 minutes.

Figure 9 shows the percentage fraction of integrated sounding time for the year 1966 at Singapore as a function of sounding time. Also shown is the number of ducts per minute of sounding time as a function of sounding time. Duct occurrence data are not included for those sounding times for which the total time amounted to a very small fraction of the integrated sounding time. It could be seen in Figure 9 that there is a reasonably positive correlation between the number of ducts per minute of sounding and the sounding time. This fact was also ascertained by running a cross-correlation check between the two quantities.

CORRELATION WITH MAGNETIC ACTIVITY

In this section, the correlation between magnetic activity and the ducting phenomenon recorded by the topside-sounder in the longitudes of Singapore in 1966 will be discussed.

Muldrew (refs. 1,3) and Loftus, VanZandt and Calvert (ref.2) concluded that the occurrence of conjugate echoes was not correlated with K_p. Muldrew used topside sounder data from Alouette-1 and -2 in his analyses. Loftus et al. used Explorer-20 fixed-frequency topside sounder observations in arriving at their conclusion.

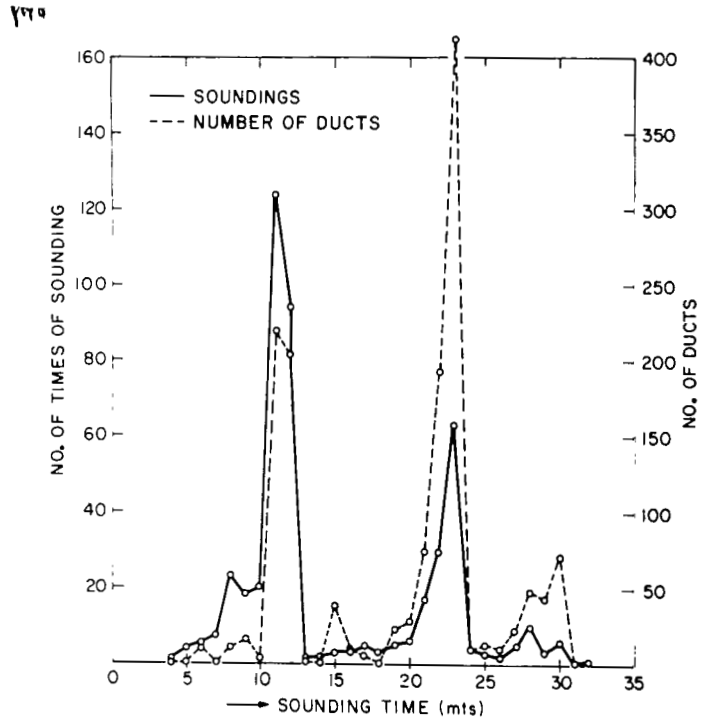

Figure 8.-Sounding time versus number of soundings and number of conjugate echo events

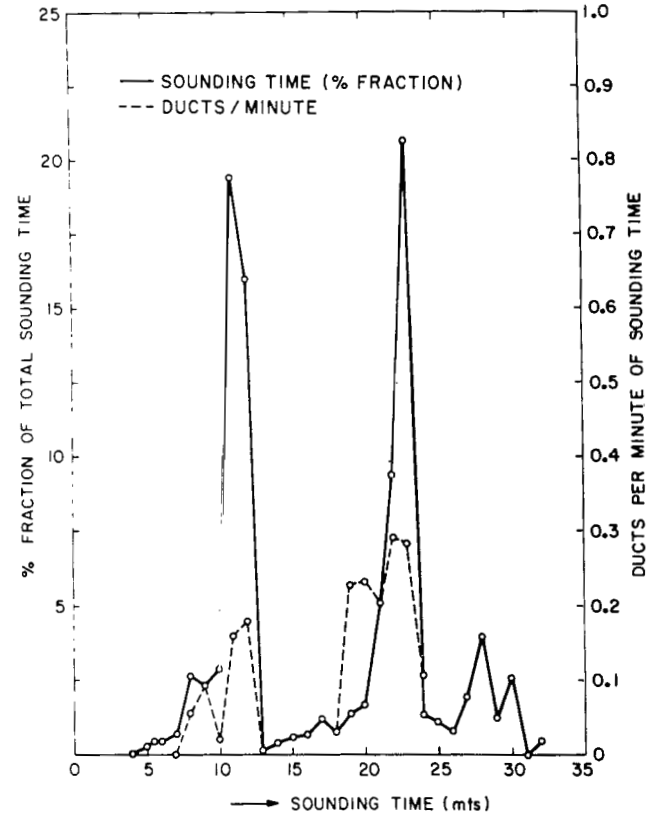

Figure 9.-Sounding time versus percentage fraction of integrated sounding time and number of conjugate echo events per minute of sounding time

At geomagnetic latitudes less than 30°, Calvert and Schmid (ref. 8), using Alouette-1 data, found a weak negative correlation between K_p and topside spread-F. This agrees with the results of Shimazaki (ref. 9) whose conclusions are based on correlation of K_p index with spread-F observed from ground-based stations. Spread-F is attributed to aspect-sensitive scatter from thin field-aligned irregularities which are thought to be part of thick irregularities or ducts. Hence, formation of magnetospheric ducts should be closely related to the formation of the thin irregularities. In other words, conjugate ducting and spread-F phenomena should show similar occurrence characteristics if they are derived from the same source. Shimazaki found that the correlation between spread-F and geomagnetic activity is strongly negative for latitude, $\theta < 20°$, and strongly positive for the latitude range, $20° \leq \theta \leq 60°$. Muldrew's (ref. 3) do not agree with those of Shimazaki. However, the characteristics of spread-F are dependent on the epoch of solar cycle and Shimazaki's results are for high sunspot activity (IGY), while the data presented by Muldrew are for low sunspot activity.

In this context, it is appropriate to consider the previously published results on correlation between whistler occurrence and magnetic activity, since whistler propagation is also attributed to the presence of magnetospheric ducts. The connection between HF and whistler ducting phenomena in the field-aligned magnetospheric ducts is discussed in Part II of this report. Storey (ref. 10) was the first to suggest the dependence of whistler occurrence on magnetic activity. Laaspere, Morgan and Johnson (ref. 11) came to the conclusion that the whistler rate increases or remains almost constant with an increase of the K_p index up to about $K_p = 4$ or 6. The whistler rate then decreases with a further increase in K_p. They suggest that the decrease in the whistler rate with increasing magnetic activity may be due to the absorption of whistlers in passing through the lower ionosphere. Barrington and Thomson (ref. 12), on the other hand, attribute K_p values to the destruction or discontinuity of the ducts in the outer ionosphere due to overall turbulence caused by increased magnetic activity. However, Kimpara (ref. 12) reported enchanced whistler activity at low latitudes one or two days after the onset of a magnetic storm. Observations of Somayajulu and Tantri (ref. 14) indicate a good positive correlation between K_p and whistler activity during a magnetic storm. Figure 10 shows their observations. It may then be concluded that the results of whistler correlations with magnetic activity do not agree with HF ducting correlation with magnetic activity.

The author has correlated HF conjugate echo events observed by the Alouette-2 topside sounder with magnetic activity and arrived at some interesting results. The approach and the results are described on the following page.

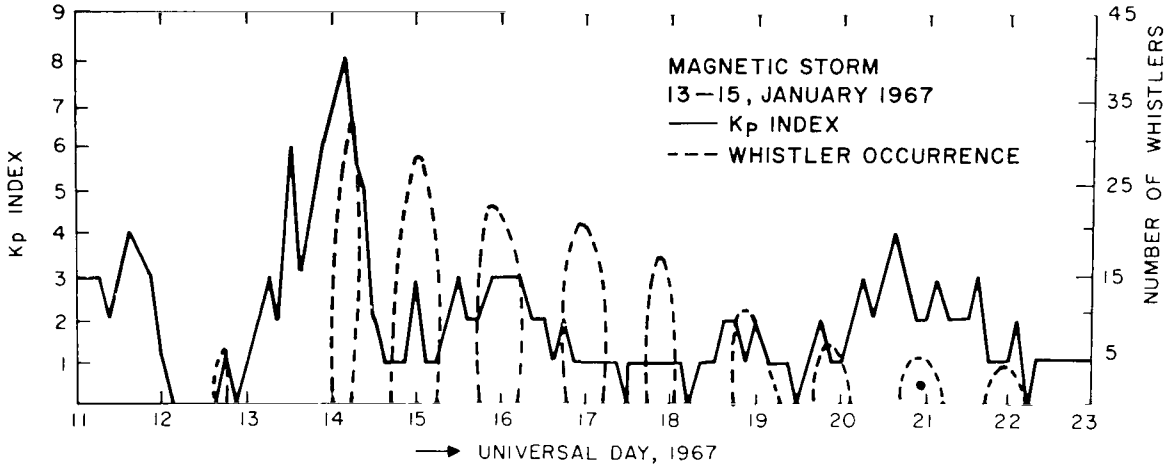

Figure 10.-Correlation of frequency of whistler occurrence with the K_p profile for the magnetic storm of January 13, 1967. (After Somayajulu and Tantri, ref. 14, p. 22)

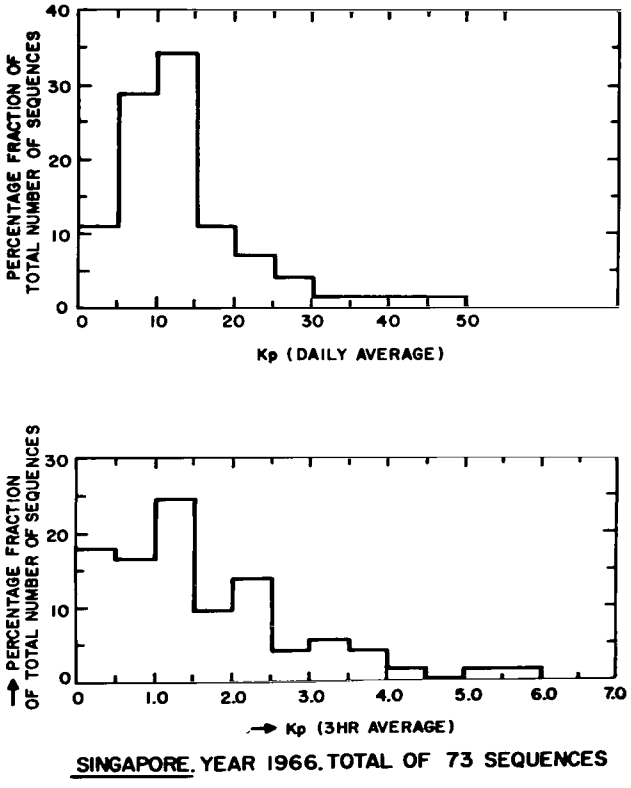

Figure 11.-Percentage fraction of total number of sequences observed at Singapore as a function of both the daily average of K_p and the 3-hour average of K_p.

Any correlative study of data from a satellite experiment with magnetic activity should take into consideration certain additional factors. If the experiment is not performed continuously, there is a need to know the dependence of the observed results on the time duration of the experiment. In the Alouette-2 topside-sounder data, two problems appear:

1. The sounding is not done continuously, but is triggered by a command signal when the satellite is in the vicinity of a tracking station and then run for a short duration (up to 33 minutes at a time). The sounder was not operated at all on many days and, on some of these days, there was magnetic storm activity.

2. Even when the sounder was operated, the sounding time duration was not always constant. In a previous section, the dependence of topside sounder observations of conjugate ducting on sounding time duration was discussed, and the existence of a definite positive correlation between the observed number of conjugate echo events per minute and the sounding time was shown.

Therefore, there is an inherent drawback in this correlative study because of the way the experiment is run. In spite of such a problem, it is possible to draw some cautious conclusions about the dependence of magnetospheric ducting on magnetic activity.

Two approaches have been taken. Since most of the Singapore conjugate echo ionograms occur in the form of sequences, each sequence is treated as an event representing the general magnetospheric condition favorable to field-aligned propagation. Then the sequences are correlated with K_p. The other approach is to treat each ionogram exhibiting conjugate echoes as a ducting event and then correlate the number of ducting events per minute of sounding time with magnetic activity. Each approach has its own advantages.

There were 50 sequences (68.5 percent) observed at Singapore during the year 1966 in the absence of any magnetic storms. The average value of K_p (3-hour average) was 1.15 with a maximum of 2.7 and a minimum of zero. Only 23 sequences (31.5 percent) were observed for the same time period in the presence of magnetic storms. The average value of K_p was 2.4 with a maximum of 7.0. As described earlier, 75 percent of all the conjugate echo ionograms observed at Singapore are parts of sequences.

Figure 11 shows the percentage fraction of total number of sequences as a function of both the daily average of K_p and the 3-hour average of K_p. In general, lower K_p values correspond to magnetically quiet periods and higher K_p values correspond to

magnetically active periods. The figure shows that the percentage occurrence of sequences is high for quiet periods. Therefore, it may be concluded that magnetic activity does not play any unique role in the formation and maintenance of magnetospheric ducts. However, one question that immediately crops up is whether there was a sufficient number of soundings at higher K_p values. For the year 1966, the sounding time amounted to 3630 minutes for magnetically quiet periods with an average ducts/min = 0.2250. For the same time period, the total sounding time for magnetically active periods was 3540 minutes resulting in an average value of ducts/min = 0.1830. Hence, the sounding time is equally divided between active and quiet periods. Next, the observed number of conjugate echo ionograms per minute of sounding time (ducts/min) will be correlated with magnetic activity with each ionogram treated as a ducting event. The mean value of ducts/min observed at Singapore during the year 1966 is 0.2040. During quiet periods, the average value of ducts/min is about 10 percent higher than the mean value. In the presence of magnetic storms, the average value of ducts/min is about 10 percent lower than the mean value.

In the above analysis, all the sounding times have been included, and therefore the effect of sounding time on the ultimate result is not obvious. To remove the effects of sounding time, the statistical behavior of data at sounding times of 12 minutes and 24 minutes was studied. About 50 percent of the total sounding was done at 12 minutes and about 15 percent of the total sounding was done at 24 minutes. At the sounding time of 12 minutes, during quiet periods, the average value of ducts/min is about 7.0 percent higher than the mean value of 0.1570. During magnetic storms, the average value of ducts/min is about 6.0 percent lower than the mean value. For the sounding time of 24 minutes, during quiet periods, the average value of ducts/min is about 35.0 percent greater than the mean value of 0.2710. During magnetic storms, it is about 28.0 percent lower than the mean value. Hence, there is a strong reason to believe that there is no positive correlation between ducting phenomenon and K_p. More events have been observed at lower K_p values than at higher K_p. Since the year 1966 belongs to a sunspot minimum period, the general level of magnetic activity is much weaker and the average K_p value is small. Figure 12 illustrates this fact. Shown in the figure is the percentage distribution of the daily average of K_p for the year 1966. However, as said before, the sounding times are equally distributed between quiet and active periods. Persistent occurrence of the ducting phenomenon at low K_p values and during quiet periods than in the presence of magnetic storms or at high K_p values indicates that there are other significant sources in the ambient magnetosphere which participate in the formation of magnetospheric ducts.

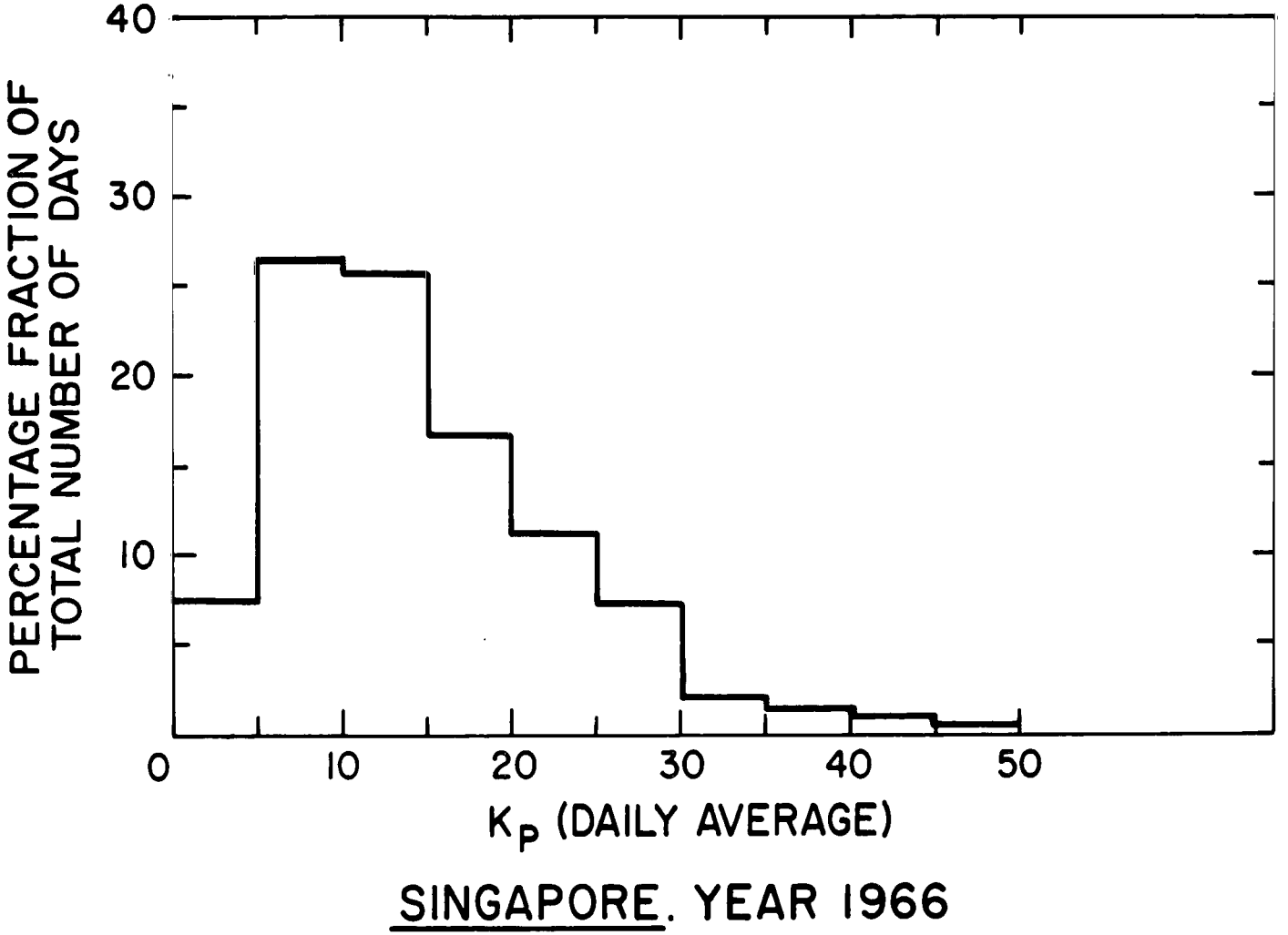

Figure 12.-Relative distribution of K_p (daily average) for 1966

OCCURRENCE CHARACTERISTICS OF DUCTING EVENTS

In a previous publication (ref. 4), the author discussed the percentage occurrence of ducting events as a function of L-value, local time, and altitude corresponding to all the equatorial and mid-latitude stations. The occurrence characteristics of conjugate ducting events observed at Singapore will now be presented.

Figure 13 shows the local time distribution of percentage occurrence of ducting events observed at Singapore. The distribution is similar to that shown in Figure 14 which corresponds to the data from all the equatorial and mid-latitude stations.

However, the local time distributions of ducting events, as shown in Figures 13 and 14, have an inherent error. The Alouette-2 satellite travels in an eccentric orbit and, therefore, its altitude is a variable. The distribution, as shown in Figures 13 or 14, is a combination of the local time distributions observed in various altitude ranges between the perigee and the apogee. For a circular orbit, the altitude is invariant and therefore there is only one local time distribution. For an eccentric orbit satellite, the local time distributions for various altitude regions are different and the distributions of all the altitude regions between the perigee and the apogee are integrated to obtain an average local time distribution, as shown in Figures 13 or 14. Such a process leads to an error since the satellite in an eccentric orbit does not spend equal amounts of time in various altitude intervals. It is possible to normalize the distribution by knowing the time spent by the satellite in various altitude ranges during a single orbit. Figure 15 provides this information. As is anticipated, the satellite spends maximum amounts of time at perigee and apogee regions.

The weight factors used to normalize individual local time distributions are derived from Figure 15. They are inversely proportional to the time spent by the satellite in the corresponding altitude range. The individual local time distributions are multiplied by the corresponding weight factors and then integrated to obtain the normalized average local time distribution. Such a distribution for Singapore for the year 1966 is shown in Figure 16. While the general nature of the distribution remains the same as in Figure 13, one can now see two distinct peaks at 2100 hours LT and 0500 hours LT. The enhanced ducting activity during after midnight hours is still apparent. The local time distribution obtained from data from all the stations and shown in Figure 17 shows the normalized local time distribution for all of the stations. This is to be compared with Figure 14.

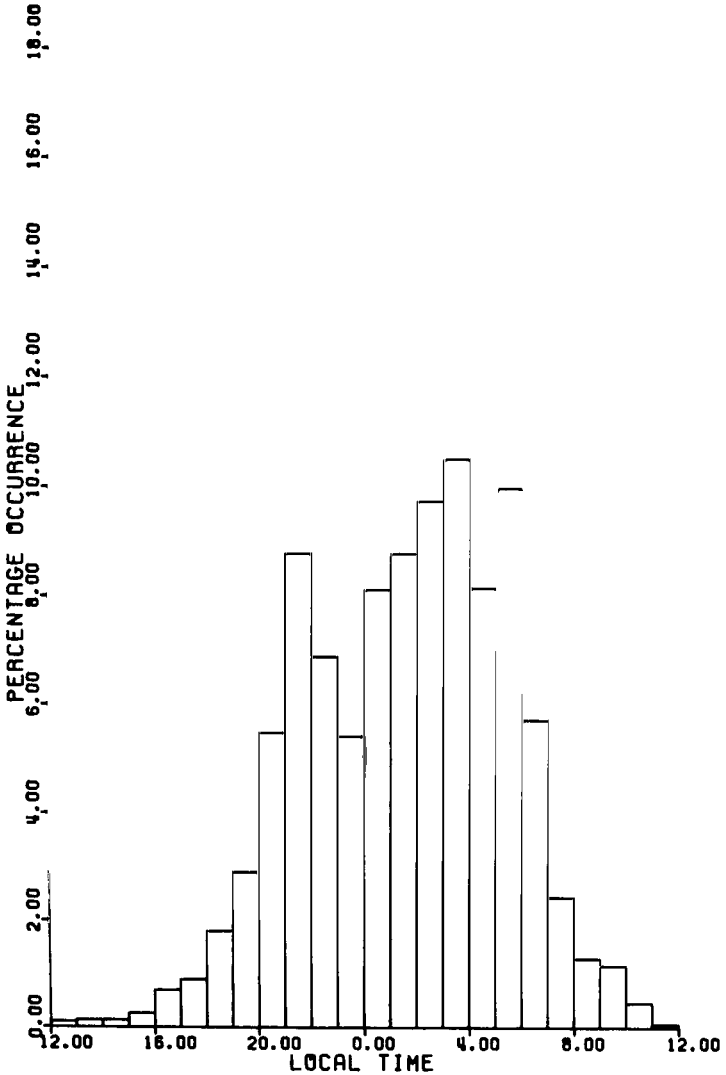

Figure 13.- Local time distribution of percentage occurrence of conjugate echo events observed at nine equatorial and mid-latitude stations

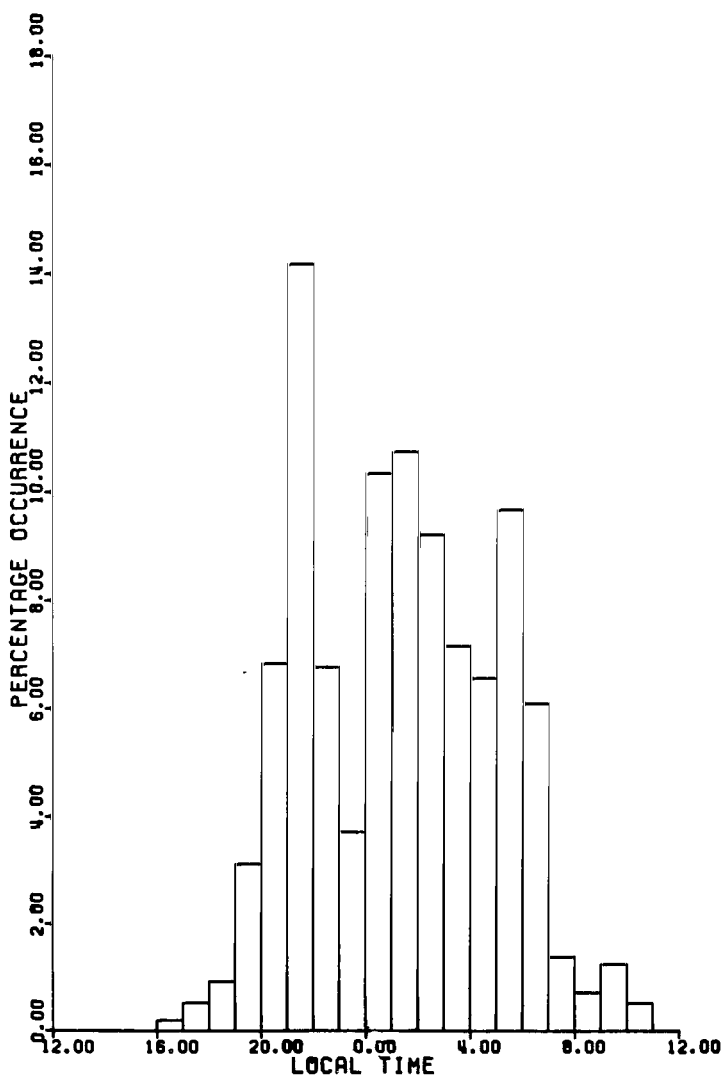

Figure 14.-Local time distribution of percentage occurrence of conjugate echo events observed at Singapore

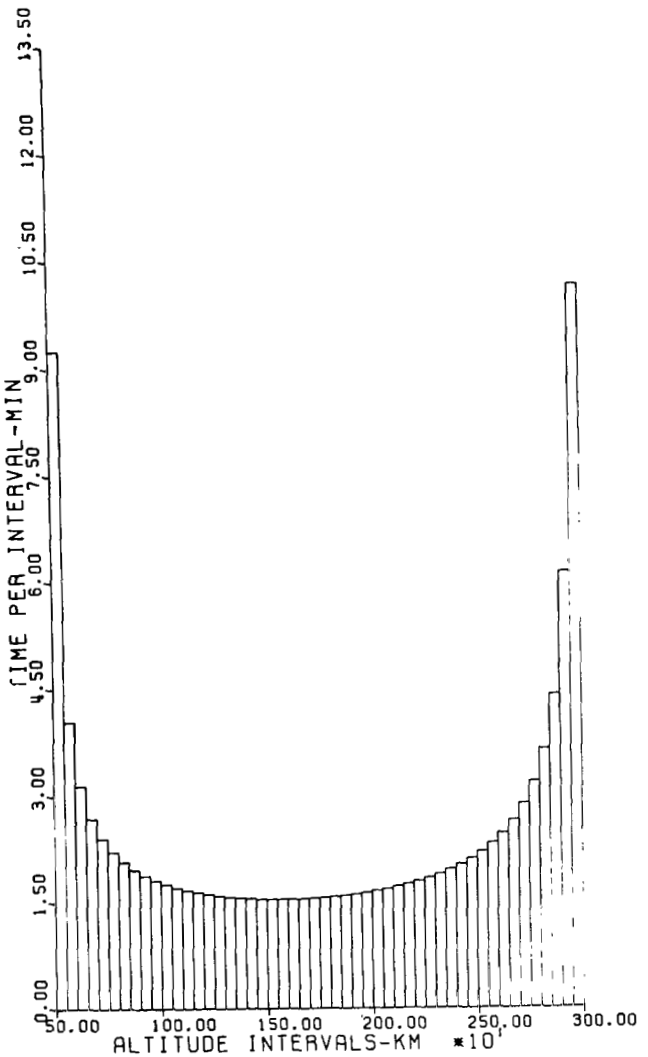

Figure 15.-Time spent by the satellite in various altitude ranges during a single orbit

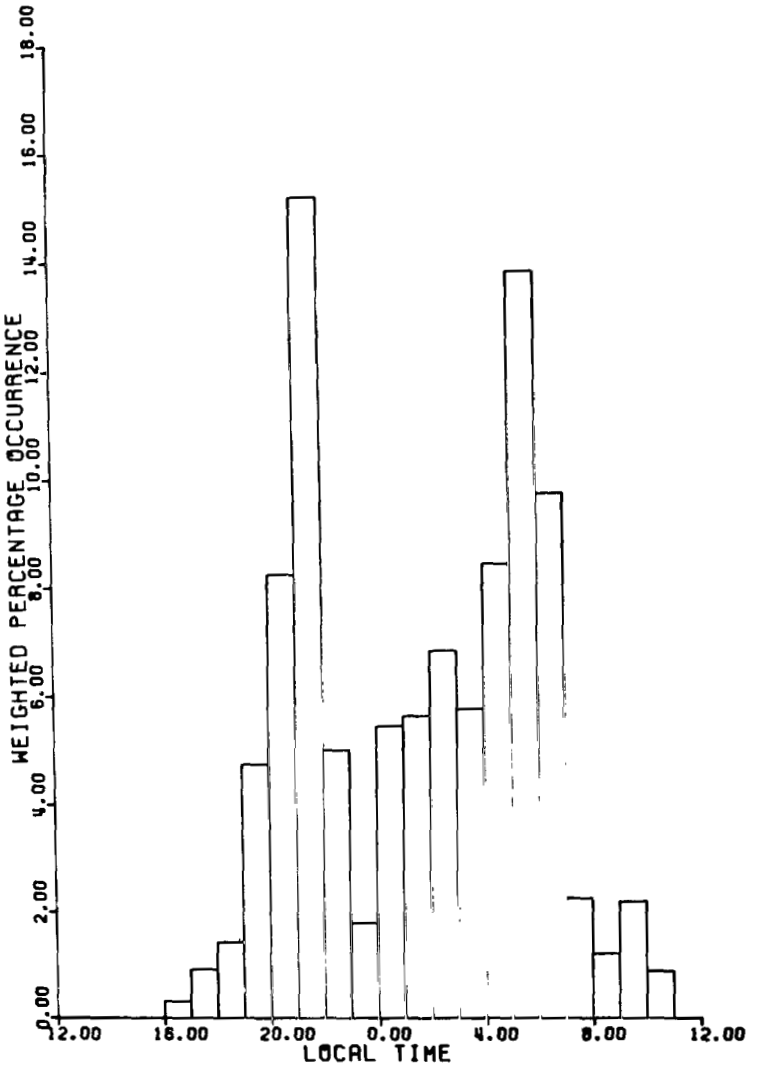

Figure 16.-Normalized local time distribution of percentage occurrence of conjugate echo events observed at Singapore

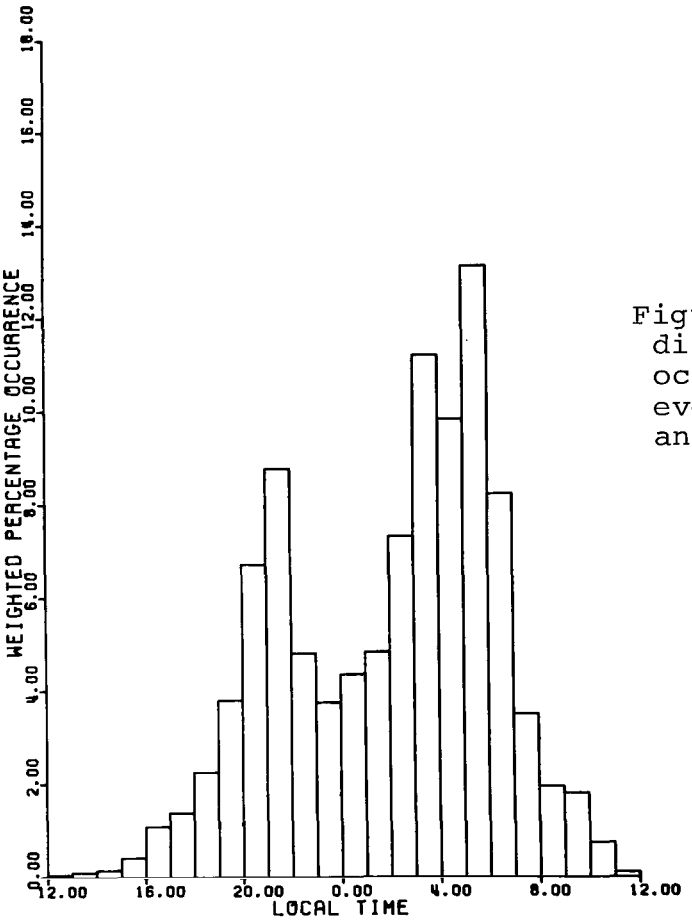

Figure 17.-Normalized local-time distribution of percentage occurrence of conjugate echo events for all the equatorial and mid-latitude stations

CONCLUSIONS

The high rate of occurrence of HF conjugate ducting events in the longitudes of Singapore and their occurrence in the form of sequences have brought forward significant information concerning the formation and maintenance of field-aligned ducts in the magnetosphere. The fact that magnetic activity does not seem to play any role in the formation of magnetospheric ducts focusses more attention on various physical mechanisms within the ambient magnetosphere. Among them are the propagating hydromagnetic waves, pressure waves, and the like. The exact way in which such mechanisms could create field-aligned ionization enhancements is still to be worked out. Nevertheless, longitudinal diffusion processes should play a very important role in the actual formation of continuous ducts in the magnetosphere.

AUTHORS' NOTE ON PART II

After this report was prepared, additional information concerning Part II was provided by Dr. T. E. Van Zandt of ESSA/ITSA and Dr. Robert Benson of NASA Goddard Space Flight Center at the 1969 Spring Meeting of URSI in Washington, D. C. They contended that the fine structure of the traces observed in Alouette-2 ionograms is solely due to an instrumentation effect and is not caused by any physical phenomenon such as the multipath ducting suggested by the authors in their unified model. Van Zandt and Benson argue that the observed fine structure and diffuseness are due to reception by the broadband receiver of various frequency side lobes of the dispersed 100-μsec pulse of the transmitter. However, subsequent discussions with several other scientists at the conference raised some questions about both the interpretations.

Both the interpretations are consistent and fully explain the observed features. However, there are some fundamental differences* between the two interpretations which need to be resolved before either of them is accepted to be correct. Then the observed fine structure of the ionogram traces could be attributed either to instrumentation effects as suggested by Van Zandt and Benson or to multipath ducting as proposed by the authors.

---

*The alternate explanation provided by Van Zandt and Benson does not answer the following questions:

(1) Why is the intensity of the sidelobe echoes in the conjugate echo traces so high? One would expect that the sidelobe returns should be less intense at such long delays.

(2) Why does the fine structure in some ionograms indicate skew traces? This does not conform to the Van Zandt-Benson explanation.

(3) Why doesn't the observed diffuseness in the horizontal region of some of the ionogram traces agree with the Van Zandt-Benson explanation?

PART II

A UNIFIED MODEL OF FIELD-ALIGNED DUCTS IN THE MAGNETOSPHERE

INTRODUCTION

Past experimental observations made with HF and VLF techniques have given credence to the fact that there exist in the magnetosphere electron density irregularities or ducts aligned along magnetic lines of force and responsible for guiding electromagnetic waves. The same irregularities are responsible, in general, for guiding both the VLF (whistler) and HF waves. HF and VLF observations in the past have shown that field-aligned irregularities have been observed from ionospheric heights to regions near plasma pause ($L \approx 4$). Detailed discussions of previous HF and VLF investigations pertaining to magnetospheric ducting phenomena could be found in references 4 and 15.

However, the duct characteristics like scale size and peak fractional enhancement or depletion of electron density that are deciphered from VLF and HF observations do not agree with each other. The scale sizes deduced by VLF investigators are rather large compared to the scale sizes required for substantiating the ducting phenomena observed at high frequencies. The measurement of the irregularity size is, of course, dependent on the radio wavelength employed. VLF measurements must of necessity find larger irregularities than HF measurements made at shorter wavelengths. Also, simultaneous existence of a spectrum of irregularity sizes should not be discounted. It is therefore of considerable theoretical interest to combine the results of VLF whistler observation and HF conjugate echo observations and develop a unified model for the magnetospheric irregularities (ducts).

The irregularities detected by Knecht, Van Zandt and Russell (ref. 16) in their rocket-borne HF sounding experiment exhibited individual thicknesses of about 1.0 to 10.0 km transverse to the guiding magnetic field line. The median thickness of the most intense ducts was about 3 km while the mode was about 1.4 km. Thicknesses of conjugate ducts observed by Explorer 20 (ref. 2) range from 1.0 to 40 km. The Alouette-1 conjugate ducts observed by Muldrew (ref. 1) had a median thickness of 0.6 km. Estimates of irregularity sizes based on VLF observations are somewhat larger than those of HF being on the order of 20 to 40 km transverse to the magnetic field (refs. 7,17) during quiet periods. Somayajulu and Tantri (ref. 14) have reported whistler ducts as large as 180 km during magnetic disturbances.

To explain HF ducted echoes, Pitteway and Cohen (ref. 18), Knecht and Russell (ref. 19), and others have suggested that it is the depletion in electron density that constitutes the ducts. However, Booker (ref. 20), Muldrew (refs. 1,3), Ramasastry, Walsh, and Herman (refs. 4,5), and others have suggested enhancement models. The prevailing opinion is also confusing among VLF investigators. Smith (ref. 17), and Helliwell (ref. 7) prefer depletion ducts, but Somayajulu and Tantri (ref. 14) have adapted an enhancement model. The authors have argued in the past (ref.4) that the HF waves are trapped in a whispering gallery mode on the inside of an enhancement duct. The authors' model has been able to explain the observed conjugate echoes in the Alouette and Explorer 20 data. Therefore, an enhancement duct has been adapted as the basic model in proposing a unified model for the magnetospheric ducts.

CHARACTERISTICS OF CONJUGATE ECHO TRACES

In this section, the manner in which the appearance of the various conjugate echoes (near-end, far-end, round-trip, etc.) is affected by the position of the satellite with respect to the field-aligned duct will be discussed.

Figure 18 is an ionogram showing conjugate echoes recorded at Singapore on 1966. Enlargements of the regions within the dashed lines are shown in Figures 18a and 18b. Why should the near-end echo begin at a much lower frequency than the other echoes which all seem to begin abruptly at a higher frequency? The answer to this question can be obtained by examining the satellite position as a function of frequency. The satellite was at a geomagnetic latitude of 14.02°N and moving southwards. This means that the satellite travels from the outside to the inside of the field lines it crosses. The transmitter frequency is swept linearly with time and therefore the frequency axis of the ionogram can be converted to either universal time or satellite position. Figure 19 shows the geometry of the satellite path corresponding to the ionogram shown in Figure 18. For the relatively small distance traversed by the satellite during the recording of the portion of the ionogram as shown in Figure 18, the satellite trajectory and the field lines can be represented by straight lines. The field lines are taken to be parallel to the abscissa. The satellite velocity and the angle between it and the field lines can be calculated from the ephemeris data. The satellite positions along its trajectory when the near-end, far-end, and round-trip traces begin and end are denoted in the figure.

The explanation hinges on the postulate that it is not possible for a duct located at a particular field line to support far-end echoes while the satellite is outside that field line.

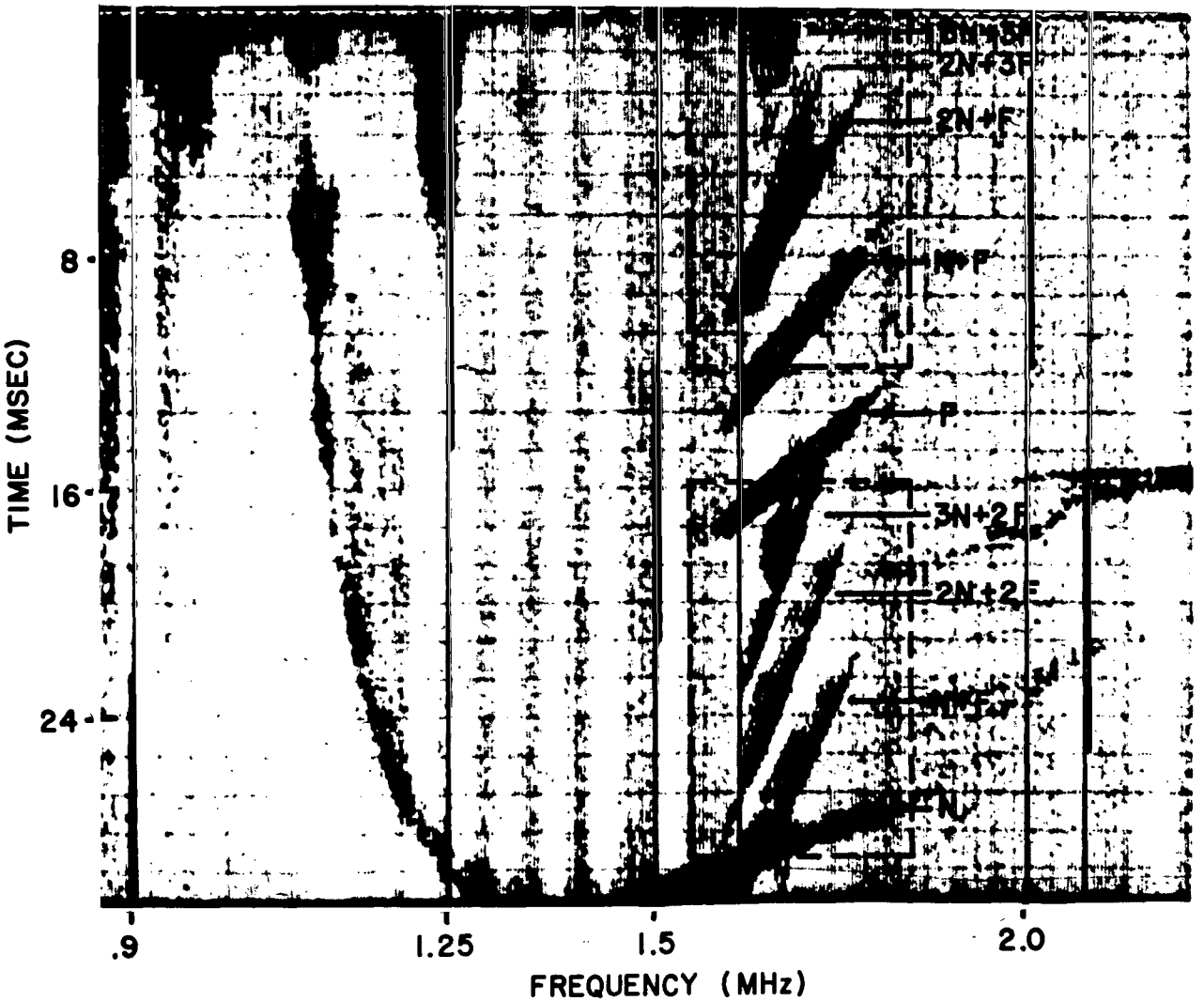

Figure 18.-Ionogram recorded at Singapore on June 27, 1966, at 12:00:04 UT(20:00:01LT).

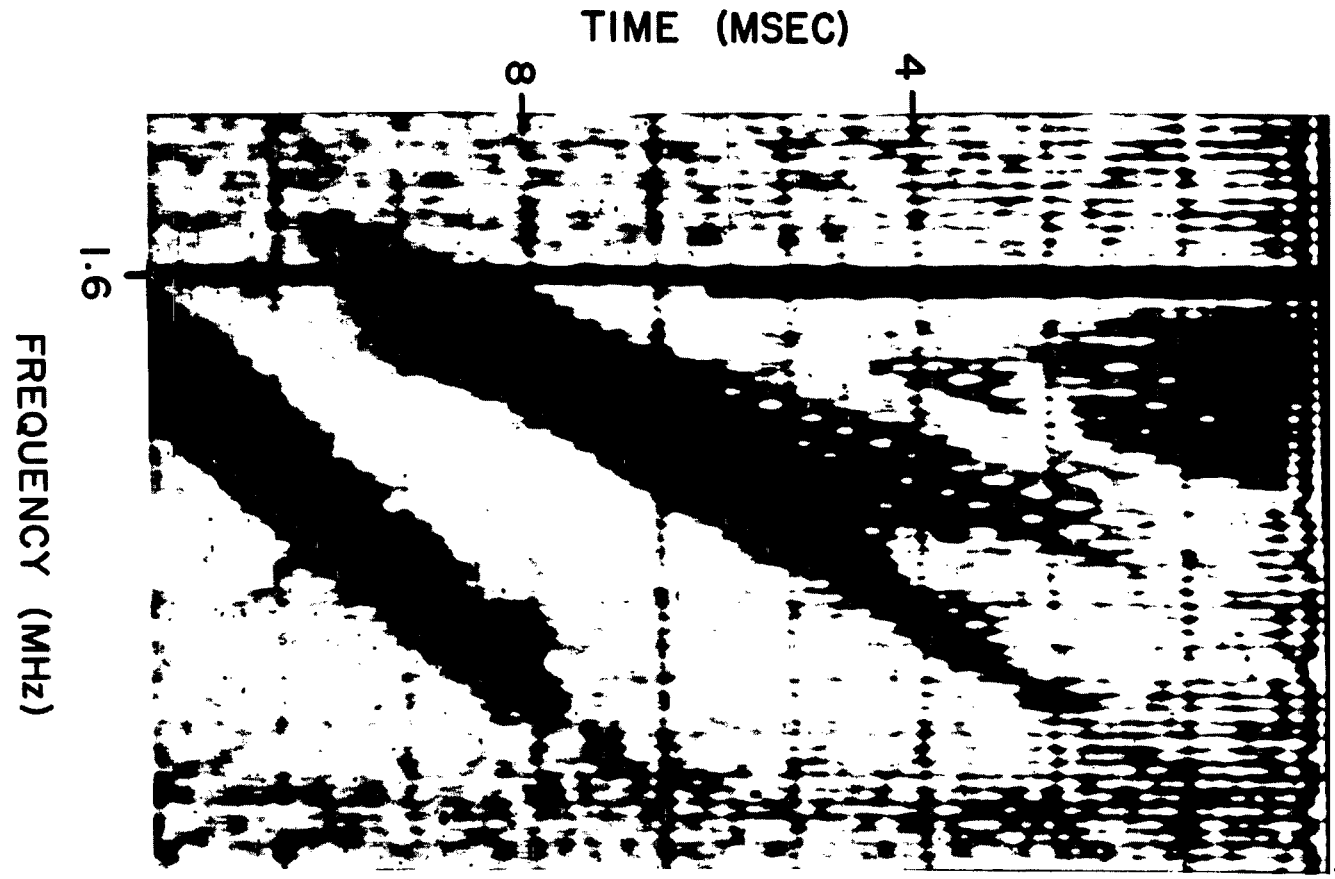

Figure 18a.-Enlargement of the upper portion of figure 18 enclosed by dashed lines

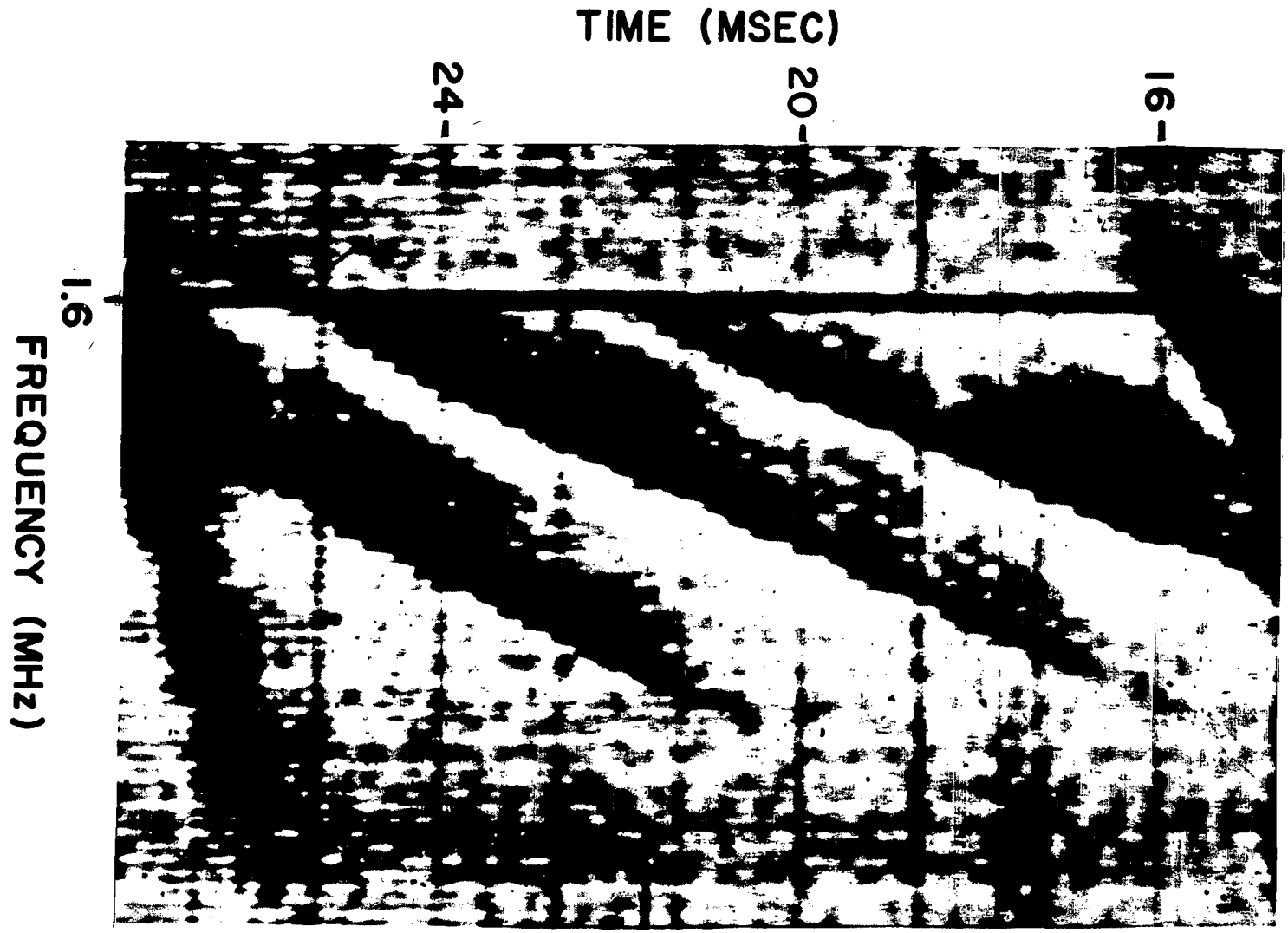

Figure 18b.-Enlargement of the lower portion of figure 18 enclosed by dashed lines

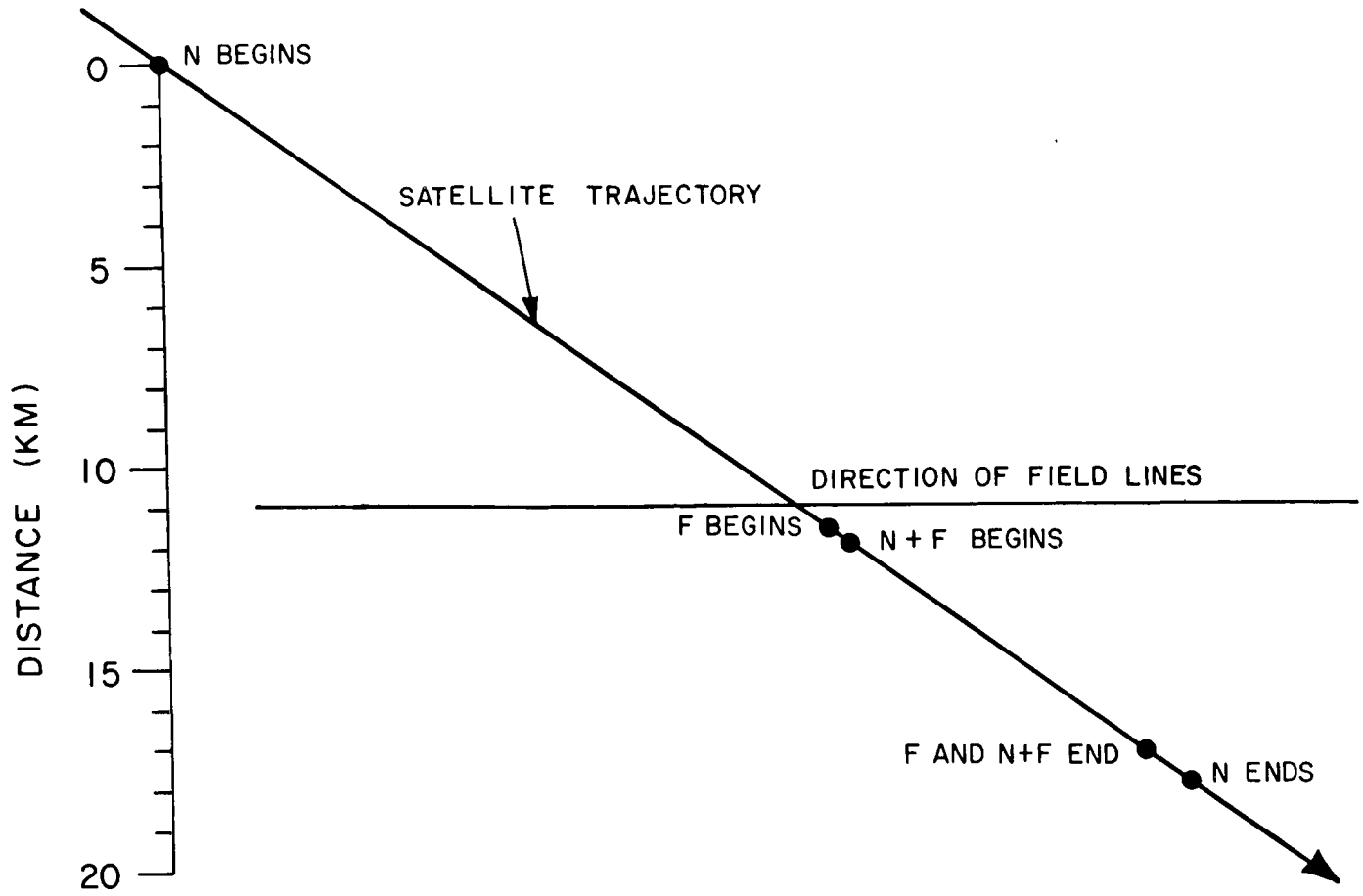

Figure 19.-Diagram of the satellite trajectory relative to the magnetic field lines at the time the ionogram of figure 18 was recorded; also shown in the figure are the relative locations of the satellite when the near-end(N), far-end(F), and first round-trip(N+F) echoes were received

The ducts become more tenuous along with the medium as one travels along a field line towards the equator. It is at the equator that the radius of curvature of the field line is the smallest and requires the largest electron density gradient for trapping radiowaves. When the signals are able to penetrate through the duct from outside the field line, the more tenuous medium towards the equator is unable to guide the rays along the field line. Existence of high electron density gradients needed to contain the rays is unlikely. On the other hand, the medium becomes more dense and the ducts become more effective in trapping as one travels towards the Earth along the field line from the satellite position. Also, the radius of curvature of the field line becomes larger. This means that the signals which penetrate through the duct from outside could easily be guided to the near-end reflection level and back to the satellite. Hence, when the satellite is located outside a field line, the near-end echo is easily observed while the far-end and round-trip traces either cannot exist or exist under extraordinary magnetospheric conditions.

Once the satellite passes through to the inside of the field line, the signals directed towards the equator are also guided, and both the far-end and round-trip traces are obtained as well as the near-end trace which had begun earlier. As the satellite travels further inside the field and also as the signal frequency increases, a time is finally reached when it is no longer possible for the duct to trap the signals in either direction.

On the other hand, when the satellite is approaching the duct from the inside, it is possible for both the signals towards and away from the equator to be trapped. Such a situation is demonstrated in Figure 20 which shows an ionogram recorded when the satellite was at a geomagnetic latitude 11.02°N and travelling northward. Figures 20a and 20b show enlargements of the regions within the dashed lines in Figure 20. Figure 21 shows the satellite positions along its trajectory when the near-end, far-end, and round-trip traces began and ended.

Figure 22 shows an ionogram recorded when the satellite was in the southern hemisphere (-14.97°S Geomagnetic) and travelling northward so the satellite is moving from the outside to the inside of the field lines. Figures 22a and 22b are enlargements of the regions shown within dashed lines in Figure 22. The physical situation is analogous to that of Figure 15, but in the opposite hemisphere and the patterns are similar. The satellite path geometry corresponding to Figure 22 is shown in Figure 23. The abrupt cut-off at 2 MHz of the echo traces in Figure 22 is caused by the sounder sweep-rate changes from 0.15 to 1.0 MHz/sec when the sounder frequency reached 2.0 MHz. At so high a sweep-rate as 1.0 MHz/sec, the receiver is completely detuned by the time the various echoes return, except for the near-end echo.

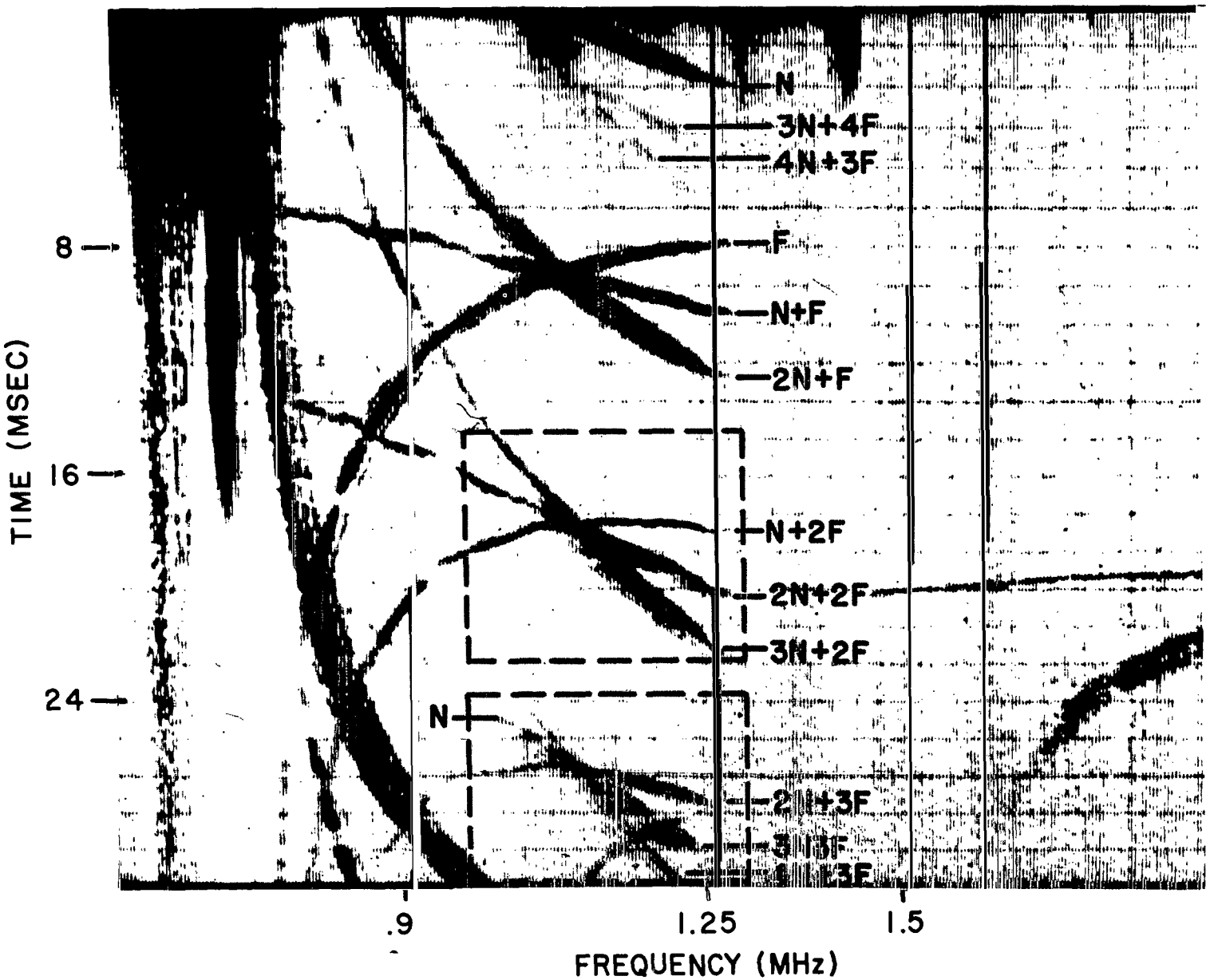

Figure 20.-Ionogram recorded at Singapore on February 3, 1966, at 19:25:19UT (01:40:12LT)

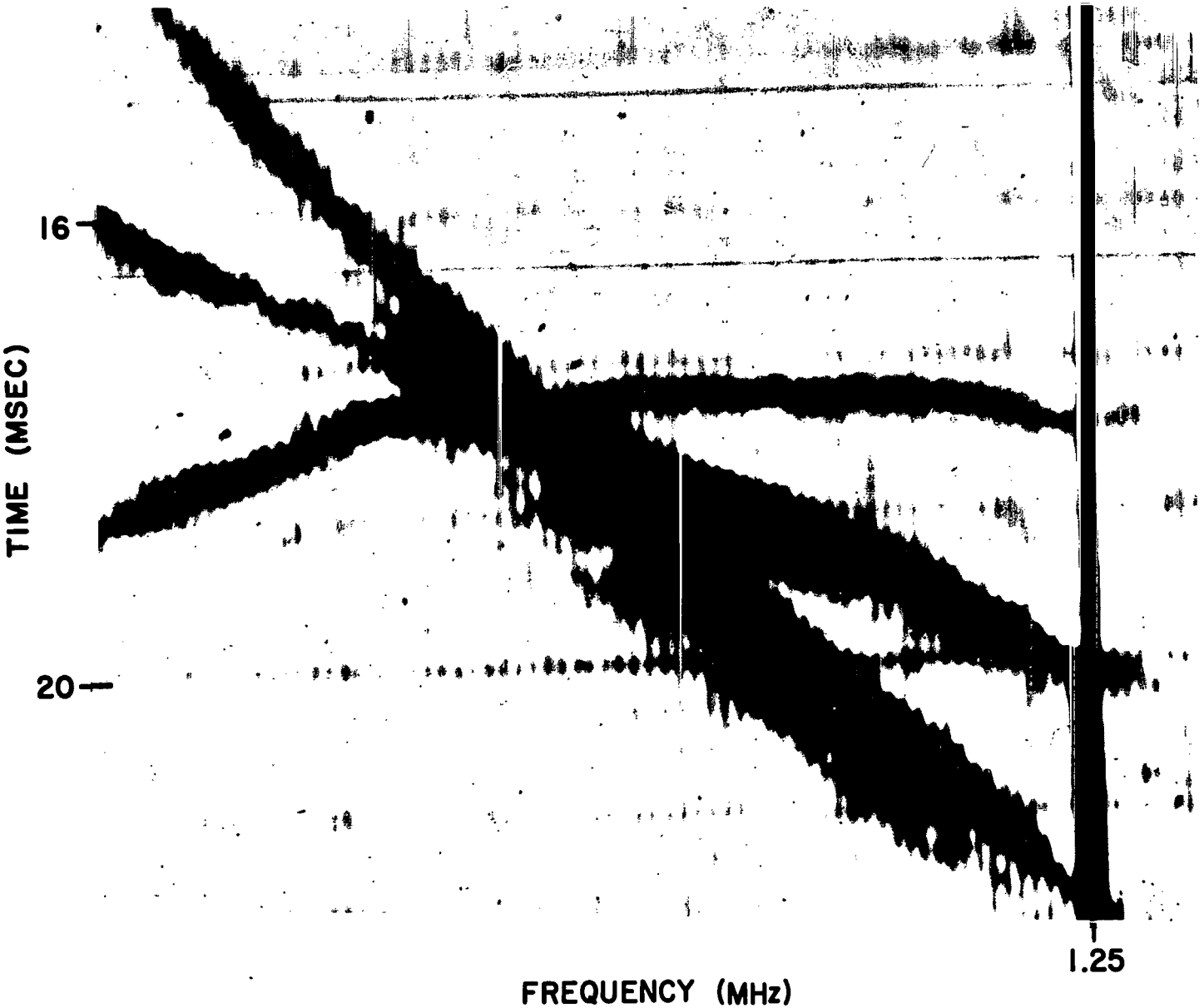

Figure 20a.-Enlargement of the upper portion of figure 20 enclosed by dashed lines

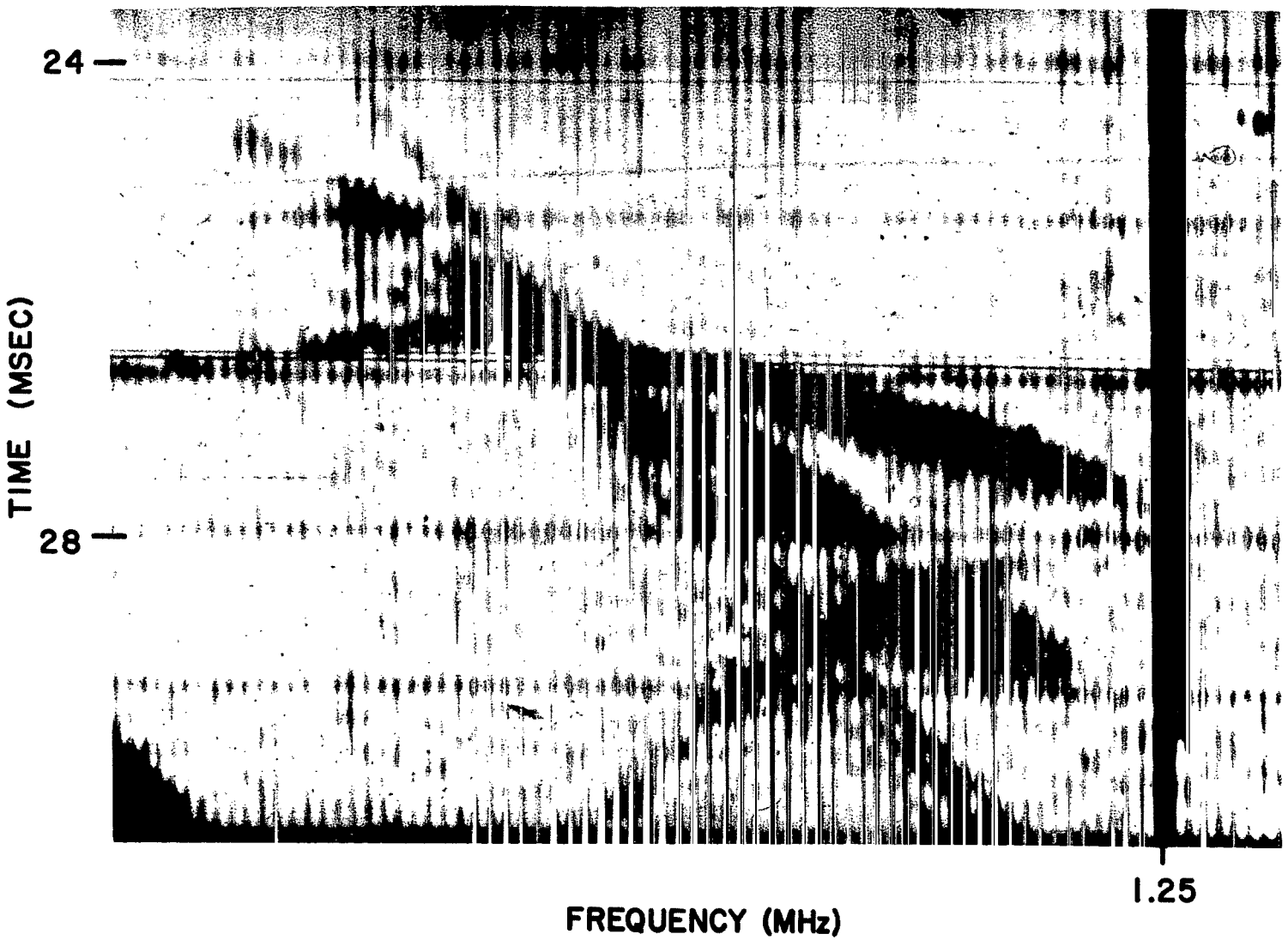

Figure 20b.-Enlargement of the lower portion of figure 20 enclosed by dashed lines

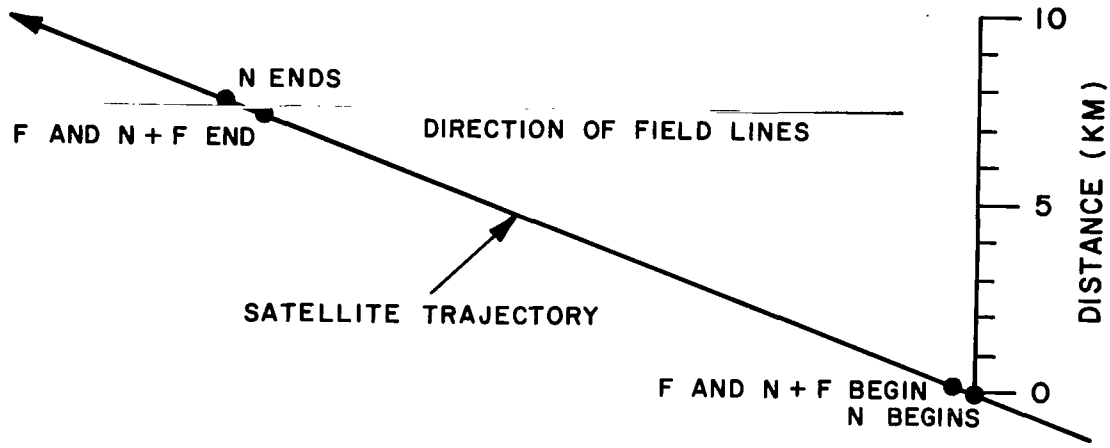

Figure 21.-Diagram of the satellite trajectory relative to the magnetic field lines at the time the ionogram of figure 20 was recorded; relative satellite locations corresponding to the N, F, and N+F traces are also shown

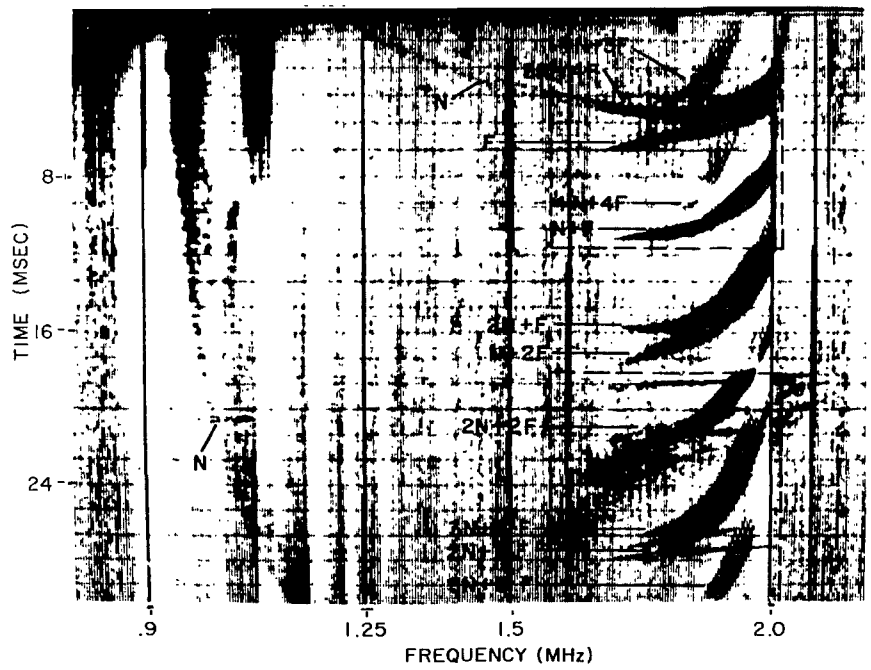

Figure 22.-Ionogram recorded at Singapore on February 10, 1966 at 17:15:49 UT (00:31:48 LT).

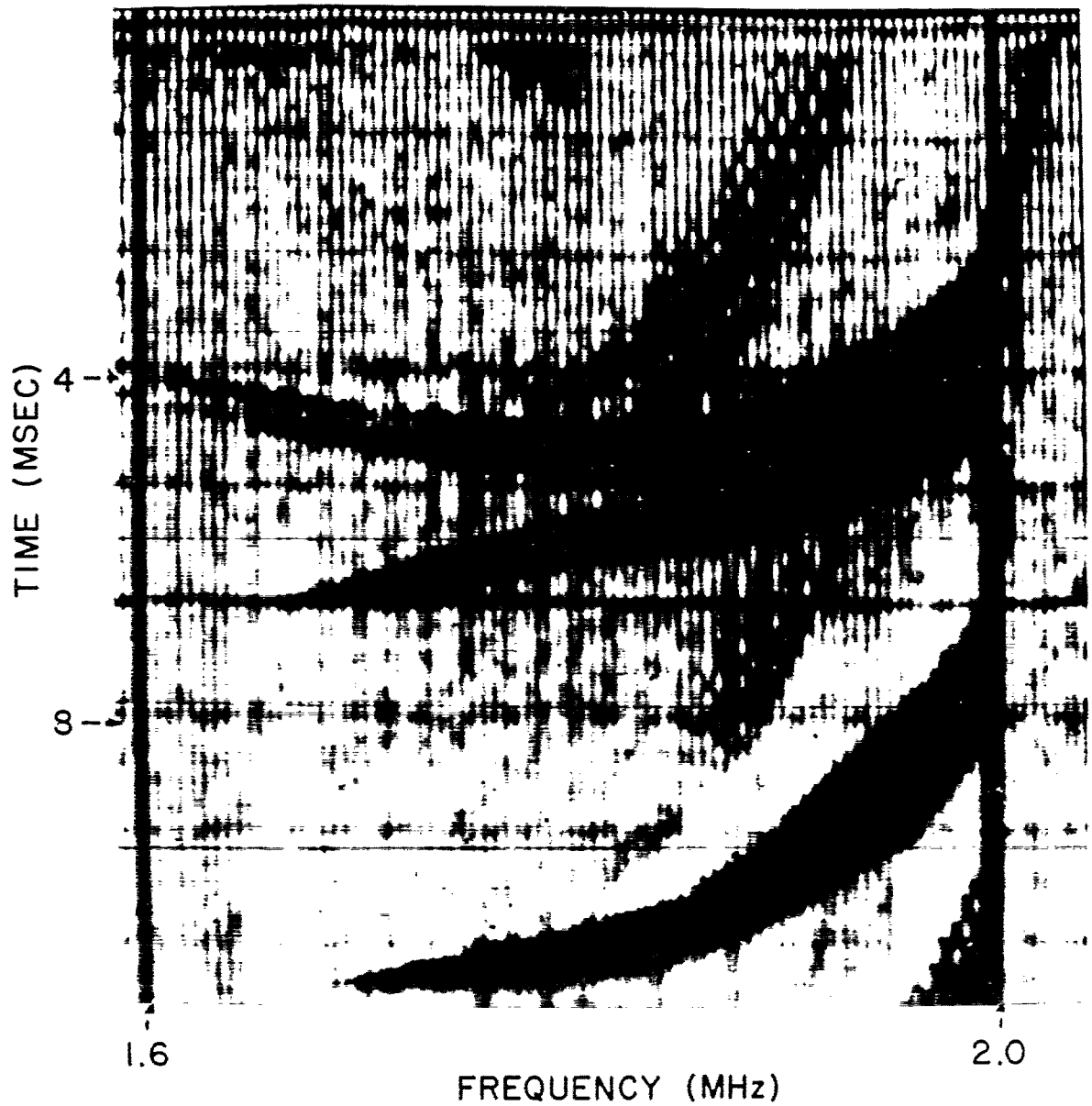

Figure 22a.-Enlargement of the upper portion of figure 22, enclosed by dashed lines

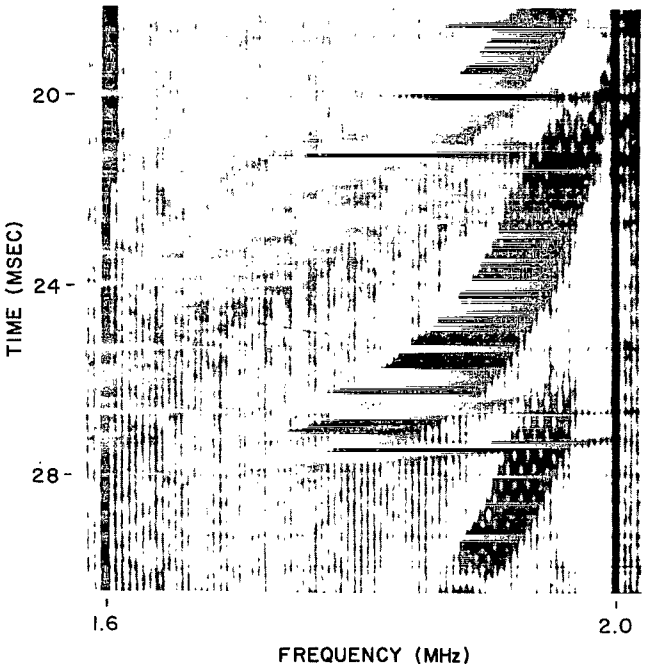

Figure 22b.-Enlargement of the lower portion of figure 22 enclosed by dashed lines

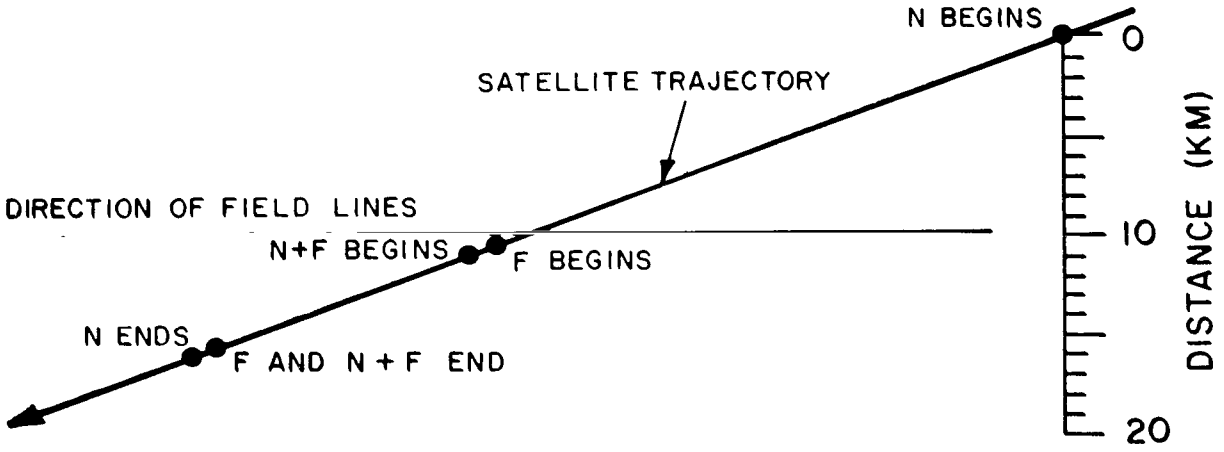

Figure 23.-Diagram of the satellite trajectory relative to the magnetic field lines at the time the ionogram of figure 22 was recorded; the satellite locations corresponding to the near-end(N), far-end(F), and round-trip (N+F) traces are also shown

DIFFUSENESS OF CONJUGATE ECHO TRACES

The diffuseness and fine structure of the conjugate echo traces is caused by multipath ducting. An examination of the enlargements of Figures 18, 20, and 22 reveals the existence of a fine structure in the echo traces. Each trace is actually made up of a number of individual, closely spaced traces. A model for guided propagation of electromagnetic waves in the magnetosphere is presented in this report. The proposed model has evolved out of an effort to explain the diffuseness and fine structure of conjugate echo traces in topside sounder ionograms. Many investigators (ref. 5,6,14,21) have explained the diffuseness of whistler traces as due to the whistler energy propagating in closely spaced paths, the path lengths of which are slightly different. Whistler energy propagating in the various paths will have slightly differing group delays and hence give rise to the observed diffuseness on the whistler traces. It is the geometrcal difference in the path length between neighboring paths and not the duct structure that is invoked to explain the diffuseness of whistlers. This type of explanation cannot account for the diffuseness of HF conjugate echo traces since it results in a much smaller value for the diffuseness than is observed. The authors feel that the same magnetospheric ducts are responsible for the guided propagation of both VLF and HF waves. Therefore, any model postualted to explain the diffuseness of one type of wave should also be able to explain the diffuseness and fine structure characteristics of the other type.

No work has been reported hitherto about the fine strucutre and diffuseness of the HF conjugate echo traces observed in topside sounder ionograms. While the mixed modes of propagation (in which the signal travels along the field line down to the reflection and then returns directly to the satellite), as shown in Figures 24a and 24b, might provide an explanation for the diffuseness of the near-end traces, they are unable to explain the diffuseness and fine structure of the far-end and round-trip traces.

The model for the magnetospheric duct proposed by the authors is in the form of a large-scale, field-aligned, gaussian enhancement of electron density with a superimposed fine structure of small-scale gaussian ripples so that the large scale variation has a ribbed rather than a smooth structure. The parameters of this model, namely, the scale sizes and fractional enhancements, are derived from the analysis of the diffuseness of the various echo returns the Alouette-2 ionograms, the number of individual traces making up a single diffuse echo, the relative positions of the satellite when various echoes begin and end, and a knowledge of the electron density gradients required for trapping. Figure 25a, which is an example of the proposed duct model, shows

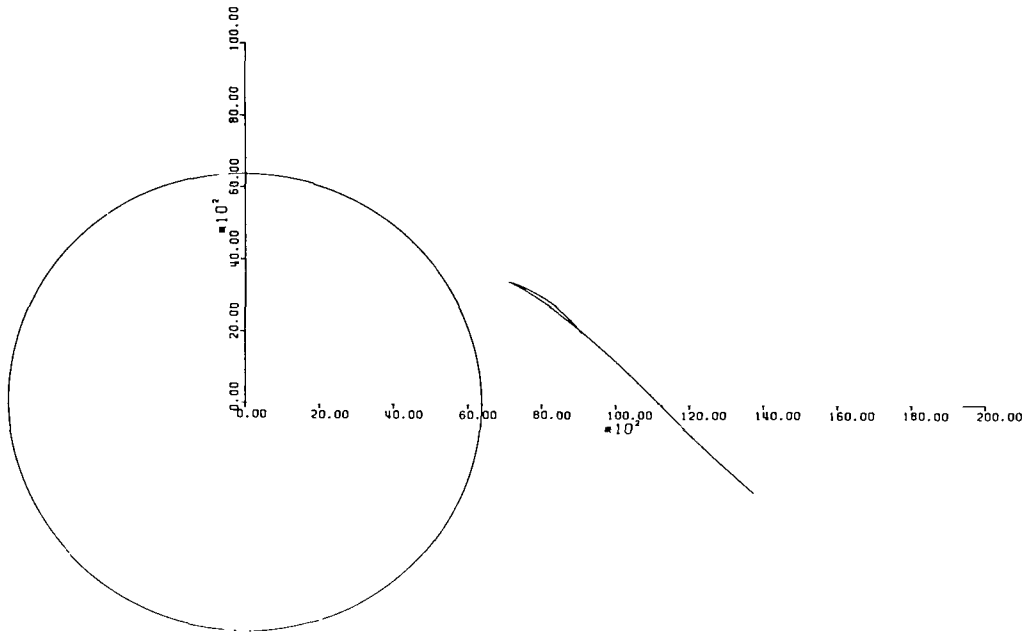

Figure 24a.-Diagram showing mixed modes of propagation; the signal is ducted along the field-line from the satellite to the reflection level, but returns directly to the satellite after reflection

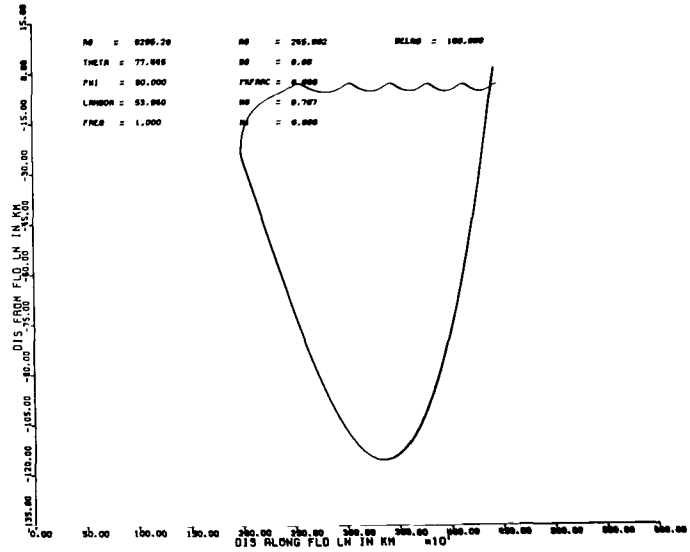

Figure 24b.-Diagram showing mixed modes of propagation; the signal is ducted along the field-line from the satellite to the reflection level, but returns directly to the satellite after reflection

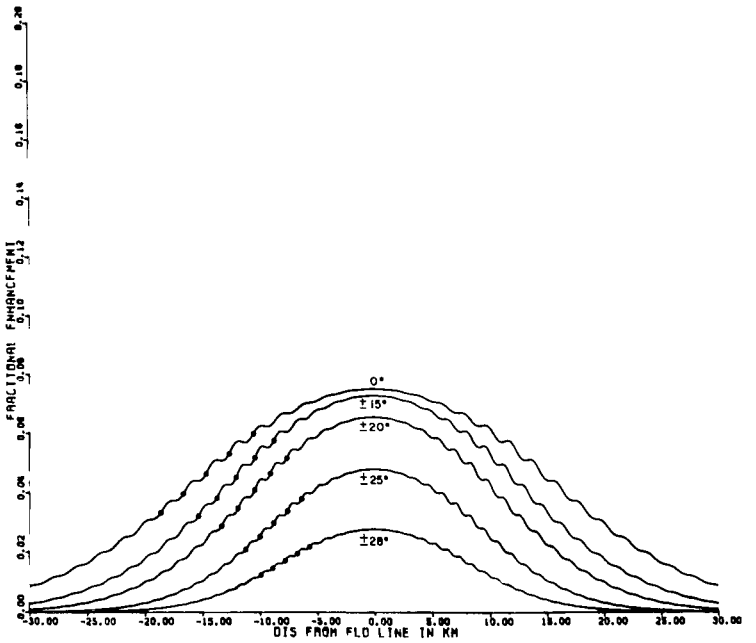

Figure 25a.-Model of the enhancement duct showing percentage enhancement as a function of distance normal to the field-line (L = 1.47)

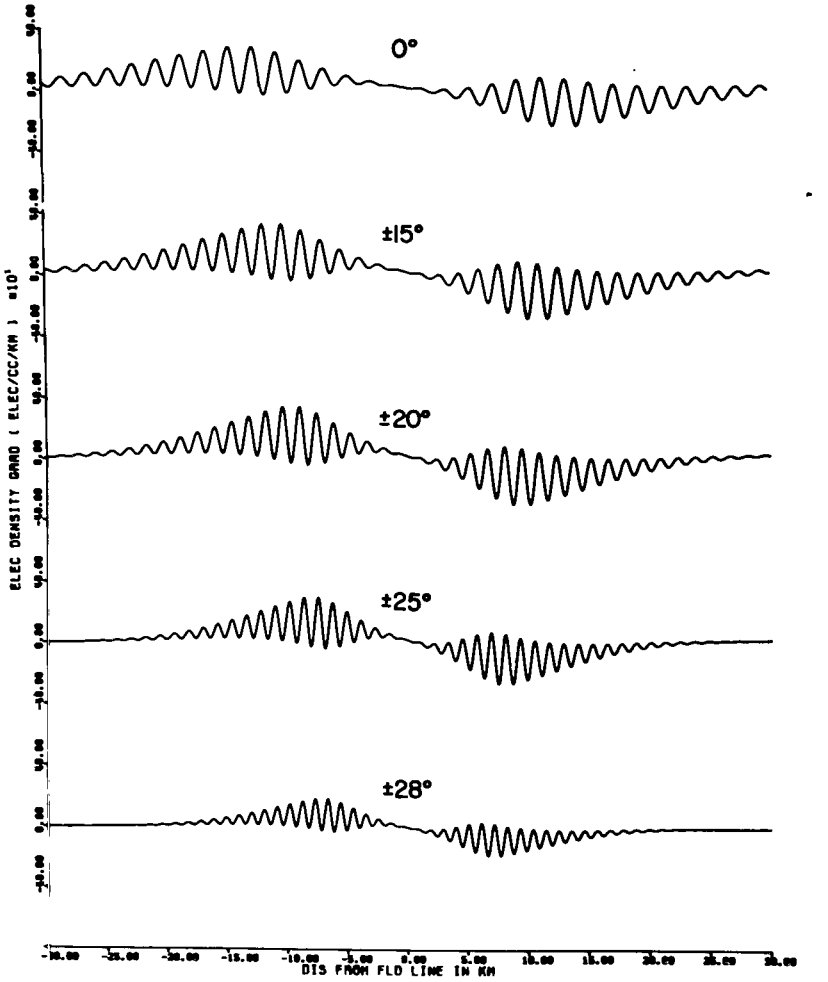

Figure 25b.-The gradient of electron density enhancement as a function of distance normal to the field-line for the model shown in figure 25a

the cross-sectional variation of the ionization enhancement at dip latitudes of 0, ±15, ±20, ±25, and ±28° along a field line of L-value equal to 1.47. The derivative of the electron density with respect to the distance normal to the field line for the various dip latitudes is shown in Figure 25b.

In this basic model of the magnetospheric ducts (refs. 4 and 5) and the present unified model, the duct width and peak fractional enhancement change with distance along the field line. The duct width is proportional to the transverse (meridional) dimension of the tube of magnetic flux. The expression for that variation is:

$$t/t_o = \frac{\text{Meridional Width at } (r,\ \theta)}{\text{Meridional Width at } (r_o,\ \theta_o)}$$

$$= \frac{\sin^3\theta \left(4 - 3 \sin^2\theta_o\right)^{1/2}}{\sin^3\theta_o \left(4 - 3 \sin^2\theta\right)^{1/2}} \qquad (1)$$

where r is the radius, θ is the colatitude of any point of the field line, and r_o and θ_o are the corresponding values at the initial position.

Similarly, the peak electron density enhancement in the duct is assumed to vary inversely as the transverse dimensions of the tube of magnetic flux. If the peak enhancement is denoted by ΔN, its variation along the field line can be expressed as,

$$\Delta N = \Delta N_o * \frac{1}{(t/t_o)} \qquad (2)$$

where ΔN_o is the peak enhancement at r_o, θ_o. This means that the peak fractional enhancement

$$\frac{\Delta N}{N} = \frac{\Delta N_o}{N} * \frac{1}{(t/t_o)} \qquad (3)$$

is inversely proportional to the duct width and the ambient electron density N. In this way, the high values of peak fractional enhancement required in the less dense equatorial regions of the

high latitude field lines (high L values) are obtained while maintaining reasonable values of peak fractional enhancement in the dense regions at the reflection levels near the topside F-region.

In Figure 25a the large-scale structure (20 to 30 km) has a peak enhancement of approximately 3 percent above the ambient at a latitude of 28° and is capable of guiding whistler modes. The small-scale variations (≈1 km), which constitute the ribbed structure, would not affect propagation of the whistler waves, the wavelengths of which are too large. On the other hand, the small electron density gradients that are characteristic of the large-scale variation are too small to guide the HF waves. However, in the small-scale ribbed structure, there exist gradients in electron density which are sufficiently large enough to trap HF waves. The scale sizes of the order of a kilometer are also large enough to constitute a duct for the HF waves. Therefore, HF waves could be trapped in these ribbed structures. The positions of five possible trapping regions for the high-frequency waves are indicated by dots on the respective profiles in Figure 25a.

The diffuseness of the HF conjugate echo traces is due to the relative differences in the ambient electron densities among these ripples which guide the HF waves. The difference in electron densities causes the group refractive indices to be slightly different. Since these ribbed structures are closely spaced, portions of HF energy can propagate in each of the individual structures which have large enough gradients. If five of the small-scale ribs have sufficiently large gradients to guide HF energy, then the returning echoes will have five slightly different delay times due to the differences in the group velocities. On an ionogram, the five individual traces overlap to form a diffuse trace. The fine structure of the diffuse trace generally is not discernible in the lower order traces (near-end, far-end, first round trip) because the differences in delay times among the signals travelling in the closely spaced paths are very small. As the number of times the signals traverse the paths increases, the time differences increase and the fine structure of the traces becomes apparent. Traces corresponding to individual raypaths could then be seen. This behavior is evidenced in Figures 18, 20, and 22.

Figures 18 and 22 refer to the same field-line (L = 1.47) and approximately the same geomagnetic positions but in opposite hemispheres -- 14.02°N and 14.97°S. The third round-trip echo (3N + 3F) of Figure 22 exhibits five distinct traces. From Figure 23 it may be seen that the region in which most of the signal energy is trapped is about 7 km wide. Therefore, within a 7-km region, there must be five ripples at the satellite position

capable of ducting HF energy. Figure 18 also shows four distinct traces making up the higher order echoes. In Figure 19 this trapping region is shown to be just over 5 km.

The fine structure in Figure 20 is very faint but there are indications of four traces composing the echoes. Figure 21 shows the trapping region corresponding to Figure 20 to be roughly 7 km. The ionogram corresponds to almost the same field-line (L = 1.48), but a lower geomagnetic latitude (11.02°N).

Although the three ionograms shown in Figures 18, 20, and 22 were recorded on different days of the year and at different local times, the deduced spacing of the ripples fits very well with the spacing of the ripples indicated by dots in the unified model shown in Figure 25a.

MATHEMATICAL ANALYSIS OF DIFFUSENESS

In this section, an approximate expression for diffuseness is developed by relating the change in group velocity to the change in electron density. The longitudinal approximation for refractive index in a collisionless plasma is given by

$$\mu^2 = 1 - \frac{x}{1 - y} \tag{4}$$

where

$$x = \frac{f_N^2}{f^2} = \frac{8.06 \times 10^7}{f^2} N \text{ and } y = \frac{f_H}{f}$$

The term f_N is the electron plasma frequency, f is the wave frequency, N is the electron density, and f_H is the electron gyro frequency.

The group refractive index is then given by

$$\mu' = \mu + f \frac{\partial \mu}{\partial f} = \frac{1 + \frac{1}{2} \frac{xy}{(1 - y)^2}}{\left(1 - \frac{x}{1 - y}\right)^{1/2}} \quad . \tag{5}$$

Differentiating Eq. (5) with respect to the electron density parameter yields:

$$\frac{d\mu'}{dx} = \frac{1}{2(1-y)\left[1-\frac{x}{1-y}\right]^{3/2}} \left\{1 - \frac{1}{2}\frac{xy}{(1-y)^2} + \frac{y}{1-y}\right\} . \quad (6)$$

Let

$$\Delta\mu' = \frac{d\mu'}{dx}\,\Delta x \ ; \quad (7)$$

then, using Eqs. (5), (6), and (7):

$$\frac{\Delta x}{x} = -2\,\frac{\Delta\mu'}{\mu'} \cdot \frac{(1-\frac{1}{\alpha})(1+\frac{1}{2}\alpha\beta)}{1+\beta(1-\frac{\alpha}{2})} \quad (8)$$

where

$$\alpha = \frac{x}{1-y} \quad \text{and} \quad \beta = \frac{y}{1-y} \ .$$

The parameter f_x is defined as the critical frequency of the extraordinary mode. At this frequency,

$$x = 1 - y \quad \text{(reflection level)} \quad (9)$$

In other words:

$$\alpha\big|_{f=f_x} = 1 \ . \quad (10)$$

If f increases or N and f_H decrease, x and y decrease so that

$$\alpha\big|_{f>f_x} < 1 \ . \quad (11)$$

The near-end echo begins with zero time delay when $f = f_{XS}$ (the value of f_X at the satellite position). As f increases, the delay increases since the signal has to travel further down the field line to reach the reflection point where $f = f_X$. For frequencies above f_{XS}, the value of α is less than 1 at the satellite. Along the signal path from the satellite position to the reflection point down the field line, α gradually increases from its value at the satellite position and approaches unity at the reflection point. For signals travelling up the field line away from the Earth, α would first decrease, reaching some minimum value at the equator, and then increase to 1 as the reflection level in the opposite hemisphere is approached. Even at the equator, the value of α cannot be too small if the ray is to be trapped (ref. 19). Since the refractive index may be approximated by

$$\mu = (1 - \alpha)^{1/2} \quad , \tag{12}$$

it can be seen that the medium approaches free space ($\mu = 1$) as α approaches zero. If α is too close to zero, the medium will be unable to bend the ray so that the ray curvature becomes equal to the curvature of the field line. Under such conditions, the ray would escape.

The frequency at which the conjugate traces occur in Figure 22 is greater than five times the gyro frequency at the satellite. Then, Eq. (8) may be approximated by

$$\frac{\Delta x}{x} \approx -2 \frac{\Delta \mu'}{\mu'} \left(1 - \frac{1}{\alpha}\right) \tag{13}$$

Equation (13) is also a good approximation when α is near 1, regardless of the value of β. With the relationship,

$$\frac{\Delta \mu'}{\mu'} \approx - \frac{\Delta v_g}{v_g} \quad , \tag{14}$$

where v_g is the group-velocity, Eq. (13) may be simplified to

$$\frac{\Delta v_g}{v_g} = - \frac{1}{2} \gamma \frac{\Delta x}{x} = - \frac{1}{2} \gamma \frac{\Delta N}{N} \tag{15}$$

where $\gamma = \alpha/(1-\alpha)$. If the third round-trip trace (3N + 3F), is examined in Figure 22, it is seen to be composed of five individual traces with a total time spread (diffuseness) which increases slightly with frequency but has an average value of 2.2 msec. Because the third round-trip trace returned with a delay time of 317 msec, the diffuseness could be explained by an average fractional change in group-velocity $(\Delta v_g/v_g)_{avg}$ of 0.007 between the first and the last traces of the echo. The average fractional change in group velocity is given by the expression

$$\left(\frac{\Delta v_g}{v_g}\right)_{avg} = \frac{1}{s}\int_{Path} \frac{\Delta v_g}{v_g}\, ds \approx \frac{1}{2s} \int_{Path} \gamma\, \frac{\Delta N_{eff.}}{N}\, ds \qquad (16)*$$

where s is the total geometrical path length along the field line. At the satellite altitude, γ is approximately equal to 1 for the frequency range being considered in the example. If γ were constant along the path, then the required fractional change in electron density at the satellite altitude (and all along the field line) between the positions where the first and last traces were guided would be 1.4 percent. But α and γ are not constant along the field line. Figure 26 shows a plot of γ versus α. At the equator, α has its lowest value and at the reflection level it approaches a value of 1.

A gaussian variation centered around the corresponding magnetic field line was selected as a reasonable model for the broad enhancement. The superimposed small-scale ripples that are effective in guiding the HF rays are located in the region of the point of maximum slope of the broad gaussian distribution. This is the region where the maximum variation in the ambient electron density takes place. The slope of the large-scale enhancement will also reinforce the ability of the small ripples to trap the HF rays. At the center of the broad enhancement, the electron density gradients are too small to contain the HF rays. Ripples on the outside of the large-scale enhancement would less likely be able to trap the rays because the large-scale slope would then be negative and hence decrease the gradients in the ripples. Occasionally, however, the ripples on the outside of the broad enhancement do have sufficient gradients to trap the radio energy. A typical example is shown in Figure 27. Another figure showing the same feature is the 23rd ionogram in the sequence observed at Singapore, August 9, 1966. It is from

*The meaning of $\Delta N_{eff.}$ is discussed in the appendix.

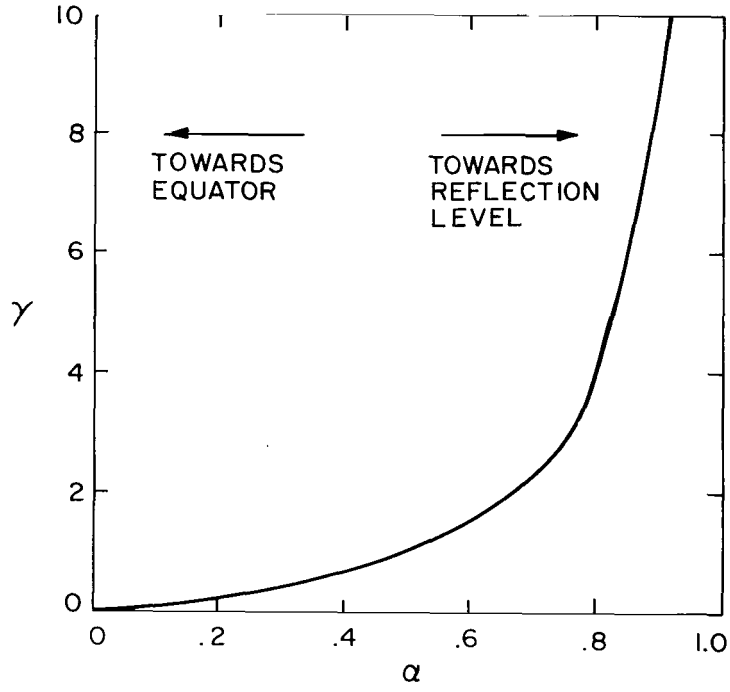

Figure 26.-Diagram showing γ versus α

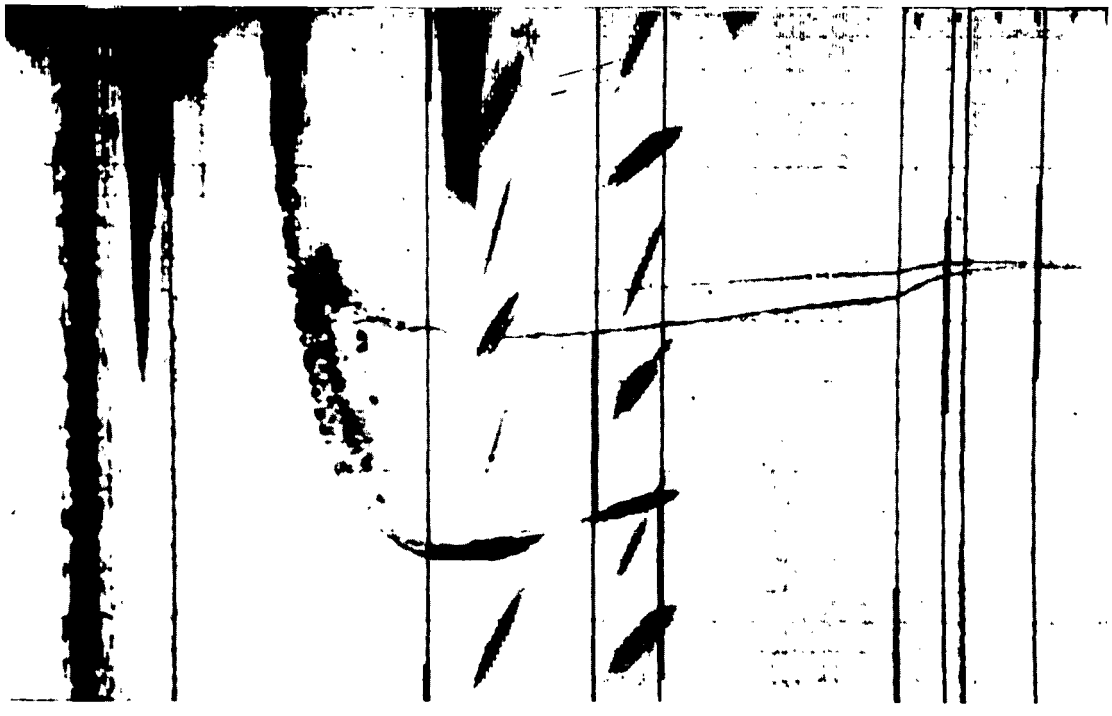

Figure 27.-Ionogram recorded at Santiago on July 20, 1966, at 21:11:34 UT.

these types of ionograms that the width of the large-scale enhancement structure could be obtained.

In the 23rd ionogram of the Singapore sequence, the satellite is travelling from the inside to the outside of the field lines. So, all the traces begin simultaneously after $f > f_{XS}$. Later on, all of the traces, except the near-end trace, end abruptly. A few second later all the traces begin again. The first ducting region corresponds to the satellite being at the ripples on the inside slope of the broad enhancement. As the satellite approaches the center of the broad enchancement where there are insufficient electron density gradients for trapping, the traces vanish on the ionogram. Finally, the satellite approaches the second ducting region on the outside slope of the broad enhancement and the signals are trapped again, resulting in a resumption of traces on the ionogram. The near-end echo does not suffer this discontinuity for reasons discussed earlier.

In Figure 27, the satellite is travelling from the outside to the inside of the field line so that the near-end echo begins considerably earlier than the other echoes. Here the first trapping region corresponds to the ripples on the outside slope of the broad enhancement and the second trapping region corresponds to the region on the inside slope. The various conjugate echoes observed in the ionogram of Figure 27 are identified and arranged according to their actual delay times in Figure 28. The satellite positions relative to the field line for the frequencies of interest are shown in Figure 29. It is through the types of echoes observed in the ionogram of Figure 27 that the size of the broad enhancement can be determined. The satellite was near perigee when the ionogram was recorded and the trapping regions are 4 and 5 km wide with a separation of 7 km. An anlaysis of the diffuseness of the first round-trip trace of Figure 27 indicates a variation in the group-velocity of approximately 0.8 percent.

In the ionogram of Figure 27, the higher order traces show less fine-structure and diffuseness compared to the lower order traces. This is opposite to what we have observed in the previous examples. The significant factor that differentiates the present example from the previous examples is the high L-value of the satellite position. The L-value corresponding to the ionogram of Figure 27 is 2.53. Along the field-line of such a high L-value, the ducts are probably more tenuous and, no doubt, more leaky than the ducts' lower L-values corresponding to previously considered examples. On succeeding hops, the energy escapes from the ripples having smaller gradients of electron density and this leads to less diffuseness in higher order traces. Only those paths along which ducting is stable persist in the higher order traces.

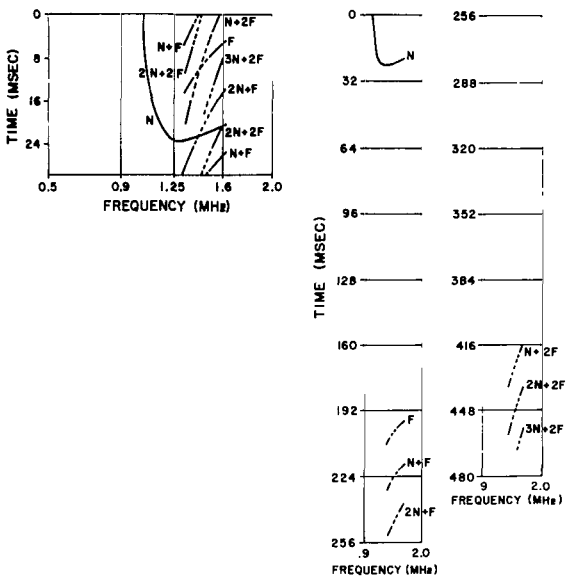

Figure 28.-Diagram corresponding to figure 27 showing the actual time-delays and the frequency variations with the missing portions indicated by dashed lines

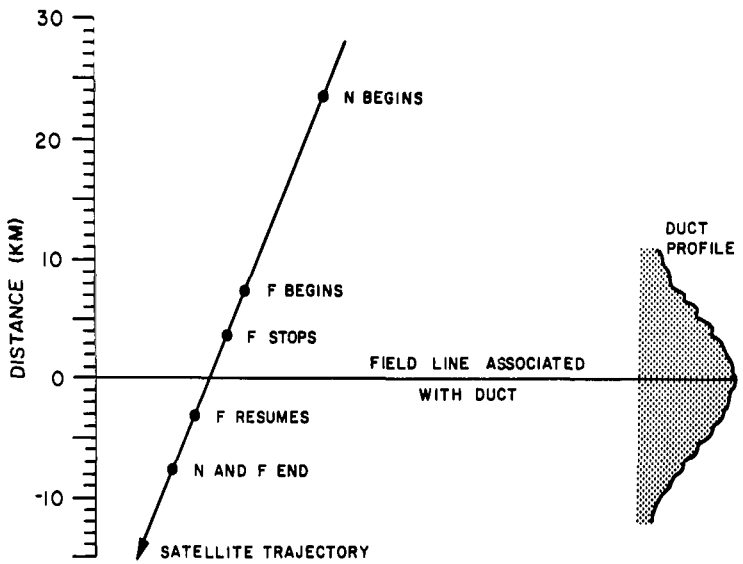

Figure 29.-Diagram of the satellite trajectory relative to the magnetic field-lines at the time the ionogram of figure 24 was recorded; also shown are the relative satellite locations when the near-end (N) and far-end (F) echoes were received

Figure 30 shows an ionogram corresponding to a lower L-value (L = 1.81). This ionogram exhibits both pronounced fine-structure and two trapping regions. An enlarged portion of Figure 30 is shown in Figure 30a. The traces are identified and arranged according to their actual delay times in Figure 31. The satellite trajectory corresponding to Figure 30 is shown in Figure 32. The satellite was travelling from the inside to the outside of the field-line so all the echoes begin at virtually the same time. Although the field-line has a larger L-value (L = 1.8) than that for the model presented in Figure 25a (L = 1.47), the indicated spacing of the ripples and the size and spacing of the two ducting regions agree fairly well with the model when the same altitude ranges are considered. The diffuseness of the second round-trip trace (2N + 2F) indicates a change in group-velocity of 1.0 percent over a distance of five ripples. Figure 30 is an example of an ionogram corresponding to a relatively higher L-value, but still capable of showing the fine structure and diffuseness as discussed in Figure 25a. Figure 27 is an example of an ionogram of much higher L-value where the ducting process is different from the others discussed earlier.

The duct model, as shown in Figure 25a, was developed by the authors from analysis of topside-sounder ionograms and digital ray-tracing results. Using the proposed model for magnetospheric ducts in the ray-tracing program, the authors have obtained values for the diffuseness of HF conjugate echoes which are in good agreement with the observed values in the topside-sounder ionograms.

Figure 33a shows the results of a digital ray-tracing program showing the trapped ray paths in the ripples indicated by dots in the model of Figure 25. All the rays were launched from a latitude of 3.808° towards the near-end on the field line of L = 1.47. Although the total path is not shown in Figure 33a because of the limited calcomp storage volume, all the rays were reflected at the near-end and guided to a far-end reflection level where the computer run was terminated. The ray paths relative to the Earth are shown in Figure 33b. The computed delay-times agree well with the observed values.

CONCLUSION

The basic ideas used in developing the model will now be reviewed. The distance travelled by the satellite normal to the field lines indicates the size of the ducting regions. The separation distance between two ducting regions as determined by the ionograms provides information on the width of the broad enhancement. The fine structure of the various echoes in an ionogram determines the number of ripples in the trapping region and

Figure 30.-Ionogram recorded by the Alouette-2 topside-sounder at Singapore on April 8, 1966, at 23:01:13 UT.

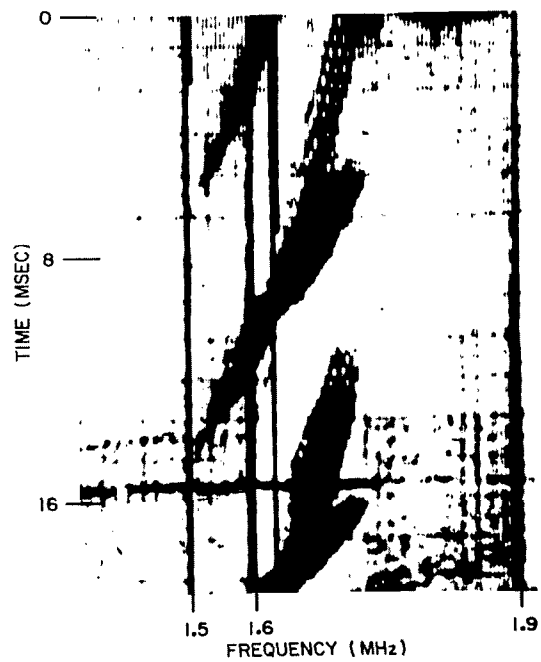

Figure 30a.-Enlargement of the upper portion of figure 30 indicated by dashed lines

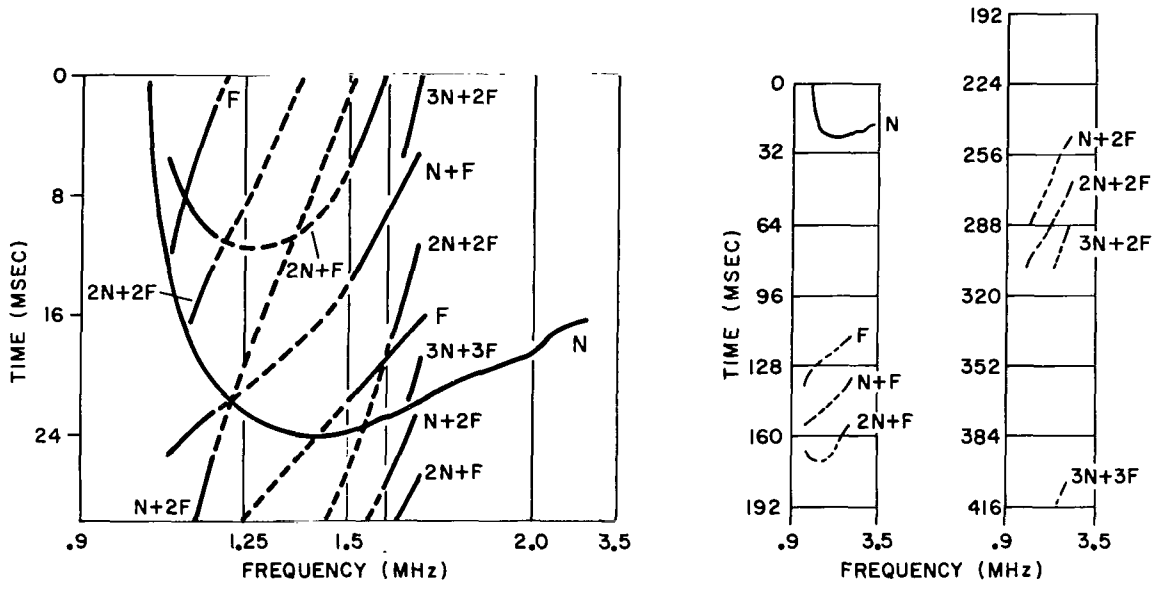

Figure 31.-Diagram corresponding to figure 30 showing the actual time-delays and the frequency-variations with the missing portions indicated by dashed lines

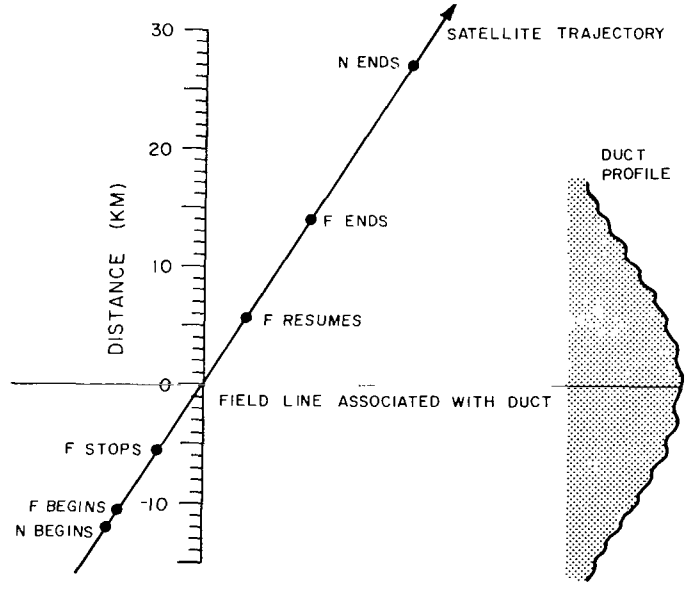

Figure 32.-Diagram of the satellite trajectory relative to the magnetic field lines at the time the ionogram of figure 30 was recorded; also shown are the relative satellite locations when the near-end(N) and far-end(F) echoes were received

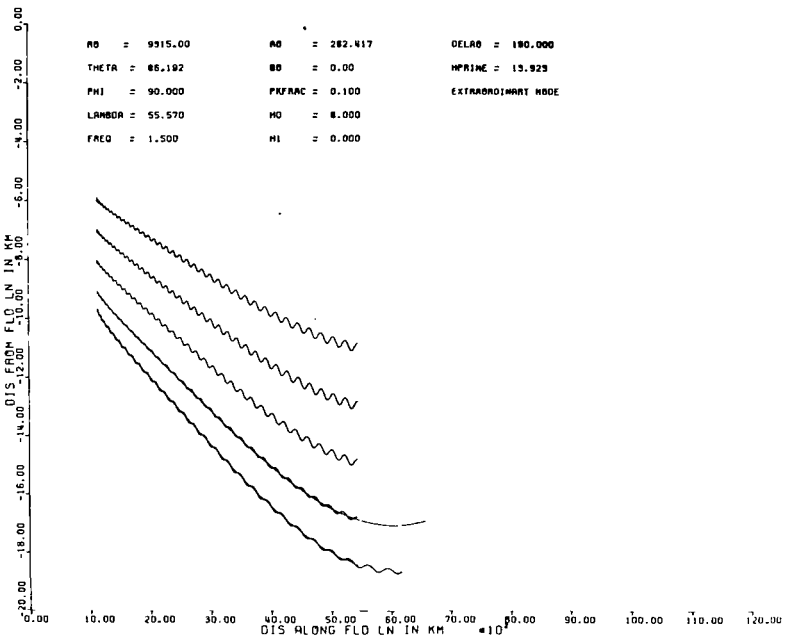

Figure 33a.-Calcomp plot produced by the digital ray-tracing program showing five rays trapped in the ripples indicated by dots in the proposed duct model shown in figure 25

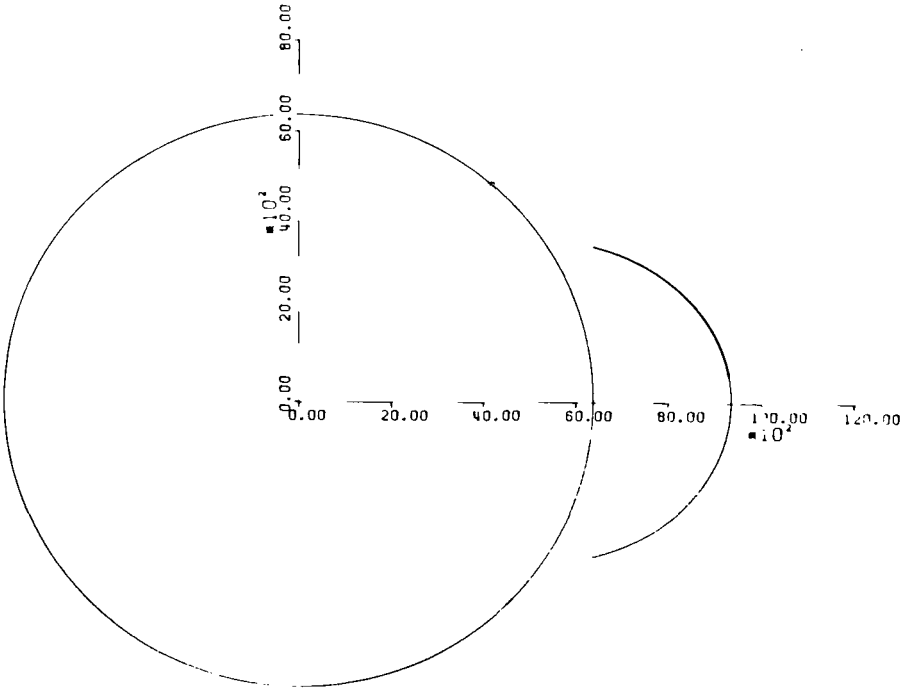

Figure 33b.-Calcomp plot of the ray-paths relative to Earth

therefore their spacing. The diffuseness indicates the electron density gradient in the braod enhancement which, in turn, determines the peak value of fractional enhancement. The amplitude of the broad enhancement determines the diffuseness, whereas the amplitude of the ripples determines the number that can trap the radio waves.

Much research remains to be done on the ducting phenomenon itself, but the basic physical structure of the model as postulated by the author seems to be consistent with the observed results.

REFERENCES

1. Muldrew, D. B.: Radio Propagation Along Magnetic Field-Aligned Sheets of Ionization Observed the Alouette-1 Topside Sounder. J. Geophys. Res., vol. 68, 1963, pp. 5355-5370.

2. Loftus, B. T., Van Zandt, T. E., and Calvert, W.: Observations of Conjugate Ducting by the Fixed-Frequency Topside-Sounder Satellite. Ann. de Geophys., vol. 22, 1966, pp. 530-537.

3. Muldrew, D. B.: MF Conjugate Echoes Observed on Alouette-2 Topside-Sounder Data. Can. J. Phys., vol. 45, no. 12, 1967, pp. 3935-3944.

4. Ramasastry, J., Walsh, E. J. and Herman, J. R.: Research on Field-Aligned Propagation of HF Radio Waves Using Alouette-2 Topside-Sounder Data and Digital Ray-tracing Techniques. NASA TN D-4748, August 1968.

5. Ramasastry, J., Walsh, E.J. and Herman, J.R.: Conjugate Echoes in Alouette-2 Topside-Sounder Data. IEEE Trans. on Antennas and Propagation, vol. AP-16, no. 6, November 1968, pp. 771-775.

6. Helliwell, R. A.: Whistler Paths and Electron Densities in the Outer Ionosphere. Proc. of the Symposium on Physical Processes in the Sun-Earth Environment, DRTE No. 1025, Defence Research Telecommunications Establishment, Ottawa, Canada, 1960, pp. 165-175.

7. Helliwell, R. A.: Whistlers and Related Ionospheric Phenomena. Stanford University Press, Stanford, California, 1965.

8. Calvert, W., and Schmid, C. W.: Spread-F Observations by the Alouette Topside-Sounder Satellite. J. Geophys. Res., vol. 69, 1964, pp. 1839-1852.

9. Shimazaki, T.: A Statistical Study of World-Wide Occurrence Probability of Spread-F. J. Radio. Res. Labs. (Japan), vol. 6, no. 28, 1959, pp. 669-704.

10. Storey, L. R. O.: An Investigation of Whistling Atmospherics. Phil. Trans. Roy. Soc. (London), vol. 246A, 1953, pp. 113-141.

11. Laaspere, T., Morgan, M. G. and Johnson, W.C.: Some Results of Five Years of Whistler Observations from Labrador to Antarctica. Proc. IEEE, vol. 51, no. 4, 1963, pp. 554-568.

12. Barrington, R. E., and Thompson, W. E.: Whistlers and Magnetic Activity. Can. J. Phys., vol. 40, 1962, pp. 775-781.

13. Kimpara, A.: Correlation of Occurrence of Whistlers and Geomagnetic Activities. Nature, vol. 186, 1960, pp. 230-246.

14. Somayajulu, V. V., and Tantri, B. A. P.: Effect of Magnetic Storms on Duct Formation for Whistler Propagation. J. Geomagnetism and Geoelectricity, vol. 20, no. 1, 1968, pp. 21-31.

15. Ramasastry, J.: Review of High-Frequency Ducting in the Magnetosphere of the Earth, NASA TM X-1457, 1967.

16. Knecht, R. W., Van Zandt, T. E., and Russell, S.: First Pulsed Radio Soundings of the Topside of the Ionosphere, J. Geophys. Res., vol. 66, 1961, pp. 3078-3081.

17. Smith, R. L.: Propagation Characteristics of Whistlers Trapped in Field-Aligned Columns of Enhanced Ionization J. Geophys. Res., vol. 66, 1961, pp. 3699-3707.

18. Pitteway, M. L. V., and Cohen, R.: A Wave-guide Interpretation of Temperate-Latitude Spread-F on Equatorial Ionograms. J. Geophys. Res., vol. 66, 1961, pp. 3141-3156.

19. Knecht, R. W., and Russell, S.: Pulsed Radio Soundings of the Topside of the Ionosphere in the Presence of Spread-F. J. Geophys. Res., vol. 67, 1962, pp. 1178-1182.

20. Booker, H. G.: Guidance of Radio and Hydromagnetic Waves in the Magnetosphere. J. Geophys. Res., vol. 67, 1962, pp. 4135-4162.

21. Gothard, N.: Guidance in the Magnetosphere Along Field-Aligned Irregularities. Radio Science, vol. 3 (new series), no. 3, 1968, pp. 235-243.

APPENDIX

The reason for using $\Delta N_{effective}$ instead of ΔN is the following. The difference in the enhancements at the various ripples causes the corresponding ducted signals to be reflected at slightly different altitudes, since they require the same electron density for reflection. To allow for this effect, the various ripples could be imagined to be shifted slightly in the direction parallel to the field line so that the various reflection points are shifted to the same altitude. As a result, ΔN is zero in the region where γ is singular and has increasingly higher values as the equator is approached. Under such circumstances, Eq. (16) could be integrated. This procedure is roughly equivalent to using a $\Delta N_{effective}$ in Eq. (16), which is less than the actual value at any level by an amount equal to ΔN at the reflection level. If the satellite is located at a geomagnetic latitude of 15° on a field line of L-value 1.47, the enhancement model of Figure 25a indicates that $\Delta N_{effective}$ is approximately equal to 2 percent at that position which is a reasonable value.

NATIONAL AERONAUTICS AND SPACE ADMINISTRATION
WASHINGTON, D. C. 20546

OFFICIAL BUSINESS

FIRST CLASS MAIL

POSTAGE AND FEES PAID
NATIONAL AERONAUTICS AN
SPACE ADMINISTRATION

POSTMASTER: If Undeliverable (Section 158 Postal Manual) Do Not Return

"The aeronautical and space activities of the United States shall be conducted so as to contribute . . . to the expansion of human knowledge of phenomena in the atmosphere and space. The Administration shall provide for the widest practicable and appropriate dissemination of information concerning its activities and the results thereof."

—NATIONAL AERONAUTICS AND SPACE ACT OF 1958

NASA SCIENTIFIC AND TECHNICAL PUBLICATIONS

TECHNICAL REPORTS: Scientific and technical information considered important, complete, and a lasting contribution to existing knowledge.

TECHNICAL NOTES: Information less broad in scope but nevertheless of importance as a contribution to existing knowledge.

TECHNICAL MEMORANDUMS: Information receiving limited distribution because of preliminary data, security classification, or other reasons.

CONTRACTOR REPORTS: Scientific and technical information generated under a NASA contract or grant and considered an important contribution to existing knowledge.

TECHNICAL TRANSLATIONS: Information published in a foreign language considered to merit NASA distribution in English.

SPECIAL PUBLICATIONS: Information derived from or of value to NASA activities. Publications include conference proceedings, monographs, data compilations, handbooks, sourcebooks, and special bibliographies.

TECHNOLOGY UTILIZATION PUBLICATIONS: Information on technology used by NASA that may be of particular interest in commercial and other non-aerospace applications. Publications include Tech Briefs, Technology Utilization Reports and Notes, and Technology Surveys.

Details on the availability of these publications may be obtained from:

SCIENTIFIC AND TECHNICAL INFORMATION DIVISION

NATIONAL AERONAUTICS AND SPACE ADMINISTRATION

Washington, D.C. 20546